

*IN-SITU* PRODUCTION RATES OF COSMOGENIC  $^{10}\text{Be}$  AND  $^{26}\text{Al}$   
OVER THE PAST 21,500 YEARS  
DETERMINED FROM THE TERMINAL MORaine  
OF THE LAURENTIDE ICE SHEET,  
NORTH-CENTRAL NEW JERSEY

A Thesis Presented  
by  
Patrick Luther Larsen  
to  
The Faculty of the Graduate College  
of  
The University of Vermont

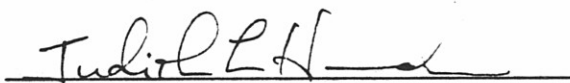
In Partial Fulfillment of the Requirements  
for the Degree of Master of Science  
Specializing in Geology

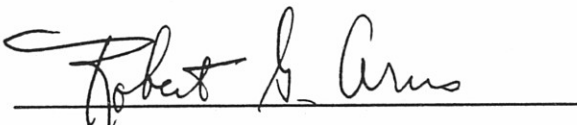
March, 1996

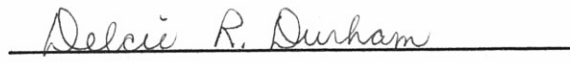
Accepted by the Faculty of the Graduate College, The University of Vermont, in partial fulfillment of the requirements for the degree of Master of Science, specializing in Geology.

Thesis Examination Committee:

  
\_\_\_\_\_  
Paul R. Bierman, Ph.D. Advisor

  
\_\_\_\_\_  
Judy Hannah, Ph.D.

  
\_\_\_\_\_  
Robert G. Arns, Ph.D. Chairperson

  
\_\_\_\_\_  
Delcie R. Durham, Ph.D. Dean,  
Graduate College

Date: October 13, 1995



## ABSTRACT

The in-situ production rates of cosmogenic  $^{10}\text{Be}$  and  $^{26}\text{Al}$  were determined in samples collected from the terminal moraine of the Laurentide ice sheet in north-central New Jersey. The minimum limiting exposure age for the Laurentide samples was assumed to be 21,500 cal  $^{14}\text{C}$  years based on numerous existing radiocarbon dates from sites on and near the terminal moraine. Statistical agreement between varying rock types and sample surfaces suggests that all samples can be considered to be from a single population and the similarity of isotope abundances between unstriated gneiss and striated quartzite sample sites indicates that erosion has been negligible since the recession of the Laurentide ice sheet. The statistical similarity between outcrop and boulder samples suggest that the boulders have not rolled and that the outcrops have not been covered with till or soil since ice sheet recession. Average concentrations of  $1.11 \pm 0.03 \cdot 10^5$  (1sem, n=12) atoms  $\text{gram}^{-1}$   $\text{SiO}_2$  for  $^{10}\text{Be}$  and  $6.47 \pm 0.22 \cdot 10^5$  (1sem, n=14) atoms  $\text{gram}^{-1}$   $\text{SiO}_2$  for  $^{26}\text{Al}$  can be used to calculate production rates of  $5.17 \pm 0.15$  (1sem) and  $30.40 \pm 1.01$  (1sem) atoms  $\text{gram}^{-1} \text{SiO}_2 \text{ year}^{-1}$  for  $^{10}\text{Be}$  and  $^{26}\text{Al}$ , respectively. These values are approximately 15-20% less than previously accepted values.

moraine of the Laurentide Ice Sheet, North-Central New Jersey, Geological Society of America Bulletin

## CITATION

Material from this thesis has been submitted for publication to Geological Society of America Bulletin on (12-15-95) in the following form:

Larsen, Patrick L., Bierman, Paul R., Stone, Byron; Caffee, M. *In-situ* production rates of cosmogenic  $^{10}\text{Be}$  and  $^{26}\text{Al}$  over the past 21,500 years determined from the terminal moraine of the Laurentide Ice Sheet, North-Central New Jersey. Geological Society of America Bulletin.

## ACKNOWLEDGEMENTS

There are several people and organizations without whose cooperation, money, time, and support this study could not have been completed.

Field work was expedited and enjoyable thanks to several people. Most notable, Byron Stone of the USGS, whose expertise and New Jersey mapping experience saved me considerable time. Byron also provided topographic and geologic maps, a couple days in the field, and numerous lively discussions. Christine Massey and Paul Bierman provided time, assistance and advise during sample collection. Personnel at the Picatinny Military Arsenal allowed me access to, and allowed me to take samples from an otherwise secured area. I am also indebted to Mike Ghia, of UVM's department of Plant and Soil Science, who arranged for me to camp on his family farm in northern New Jersey, and his brother the magician for providing nightly entertainment. Finally, field work was funded by a research grant from the Geological Society of America.

Sample preparation and analysis could not have been completed without the donations of time and analyses from several people and organizations. I am extremely indebted to Marc Caffee, Joe Koenig, John Southon, and Bob Finkle at Lawrence Livermore National Laboratories Center for Accelerator Mass Spectrometry. Livermore provided no less than \$25,000 in isotopic analyses and countless hours running samples and providing timely data. Also, numerous discussions and e-mail correspondences significantly aided in my understanding of the subject matter. Chemicals and materials for sample preparation, estimated to be approximately \$100/sample, were provided by NSF and startup grants to Paul Bierman. ICAP and SEM measurements were made with the help of Kim Hannula and Ray Coish at Middlebury College. Jennifer Larsen of the Plant and Soil Science department at UVM provided time, assistance, and free analyses on the ICP. Jill Turner provided sample preparation training and assisted during the sample preparation phase. I have numerous people to thank for baby-sitting the ultrasound and consequently, saving me many short trips into Burlington. These people include, but are probably not

limited to Kim Marsella, Alexis Richardson, Jill Turner, Jeff Frederick, Adam Brown, Paul Bierman, and basically whoever happened to answer the graduate student phone on Saturday and Sunday mornings.

I am grateful to my parents, for their continual emotional and financial support, and to the Carswell family for their support through times of crisis.

Perhaps the greatest acknowledgments should go to the good people who I have had the privilege of getting to know on a personal and social level. I have learned a great deal about myself (which is really what life is all about, not cosmogenic isotopes) thanks to interactions and friendships with the following people: Lars Cherichetti, Alexis Richardson, Jon Goldberg, Kim Marsella, Adam Schoonmaker, Adam Brown, Russ Schuck, Amy Church, Jeff Frederick, Tim Whalen, Lin Li, Jeremy Hourigan, Parker Hackett, and Todd Martin.

I am grateful to my lifelong friends, Nick Webb and Julie Talbert in New York City for giving me a place to escape to (and ultimately from) as well as providing a link to the past.

Thanks and gratitude to my advisor, Dr. Paul Bierman, who was as committed to the seemingly unprecedented two-year masters degree as I was, and whose encouragement and sincere love of science helped make this a productive and enjoyable two years.

Finally and mostly, I am grateful for the unconditional love, support, and patience of Ruth Carswell, who has added a whole new dimension to my life.



## TABLE OF CONTENTS

CITATION PAGE .....	ii
ACKNOWLEDGEMENTS .....	iii
TABLE OF CONTENTS .....	v
LIST OF TABLES .....	viii
LIST OF FIGURES .....	ix

## CHAPTER

I.	INTRODUCTION .....	1
	Cosmic rays .....	2
	Production mechanisms of cosmogenic isotopes .....	2
	Factors affecting production rates .....	3
	Significance of research .....	7
II.	COMPREHENSIVE LITERATURE REVIEW .....	10
	Introduction .....	10
	Advance of Laurentide ice sheet .....	10
	Age control .....	11
	Production rate studies for $^{10}\text{Be}$ and $^{26}\text{Al}$ .....	13
	Magnetic field fluctuation studies .....	15
	Cosmogenic isotope studies on moraines .....	16
III.	GSA BULLETIN JOURNAL ARTICLE .....	19
	ABSTRACT .....	21
	INTRODUCTION .....	22

PREVIOUS RESEARCH .....	23
Production rates of $^{10}\text{Be}$ and $^{26}\text{Al}$ .....	24
Magnetic field fluctuation and variation .....	25
in isotope production rates .....	26
FIELD SITE .....	27
Physiography .....	27
Geology .....	28
Glacial history .....	29
Ice advance .....	29
Age control for Laurentide recession .....	30
METHODS .....	32
Field methods .....	32
Lab methods .....	33
RESULTS .....	35
Isotope abundances and production rate interpretations .....	35
Statistical analyses for separability of populations .....	37
DISCUSSION .....	39
Erosion .....	40
Post-depositional movement .....	40
Snow cover .....	41
Till cover .....	41
Variations due to paleomagnetic field .....	42
Exposure age constraints .....	43
$^{26}\text{Al}/^{10}\text{Be}$ ratios .....	44
Implications .....	45
CONCLUSIONS .....	46
ACKNOWLEDGEMENTS .....	47

FIGURE CAPTIONS .....	48
TABLES .....	50
FIGURES .....	56
DATA REPOSITORY .....	66
SAMPLE DESCRIPTIONS .....	66
REFERENCES CITED .....	88
APPENDIX A-BATCH DATA .....	94
APPENDIX B-LEACH EXPERIMENT .....	119
APPENDIX C-PRECIPITATION EXPERIMENT .....	121
COMPREHENSIVE BIBLIOGRAPHY .....	124

## LIST OF TABLES

### TABLE

3.1. $^{14}\text{C}$ age estimates for deglaciation of Laurentide Ice Sheet .....	50
3.2. Sample site locations and characteristics .....	51
3.3. Laboratory sample data .....	52
3.4. $^{10}\text{Be}$ AMS data and abundances .....	53
3.5. $^{26}\text{Al}$ AMS data and abundances .....	54
3.6. Average isotopic abundances, production rates, and ratios .....	55
3.7. Preserved glacial sediments .....	62
3.8. Gneiss surface displaying characteristic weathering of quartz vein and gneiss matrix .....	63
3.9. Mean monthly snowfall values for Sussex, New Jersey .....	64



## LIST OF FIGURES

### FIGURE

1.1 Earth's magnetic field .....	6
3.1 Map of the state of New Jersey .....	56
3.2 Locations of sample sites near the terminal moraine of the Laurentide ice sheet in the Highlands physiographic province in north-central New Jersey .....	57
3.3 Generalized map showing the bedrock geology of the field area in north central New Jersey .....	58
3.4 Distribution of glacial sediments in field area in the New Jersey Highlands physiographic province in north-central New Jersey .....	59
3.5 Map showing locations of independent $^{14}\text{C}$ age controls for recession of the Laurentide ice sheet .....	60
3.6 Sampled gneissic erratic .....	61
3.7 Preserved glacial striations .....	62
3.8 Gneissic surface displaying differential weathering of quartz vein and gneiss matrix .....	63
3.9 Mean monthly snowfall values for Sussex, New Jersey .....	64

## LIST OF FIGURES

### FIGURE

1.1 Earth's magnetic field .....	6
3.1 Map of the state of New Jersey .....	56
3.2 Locations of sample sites near the terminal moraine of the Laurentide ice sheet in the Highlands physiographic province in north-central New Jersey .....	57
3.3 Generalized map showing the bedrock geology of the field area in north central New Jersey .....	58
3.4 Distribution of glacial sediments in field area in the New Jersey Highlands physiographic province in north-central New Jersey .....	59
3.5 Map showing locations of independent $^{14}\text{C}$ age controls for recession of the Laurentide ice sheet .....	60
3.6 Sampled gneissic erratic .....	61
3.7 Preserved glacial striations .....	62
3.8 Gneissic surface displaying differential weathering of quartz vein and gneiss matrix .....	63
3.9 Mean monthly snowfall values for Sussex, New Jersey .....	64

3.10 $^{26}\text{Al}$ graphed versus $^{10}\text{Be}$ .....	65
3.11. Bedrock ridge from which samples 1-4 were taken .....	67
3.12 Cross section of sampled outcrop .....	68
3.13 Bedrock ridge from which sample 5 was taken .....	70
3.14 Bedrock surface from which sample 6 was taken .....	70
3.15 Glacial erratic from which samples 7 and 8 were taken .....	72
3.16 Surface of glacial erratic .....	72
3.17 Schematic showing geometry and dimensions of erratic .....	73
3.18 Quartzite erratic .....	75
3.19 Gneissic erratic from which samples 10 and 11 were taken .....	77
3.20 Schematic showing dimensions of erratic and location of samples 10 and 11 .....	78
3.21 Schematic showing geometry and dimensions of glacial erratic .....	79
3.22 Glacially molded outcrop from which sample 13 was taken .....	81

3.23	Glacially molded outcrop from which sample 14 was taken	81
3.24	Striated outcrop	83
3.25	Schematic showing outcrop geometry and location of samples 15 and 16	84
3.26	Topographic map showing location of samples 1,2,3,4,5,6,9,15 and 16	85
3.27	Topographic map showing location of samples 7 and 8	86
3.28	Topographic map showing location of samples 10,11,12,13, and 14	87



## Chapter I

### INTRODUCTION

Cosmogenically produced isotopes are finding a wide range of applications in the earth sciences and are becoming a valuable and ubiquitous tool for geomorphic studies. Cosmogenic isotopes have been used to calculate bedrock-to-soil conversion rates (Monaghan et al., 1992), exposure ages of glacial moraines (Brown et al., 1991a), and rates of weathering (Sarda et al., 1993; Raisbeck et al., 1983; Nishiizumi et al., 1986; Nishiizumi et al., 1993; Klein et al., 1986; Nishiizumi et al., 1991a). This burgeoning popularity of in-situ produced cosmogenic isotopes is primarily due to increased analytical capabilities, a unique time frame over which such isotopes are potentially useful, and a selection of cosmogenic isotopes with different half-lives.

Recent advances in the detection capabilities of cosmogenic isotopes now make it possible to measure ratios for the isotope pairs  $^{26}\text{Al}/^{27}\text{Al}$  and  $^{10}\text{Be}/^9\text{Be}$  as low as several parts in  $10^{-15}$  (Finkle and Suter, 1993). Given these significant advancements in accelerator mass spectrometry (AMS) technology, the emphasis must now be concentrated on more precisely quantifying the production rates of cosmogenic isotopes over time. Production rates for  $^{26}\text{Al}$  and  $^{10}\text{Be}$  have been calculated for an assumed integrated exposure of 11 ky (Nishiizumi et al., 1989) and seemingly confirmed over 50 ky (Nishiizumi et al., 1991b) but production rates within and outside this temporal range are not constrained.

This thesis will follow the guidelines for a 'journal article thesis' as outlined by the graduate college of the University of Vermont. Chapter I is a basic overview with an emphasis on the fundamental concepts of cosmic radiation and the governing equations for interpretation of measured cosmogenic isotope abundances. Also, the significance of this project is explicitly stated in Chapter I. Chapter II is a comprehensive literature review in which most of the relative cosmogenic isotope and Laurentide deglaciation literature is discussed. Particular attention is given to isotope production rate studies as

well as studies which document the timing of Laurentide deglaciation from New Jersey. Chapter III is a journal article containing all the methods and results of this study. This article was written to accommodate the format specified by the Geological Society of America Bulletin and will be submitted to that journal for publication. I am the first author on the journal article, wrote the text, and am responsible for all data analysis. The appendices for this thesis include detailed sample site descriptions and photographs as well as the ICP and AMS data.

### **Cosmic rays**

The earth is continuously being bombarded by charged particles most of which are smaller than an atom. These charged particles are known as cosmic rays and it is the effects of these cosmic rays on the surface of the earth which effects provide the foundation for this study.

Eighty-five percent of the cosmic rays entering at the top of Earth's atmosphere are protons (Friedlander, 1989). Very few of these protons (primary cosmic rays) reach the surface of Earth. Essentially all primary cosmic ray protons collide with atmospheric nuclei producing atmospheric radionuclides as well as a shower of additional particles (secondary cosmic rays) resulting in what is referred to as a 'nuclear cascade'. These secondary particles have sufficient energy to reach Earth's surface and create, *in-situ*, a variety of nuclides including  $^{10}\text{Be}$  and  $^{26}\text{Al}$  (Fabryka-Martin, 1988). The origin of cosmic rays is still a subject of some debate; however, evidence suggests that there are two major sources: stars within the Milky Way galaxy reaching the explosive supernova stage, and less significantly, a solar source (Friedlander, 1989).

### **Production mechanisms of cosmogenic isotopes**

Commonly measured cosmogenic isotopes ( $^3\text{He}$ ,  $^{10}\text{Be}$ ,  $^{14}\text{C}$ ,  $^{21}\text{Ne}$ ,  $^{26}\text{Al}$ , and  $^{36}\text{Cl}$ ) are created in-situ, by several different mechanisms, when cosmic rays interact with

target nuclei in rock and soil. The four main pathways for isotope production are spallation, muon capture, neutron activation, and alpha-particle interaction (Fabryka-Martin, 1988), of which the first two are the most relevant production pathways with respect to this study.

Spallation, which is the primary production pathway of cosmogenic  $^{10}\text{Be}$  and  $^{26}\text{Al}$ , occurs when a target nucleus is split into several particles as a result of bombardment by a high energy neutron. Spallation reactions are generally negligible at depths more than a few meters below the surface.  $^{10}\text{Be}$  is produced as a result of the spallation of O, Mg, Si, and Fe, and  $^{26}\text{Al}$  is produced by the spallation of Si, Al, and Fe (Fabryka-Martin, 1988). The most common reactions are  $^{16}\text{O}(n,3n4p)^{10}\text{Be}$  and  $^{28}\text{Si}(n,n2p)^{26}\text{Al}$ .

Muon capture, a less significant isotope-producing interaction, involves charged particles with a low mass. Muons, which are secondary particles caused by interaction of primary cosmic rays with atmosphere and soil, are captured by a proton in the target nucleus. The production rates for muon capture are lower than spallation near the surface but muons penetrate to greater depths than high-energy neutrons. An example of an isotope created by muon capture would be  $^{26}\text{Al}$  from  $^{28}\text{Si}$ .

### Factors affecting production rates

There are many factors which have a direct influence on the apparent production rates of cosmogenic isotopes. These influences, which include isotope half-life, depth of sample below Earth's surface, intensity variations in the dipole field, pre-existing cosmogenic isotopes, and the latitude and elevation of the sample are best illustrated by interpretive equations. These equations are described and their variables defined in the following paragraphs.

Production rates of cosmogenic isotopes can be calculated using one of two equations. If the exposure age of the outcrop is less than the half-life of the radiogenic



isotope by at least an order of magnitude, or if the cosmogenic isotope is stable, then the production rate ( $P$ , atoms  $\text{g}^{-1} \text{yr}^{-1}$ ) is a function of the number of atoms of the cosmogenic isotope ( $N$ , atoms  $\text{g}^{-1}$ ) and the exposure age ( $t$ , yrs):

$$P = N / t \quad (\text{Eq. 1})$$

If the isotope is unstable and the exposure age of the outcrop approaches its half-life, then the production rate is a function of the decay constant ( $\lambda$ ,  $\text{yr}^{-1}$ ) as well as the exposure age ( $t$ , yrs), after a correction has been made for a pre-existing inventory of the isotope ( $B$ ):

$$N = \frac{P}{\lambda} (1 - e^{-\lambda t}) + B e^{-\lambda t} \quad (\text{Eq. 2})$$

Although the flux of galactic or primary cosmic rays is generally assumed to be constant with respect to time, there are several factors that affect the production rates of cosmogenic isotopes at Earth's surface. The three primary variables are the intensity of Earth's magnetic field, the sample elevation and latitude, and the depth of the sample below the surface.

As previously mentioned, most primary cosmic rays are positively charged particles. As such, they will be affected by magnetic fields in a manner which can be described by the following equation :

$$F = qv \times B \quad (\text{Eq. 3})$$

where the magnitude of the force on the particle ( $F$ ) is the charge ( $q$ ) times the vector product of the velocity ( $v$ ) and the magnetic field strength ( $B$ ). The magnitude of this force is expressed as



$$F = |q|vB \sin \theta \quad (\text{Eq. 4})$$

where  $\theta$  is the angle between  $v$  and  $B$ . The force acting on the charged particle will be greatest when  $\theta$  equals 90 degrees, or when the velocity vector of the particle is perpendicular to the magnetic field. The magnetic field of the earth can be modeled by analogy to the magnetic field of a bar magnet; field lines are parallel to the surface of the earth at the equator and are perpendicular to the surface of the earth at the poles (Figure 1.1). As a result, production rates of cosmogenic isotopes are less at the equator than at the poles, due to the increased angle of incidence ( $\theta$ ) between the primary cosmic rays and the field lines. There is also an abundance of evidence which suggests that the strength of Earth's magnetic field has not remained constant over the history of the earth (Bard et al., 1990; Mazaud et al., 1991; Meynadier et al., 1992), thereby making magnetic field intensity a two-dimensional variable which varies over time and space.

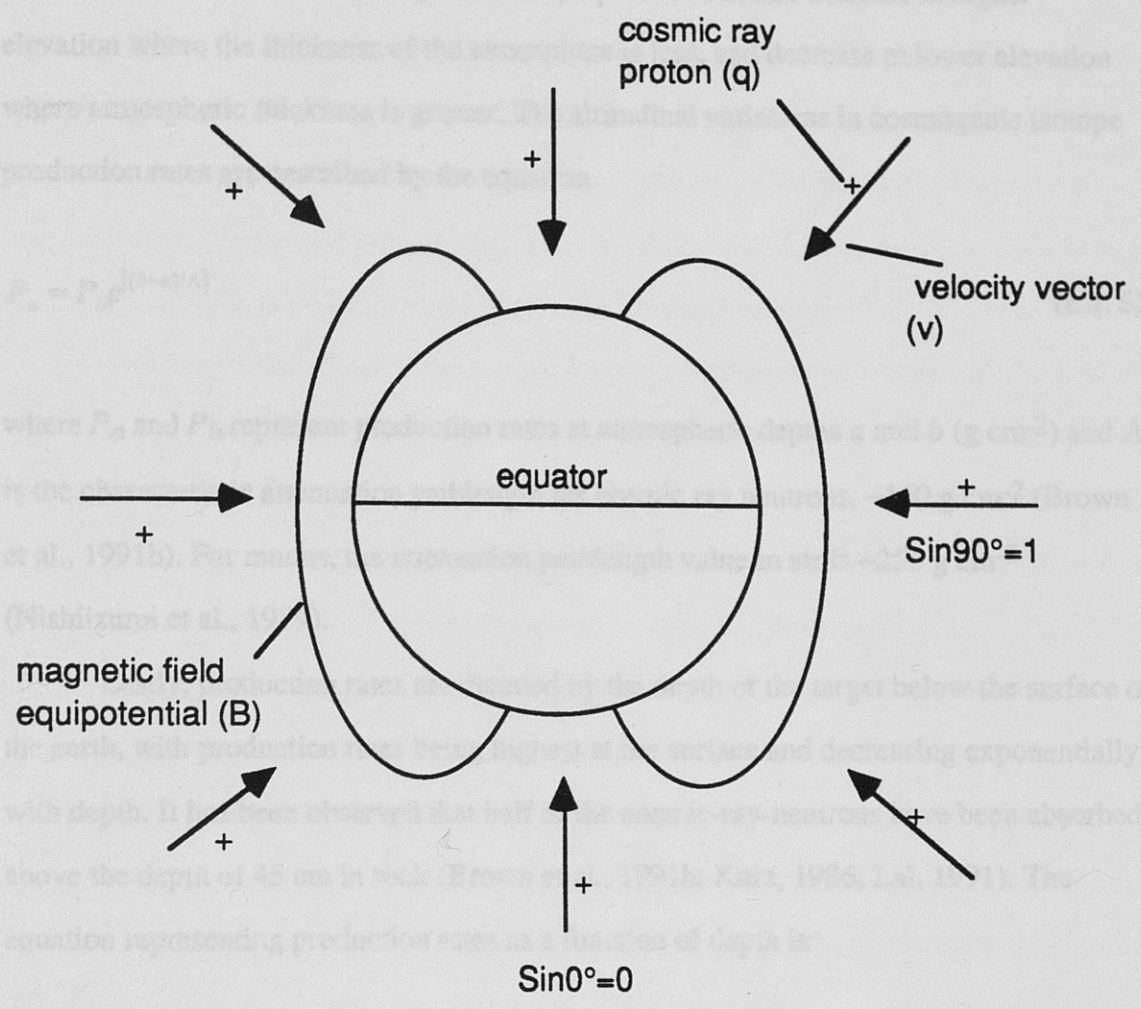


**Figure 1.1.** Earth's magnetic field. This figure shows Earth's magnetic field and its latitudinal effect on the cosmic ray flux. It is assumed that cosmic rays bombard Earth isotropically and that magnetic north equals geographic north over time. Charged particles are depleted in energy by magnetic fields according to  $F=qvB\sin\theta$  where  $\theta$  is the angle between the charged particle vector and the magnetic field line.

Cosmic rays also interact with atmospheric gases. Due to the attenuation of the cosmic ray flux by atmospheric gases, isotope production rates increase at higher elevation where the thickness of the atmosphere is less, and decrease at lower elevation where atmospheric thickness is greater. The altitudinal variations in cosmogenic isotope production rates are described by the equation

$$P_a = P_b e^{[(b-a)/\Lambda]} \quad (\text{Eq. 5})$$

where  $P_a$  and  $P_b$  represent production rates at atmospheric depths  $a$  and  $b$  ( $\text{g cm}^{-2}$ ) and  $\Lambda$  is the characteristic attenuation pathlength for cosmic ray neutrons,  $\sim 160 \text{ g cm}^{-2}$  (Brown et al., 1991b). For muons, the attenuation pathlength value in air is  $\sim 250 \text{ g cm}^{-2}$  (Nishiizumi et al., 1989).

Lastly, production rates are dictated by the depth of the target below the surface of the earth, with production rates being highest at the surface and decreasing exponentially with depth. It has been observed that half of the cosmic-ray-neutrons have been absorbed above the depth of 45 cm in rock (Brown et al., 1991b; Kurz, 1986; Lal, 1991). The equation representing production rates as a function of depth is

$$P_x = P_o e^{-(x\rho/\Lambda)} \quad (\text{Eq. 6})$$

where  $P_x$  is the production rate ( $\text{atoms g}^{-1} \text{ yr}^{-1}$ ) at depth  $x$  (cm),  $P_o$  is the surface production rate,  $x$  is the depth (cm),  $\rho$  is the density of rock ( $\text{g cm}^{-3}$ ), and  $\Lambda$  is the characteristic attenuation length for cosmic ray neutrons ( $150\text{-}170 \text{ g cm}^{-2}$ ).

### Significance of research

Existing cosmogenic exposure age and erosion rate calculations are based on the assumption that isotope production rates are temporally constant or are well represented

Cosmic rays also interact with atmospheric gases. Due to the attenuation of the cosmic ray flux by atmospheric gases, isotope production rates increase at higher elevation where the thickness of the atmosphere is less, and decrease at lower elevation where atmospheric thickness is greater. The altitudinal variations in cosmogenic isotope production rates are described by the equation

$$P_a = P_b e^{[(b-a)/\Lambda]} \quad (\text{Eq. 5})$$

where  $P_a$  and  $P_b$  represent production rates at atmospheric depths  $a$  and  $b$  ( $\text{g cm}^{-2}$ ) and  $\Lambda$  is the characteristic attenuation pathlength for cosmic ray neutrons,  $\sim 160 \text{ g cm}^{-2}$  (Brown et al., 1991b). For muons, the attenuation pathlength value in air is  $\sim 250 \text{ g cm}^{-2}$  (Nishiizumi et al., 1989).

Lastly, production rates are dictated by the depth of the target below the surface of the earth, with production rates being highest at the surface and decreasing exponentially with depth. It has been observed that half of the cosmic-ray-neutrons have been absorbed above the depth of 45 cm in rock (Brown et al., 1991b; Kurz, 1986; Lal, 1991). The equation representing production rates as a function of depth is

$$P_x = P_o e^{-(x\rho/\Lambda)} \quad (\text{Eq. 6})$$

where  $P_x$  is the production rate ( $\text{atoms g}^{-1} \text{ yr}^{-1}$ ) at depth  $x$  (cm),  $P_o$  is the surface production rate,  $x$  is the depth (cm),  $\rho$  is the density of rock ( $\text{g cm}^{-3}$ ), and  $\Lambda$  is the characteristic attenuation length for cosmic ray neutrons ( $150\text{-}170 \text{ g cm}^{-2}$ ).

### Significance of research

Existing cosmogenic exposure age and erosion rate calculations are based on the assumption that isotope production rates are temporally constant or are well represented

by average, constant values. However, numerous studies have shown that the strength of Earth's magnetic field and thus the production rate of cosmogenic nuclides have fluctuated over the past 20 ky (Bard et al., 1990; Kurz et al., 1990; Mazaud et al., 1991; Meynadier et al., 1992; Tric et al., 1992). Because accelerator mass spectrometer measurements can now be made with relatively high precision (several percent,  $1\sigma$ ), uncertainty in the rate of isotope production can easily become the dominant error term in any model used to interpret isotope abundances as exposure ages or erosion rates.

$^{26}\text{Al}$  and  $^{10}\text{Be}$  are two widely used cosmogenic nuclides for which production rates have been estimated using samples collected from glacially eroded bedrock surfaces. The exposure ages of these bedrock surfaces were estimated to be 11 cal ky based on two bog-bottom radiocarbon dates (Nishiizumi et al., 1989); however, new data suggest that the bedrock surfaces sampled were exposed at least 13 ky (Clark et al., 1995). While it seems reassuring that exposure ages calculated with these production rates appear consistent with several other production rate estimates (50 Ky, Nishiizumi et al., 1991b) and approaching saturation ( $>2$  My, Nishiizumi et al., 1991a), geophysical data suggest that exposure ages calculated for samples younger or older than the calibration age (11 ky) should be in error (Clark et al., 1995). Such discrepancy is suggested by the observation that on average, Earth's magnetic field was weaker and thus cosmic ray fluxes were higher over the past 30 ky than over the past 11 ky. Conversely, average cosmic ray fluxes and isotope production rates during periods of the Holocene have been significantly lower than the average value taken over the past 11 ky. Production rate data for cosmogenic  $^3\text{He}$ , produced in-situ, are consistent with changing field strength and isotope production rates (Kurz et al., 1990).

Despite increasing use of  $^{26}\text{Al}$  and  $^{10}\text{Be}$  for high-precision studies of climate change and glaciation in the Late Pleistocene (e.g. Evenson and Gosse, 1993; Nishiizumi et al., 1993; Gosse et al., 1995), there exists no direct calibration of  $^{26}\text{Al}$  and  $^{10}\text{Be}$  production rates over the 20 ky time frame. This study empirically determines the



production rates of  $^{10}\text{Be}$  and  $^{26}\text{Al}$  from morainal boulders and outcrops having a calibrated  $^{14}\text{C}$  age of approximately 21.5 ky based on the dating of associated organic material. The boulders and outcrops have been sampled from the terminal moraine of the Laurentide ice sheet in northwestern New Jersey where the Laurentide ice sheet's Hudson-Champlain Lobe reached its terminus. This site was chosen because the exposure age of the terminal moraine is relatively well-constrained and because the glacial erratics and outcrops are predominantly resistant quartzite and gneiss. This study addresses a fundamental uncertainty in the application of cosmogenic isotopes to geologic studies and tells us more about the behavior of Earth's magnetic field in the geologic past.

## Chapter II

### COMPREHENSIVE LITERATURE REVIEW

#### Introduction

The comprehensive literature review encompasses several topics relevant to this study. Perhaps the single most important factor in determining the production rates of cosmogenic isotopes is a well-constrained exposure age for the samples. Therefore, the first section of this chapter documents much of the previous work done on the terminal moraine of the Laurentide ice sheet. The primary focus of the selected Laurentide literature review is the timing of deglaciation, and therefore the exposure age of samples taken from the terminal moraine. The remainder of this chapter focuses on studies related to *in-situ* produced cosmogenic isotopes. Specifically, I concentrate on production rate studies for  $^{10}\text{Be}$  and  $^{26}\text{Al}$ , studies related to magnetic field fluctuation, and cosmogenic isotope studies done on glacial moraines.

I have selected the terminal moraine of the Laurentide ice sheet in northwestern New Jersey (Figure 3.1) as a calibration site for *in-situ* produced cosmogenic isotope production rates because it meets four specific criteria: 1) Samples have well-constrained exposure ages (Table 3.1); 2) the effect of erosion and till cover are negligible; 3) rocks have a significant amount of physically separable quartz and 4) the geomorphic setting is well understood. Below, I document the published ice-sheet recession ages of several authors, all of which are in radiocarbon years ( $^{14}\text{C}$  ky) unless specified as calibrated radiocarbon ages (cal  $^{14}\text{C}$ ).

#### Advance of Laurentide Ice Sheet

The extent, mode, and timing of the Late Wisconsinan glaciation in the New Jersey Highlands were studied by Stanford (1993). Based on mapping of surficial features, such as striations and drumlins, and well-log and auger-hole data, Stanford mapped the bedrock topography and the subsurface stratigraphy. From the surficial

evidence gathered, Stanford concluded that the ice moved south across the New Jersey highlands from the Wallkill-Kittatinny lowlands to abutt a southwesterly flowing lobe from the Newark basin at a sutured border. Stanford also determined that nearly 40% of the area of the New Jersey Highlands contains glacially sculpted bedrock with a thin, patchy, discontinuous cover of surficial sediments, and is therefore an ideal site for exposure age sampling. Stanford concludes, based on a series of radiocarbon dates which I discuss below, that the ice sheet reached the terminal position before 20  $^{14}\text{C}$  ky and had receded from the terminal moraine prior to 18  $^{14}\text{C}$  ky .

### Age Control

Approximately 21-23 cal  $^{14}\text{C}$  ky, the Laurentide ice sheet began to retreat from the New Jersey Highlands depositing, among various lithologies, quartzite and gneissic glacial erratics as well as leaving polished, striated, and glacially molded bedrock. The age of the terminal moraine and glacial retreat, which has been determined by several independent investigators (Table 3.1), relies on bog and lake sediment pollen assemblages, bog-bottom radiocarbon ages, as well as morphological sequence mapping and varve chronologies to determine the timing of maximum ice extent and subsequent deglaciation.

Cotter (1984), on the basis of pollen data and several radiocarbon dates, determined that deglaciation of the Ontario Lobe of the Laurentide ice sheet in western New Jersey began prior to  $18,390 \pm 200$   $^{14}\text{C}$  ka. Cotter's sample location, Francis Lake, is on the easternmost margin of the Ontario Lobe, adjacent to the Hudson-Champlain Lobe and is located at a latitude similar to the latitude of the sample sites chosen for this calibration. Due to the similarity of latitudes and the fact that this site is further north than the majority of my sample locations, Cotter's calibrated  $^{14}\text{C}$  ages are assumed to be a minimum limiting exposure age for this production rate calibration. Cotter's age estimates were based on radiocarbon dates from basal lacustrine sediments which were



correlated with tundra pollen assemblages in sediments from the same basal sedimentary horizon. The presence of the tundra pollen assemblages in the basal layer leads Cotter to the conclusion that the basal sediments were deposited shortly after deglaciation, and that deglaciation occurred prior to 18,500  $^{14}\text{C}$  years B.P. (p. 1, Cotter, 1984), which corresponds to approximately 21,500 calibrated  $^{14}\text{C}$  years (Stuiver et al., 1991).

In a similar study, Harmon (1968) collected sediment from Budd Lake just south of the terminal moraine in north-central New Jersey. Harmon obtained two radiocarbon dates, at 27 and 37 feet (8.23 m and 11.28 m), as well as pollen data from this 60 foot (18.29 m) core. The  $^{14}\text{C}$  age which corresponds with the 37 foot horizon,  $22,890 \pm 720$   $^{14}\text{C}$  years, is rejected by Harmon as being too old based on extrapolation from pollen data to the glacial chronology. She suggests making a maximum error correction and reducing the  $^{14}\text{C}$  age by 3000 years, thus yielding a corrected  $^{14}\text{C}$  age of 19,890  $^{14}\text{C}$  years. Despite the fact that the  $^{14}\text{C}$  age does not agree with the pollen data extrapolation, Harmon's correction is qualitative and arbitrary and appears to be 'adjusting' the data to fit her independent pollen data.

Evenson et al. (1983) used radiocarbon dates, stratigraphic relationships, palynological evidence from the basal tundra pollen zone to argue that ice began to retreat from the terminal moraine in New Jersey prior to 18  $^{14}\text{C}$  ky BP. Matsch (1987) also concluded from an overview of regional data that the growth of the Laurentide ice sheet ceased by 20  $^{14}\text{C}$  ka and that parts of the southern margin were retreating by 18  $^{14}\text{C}$  ka. Sirkin (1977) and Connally and Sirkin (1973), estimating deposition rates for sediments below radiocarbon dated organic horizons, suggested that recession from northern New Jersey began about 18  $^{14}\text{C}$  ky BP. In regional summaries, Fullerton (1986) and Stone and Borns (1986) assessed the regional array of limiting  $^{14}\text{C}$  ages of preglacial materials in drift and postglacial sediments and supported the estimate of deglaciation of western New Jersey prior to 18.5  $^{14}\text{C}$  ky BP. Oldale and Stone (1987) further emphasized that the ice

sheet in eastern New Jersey reached its terminal position 21-20  $^{14}\text{C}$  ky BP based on  $^{14}\text{C}$  dates on wood, bone, horn, peat, shells and whole sediment samples.

The quoted dates are in radiocarbon years, uncorrected for the change in  $^{14}\text{C}$  production rates. Corrected ages would be several thousand years older. In summary, evidence suggests that the actual exposure age of the morainal boulders and outcrop is approximately 21,500 calibrated  $^{14}\text{C}$  or sidereal years.

### **Production rate studies for $^{10}\text{Be}$ and $^{26}\text{Al}$**

Production rates of cosmogenic  $^{10}\text{Be}$  and  $^{26}\text{Al}$  were calculated over the 11 ky time period by Nishiizumi et al. (1989) and seemingly confirmed by an independent study done in Antarctica (Nishiizumi et al., 1991a) as well as an independent 50 ky calibration (Nishiizumi et al., 1991b). The production rates of  $^{10}\text{Be}$  and  $^{26}\text{Al}$  at sea level and  $> 50^\circ$  latitude were determined by Nishiizumi et al. (1989) to be  $6.03 \pm 0.3$  atoms  $\text{g}^{-1} \text{yr}^{-1}$  and  $36.8 \pm 2.7$  atoms  $\text{g}^{-1} \text{yr}^{-1}$ , respectively, assuming that the 11 ky exposure age is correct. The uncertainties in the production rates reflect only the scatter associated with the measurement of different samples, not the uncertainty associated with the calibrated age or magnetic field fluctuations.

The 11 ky calibration was performed on glacially polished granitic outcrops of Tioga age in the Sierra Nevada, California (Nishiizumi et al., 1989). The glacially polished surfaces used by Nishiizumi et al. (1989) were assumed to date from recession of Tioga glaciers, approximately 11 ka, and the glacial polish provided evidence that surface erosion had been negligible since initial exposure. The greatest uncertainty associated with this calibration is the uncertainty associated with the assumed exposure age of the polished surfaces. Nishiizumi et al.'s age estimates, which have recently been called into question (Clark et al., 1995; Larsen et al., 1995) and upon which the accuracy of the production rates rest, are based wholly on two bog-bottom radiocarbon dates.

Uncertainties in absolute production rates were calculated for possible fluctuations in the

earth's magnetic field, but were not compounded over time; uncertainties arising from errors in absolute exposure age ( $\pm 10\%$ ) were not included. The dismissal of these two corrections could potentially result in as much as a 18% error in absolute production rates; however, most studies which have utilized Nishiizumi et al.'s (1989) production rates have not propagated any uncertainty in the production rates.

The empirically derived production rates have apparently been verified by two studies, one on Antarctic rocks with exposure ages of  $>2$  my (Nishiizumi et al., 1991a), and the other on rocks with exposure ages of about 50 ky (Nishiizumi et al., 1991b). The latter, an independent study utilizing in situ  $^{10}\text{Be}$  and  $^{26}\text{Al}$ , constrained exposure ages of dolomitic ejecta blocks at Meteor Crater, Arizona (Nishiizumi et al., 1991b), thereby dating the cratering event. The maximum determined exposure age,  $49,200 \pm 1700$  years, was similar to that obtained by thermoluminescence,  $49,000 \pm 3000$  years, which was assumed to be correct, and the average of 4 cosmogenic  $^{36}\text{Cl}$  dates,  $49,200 \pm 700$  years. If the thermoluminescence age for the cratering event is correct, the  $^{10}\text{Be}$  and  $^{26}\text{Al}$  production rates averaged over 50,000 years appears to be similar to the production rate averaged over 11,000 years.

Although it appears reassuring that these independent production rate calibrations are in agreement, recent radiocarbon evidence, as well as modelling of dipole-field induced cosmic-ray flux variations would suggest that the 11 ky calibration is in error (Clark et al., 1995). A series of minimum limiting radiocarbon dates from basal lake sediments representing the end of Tioga glaciation in the Sierra Nevada suggest that the minimum exposure age for Nishiizumi's 11 cal ky calibration is no less than 13.1 cal ky BP and that the sites may have been exposed as early as 19 cal ky BP (Clark et al., 1995). The new Sierra Nevada radiocarbon evidence suggest that Nishiizumi's 11 ky production rates are probably 15-20% too high; this conclusion is confirmed by the Laurentide 21.5 ky calibration presented in this thesis.

## Magnetic field fluctuation studies

There have been two studies which directly and distinctly correlate changing isotope production rates with the changing intensity of Earth's magnetic field. The first study determined cosmogenic  $^3\text{He}$  production rates in young Hawaiian lava flows (Kurz et al., 1990); the second focused on changes in the production of atmospheric  $^{14}\text{C}$  over the last 30 ky (Bard et al., 1990).

Kurz et al. (1990) measured cosmogenic  $^3\text{He}$  to calculate production rates in young Hawaiian lava flows. Despite the absence of soil cover and negligible erosion rates, as suggested by flow morphology, they found considerable variation in production rates with respect to time. For example, from present to 2000 years ago they determined an average  $^3\text{He}$  production rate of  $125 \pm 30$  atoms  $\text{g}^{-1} \text{yr}^{-1}$ . The  $^3\text{He}$  production rate was  $55 \pm 15$  atoms  $\text{g}^{-1} \text{yr}^{-1}$  from 2,000 to 7,000 years BP, and  $127 \pm 19$  atoms  $\text{g}^{-1} \text{yr}^{-1}$  from 7,000 to 10,000 years BP. The minimum values for the 2,000 to 7,000 year time period apparently corresponds to a maximum in the earth's magnetic dipole field strength, indicated by the archaeomagnetic measurements compiled by McElhinny and Senanayake (1982).

Observations by Bard et al. (1990) also established a link between variations in cosmogenically produced atmospheric  $^{14}\text{C}$  and temporal intensity variations in Earth's magnetic field. They compared U-Th ages with  $^{14}\text{C}$  ages of Barbados corals over the last 30,000 years and found the  $^{14}\text{C}$  ages before 9000 years ago were systematically younger than the U-Th ages, indicating increased atmospheric concentration and presumably increased production rates of atmospheric  $^{14}\text{C}$  over that time period. The U-Th ages, which are not influenced by the cosmic ray flux, were determined to be accurate as they were in accord with a dendrochronological  $^{14}\text{C}$  calibration over the first 10,000 years of the record. Ultimately, the authors concluded that the discrepancy between U/Th ages and  $^{14}\text{C}$  ages are the result of a time-variant magnetic field and the resulting variations in  $^{14}\text{C}$  production.



## Cosmogenic isotope studies on moraines

Several studies have used cosmogenic isotopes to better understand glacial chronologies and relative ages of glacial moraines. Cosmogenic  $^{10}\text{Be}$ ,  $^{26}\text{Al}$ , and  $^3\text{He}$  abundances in bedrock and boulder surfaces have been used to better constrain glacial chronologies by surface exposure dating of morainal deposits in Antarctica, Wyoming, and the Sierra Nevada Mountains, California.

Brook et al. (1993) measured  $^3\text{He}$  and  $^{10}\text{Be}$  abundances in samples from quartz sandstone boulders on glacial moraines in Antarctica. In order to provide time constraint for a series of moraines, as well as to get a better understanding of the factors affecting  $^3\text{He}$  abundances, the investigators measured  $^3\text{He}$  and  $^{10}\text{Be}$  abundances for the top surfaces of sandstone erratics. Brook et al. (1993) collected 37 samples, 21 of which provided  $^{10}\text{Be}$  exposure ages. They found that there was a broad age distribution within a single moraine;  $^3\text{He}$ , 74-192 ky and  $^{10}\text{Be}$ , 43-370 ky. The authors conclude that this variation was most likely due to previous exposure to cosmic rays, varying erosional histories, a history of soil cover, possible post-depositional movement, and lastly, radiogenic production and diffusive loss of  $^3\text{He}$ . Although their data show considerable variation for exposure ages within single moraines, the exposure ages still provide broad chronological constraints for the series of moraines.

The samples were taken from horizontal (dip angle  $< 10^\circ$ - $15^\circ$ ), up-facing boulder surfaces located, when possible, on the crests of moraines. The authors indicate that the effects of shielding were negligible, although they do not document the horizon geometry. They also make no corrections for boulder geometry and make no mention of the position of the sample with respect to the edges of the boulder. Corrections were made for sample thickness, and radiogenic production of  $^3\text{He}$ . They assume that mass lost due to erosion is relatively minor and, therefore, make no correction for erosion on the  $^{10}\text{Be}$  ages.

In a similar study, Phillips et al. (1990) measured  $^{36}\text{Cl}$  abundances from boulders on the crests of moraines in order to better constrain the glacial chronology at Bloody Canyon in the eastern Sierra Nevada. The need for this study, as expressed by Phillips et al. (1990) was based on the large uncertainties associated with limiting age techniques such as  $^{40}\text{Ar}/^{39}\text{Ar}$  dates on inter-morainal lava flows. Bloody Canyon was chosen as the sample site based on the well-preserved moraine morphology, the easily recognized relative ages of the moraines, as well as the fact that the field area has been studied by numerous investigators although with somewhat ambiguous results.

Thirty one samples were taken from large erratics (0.5-5.4 m) located on the crests of 5 different moraines. The size and geomorphic setting of the erratics ensured that the erratics had not rolled to their present location as well as reduced the chance of the erratic having been exposed by erosion of the moraine crest. The upper surfaces of the boulders were also assumed to be above the average snow depth. The  $^{36}\text{Cl}$  exposure ages of Phillips et al. (1990) show tight grouping for the younger moraines with the  $^{36}\text{Cl}$  exposure ages becoming more scattered on the older moraines. The scatter in their exposure ages is explained by random and systematic errors such as analytical error, variable erosion of sampled surfaces, snow cover, till cover, previous cosmic ray exposure, and preferential leaching of  $^{36}\text{Cl}$ . Except for previous exposure, all other systematic errors would generate younger exposure ages. When mean moraine ages were calculated, samples with anomalously young exposure ages were not calculated into the mean.

In a more recent study, Brook et al. (1995) used cosmogenic  $^3\text{He}$ ,  $^{10}\text{Be}$ , and  $^{26}\text{Al}$  to constrain better the absolute and relative glacial chronology in McMurdo Sound, Antarctica. This site was chosen based on the need for a better absolute glacial chronology in Antarctica as well as well as the abundance of well-preserved glacial drift sequences. Previous numerical age estimates relied on deltaic sediment  $^{14}\text{C}$  dates which

do not constrain the chronology of the advancing ice sheet, nor of glaciations beyond the  $^{14}\text{C}$  time scale.

Brook et al. (1995) collected 26 samples from olivene-bearing basalts, quartz-rich granites, and unspecified metamorphic rocks and sandstones. Their samples were collected from the horizontal, up-facing surfaces of large clasts located on moraine crests. The production rates of Nishiizumi et al. (1989) and the latitude/altitude scaling factors of Lal (1991) were used to calculate the  $^{10}\text{Be}$  and  $^{26}\text{Al}$  exposure ages. The uncertainties associated with the reported isotope concentrations are reported as a function of accelerator counting statistics and variation in AMS stability. Brook et al.'s (1995) exposure age calculations rely on the assumption that erosion rates are negligible (Brown et al., 1991a; Nishiizumi et al., 1991a). This assumption is based on previous erosion rate estimates for Antarctica.

**Chapter 3.**  
**GSA BULLETIN JOURNAL ARTICLE**



FOR SUBMISSION TO GEOLOGICAL SOCIETY OF AMERICA BULLETIN

*In-situ* production rates of cosmogenic  $^{10}\text{Be}$  and  $^{26}\text{Al}$   
over the past 21,500 years determined  
from the terminal moraine of the Laurentide ice sheet,  
north-central New Jersey

Patrick L. Larsen and Paul R. Bierman

Department of Geology

University of Vermont

Burlington, VT 05405

plarsen@moose.uvm.edu

pbierman@moose.uvm.edu

(802) 656-3398

Byron Stone

United States Geological Survey

450 Main, Federal Bldg.

Hartford, CT 06103

Marc Caffee

Lawrence Livermore National Laboratory

Livermore, CA 94550

## ABSTRACT

New  $^{10}\text{Be}$  and  $^{26}\text{Al}$  measurements from the Laurentide terminal moraine provide the first production rate estimates for *in-situ* cosmogenic  $^{10}\text{Be}$  and  $^{26}\text{Al}$  over the past 21.5 cal  $^{14}\text{C}$  ky. Sixteen samples of quartzite and gneiss were collected from striated and/or glacially molded outcrops and large glacial erratics on or just behind the terminal moraine of the Laurentide ice sheet in north-central New Jersey. The recession of the Laurentide ice sheet, and thus the exposure age for our samples, is estimated to be  $\sim 21.5$  ky sidereal years on the basis of numerous limiting  $^{14}\text{C}$  ages. Average concentrations of  $1.11 \pm 0.03 \times 10^5$  (1sem,  $n=12$ ) atoms  $\text{g}^{-1}$   $\text{SiO}_2$  for  $^{10}\text{Be}$  and  $6.47 \pm 0.22 \times 10^5$  (1sem,  $n=14$ ) atoms  $\text{g}^{-1}$   $\text{SiO}_2$  for  $^{26}\text{Al}$  can be used to calculate integrated sea-level, high latitude production rates and associated standard errors of the mean of  $5.17 \pm 0.15$  and  $30.40 \pm 1.01$  atoms  $\text{g}^{-1}$  year $^{-1}$  for  $^{10}\text{Be}$  and  $^{26}\text{Al}$ , respectively. The isotope abundances show no significant variation between boulder and outcrop sample locations and quartzite and gneiss sample lithologies implying that the effects of erosion and till cover are negligible. Samples of different lithology and type were assumed to be from a single population based on the results of a two-sample *t* test for the comparison of the means of two populations. The integrated production rates calculated over the past 21.5 ky period are about 18% lower than previously determined integrated production rates over the 11 ky (Nishiizumi et al., 1989) and 50 ky (Nishiizumi et al., 1991b) year time frames. We attribute this difference to an underestimated exposure age for the 11 ky calibration. The  $^{10}\text{Be}$  and  $^{26}\text{Al}$  production rates presented in this paper are the first to be determined for the 21.5 ky time frame. This study also provides the first direct comparison of cosmogenic isotope abundances in boulder and outcrop surfaces as well as quartzite and gneiss rock types.

## INTRODUCTION

In-situ produced cosmogenic isotopes are finding a wide range of applications in the earth sciences and are becoming a valuable and ubiquitous tool for geomorphic studies (Bierman, 1994; Cerling and Craig, 1994). Cosmogenic isotopes have been used to calculate exposure ages of glacial moraines (Brown et al., 1991a; Phillips et al., 1990; Brook et al., 1995; Brook et al., 1993; Gosse et al., 1995), and rates of weathering (Sarda et al., 1993; Nishiizumi et al., 1986; Nishiizumi et al., 1991a; Nishiizumi et al., 1993). The burgeoning popularity of in-situ produced cosmogenic isotopes is primarily due to increasing analytical capabilities, a unique time frame over which cosmogenic dates and erosion rates are potentially useful, and the ability for these isotope systems to provide ages where organic material is absent.

Recent advances in the detection capabilities for cosmogenic isotopes, now make it possible to measure ratios for the isotope pairs  $^{26}\text{Al}/^{27}\text{Al}$  and  $^{10}\text{Be}/^9\text{Be}$  as low as several parts in  $10^{-15}$  (Elmore and Phillips, 1987; Finkle and Suter, 1993). As a result, the accuracy and precision of model cosmogenic ages and erosion rates for many samples is now limited by our knowledge of production rates and their variability over time and space. Production rates for  $^{26}\text{Al}$  and  $^{10}\text{Be}$  have been estimated for exposures integrated by rock surfaces since the Late Pleistocene (11 cal ky, Nishiizumi et al., 1989) and seemingly confirmed over the 50 ky thermoluminescence time frame (Nishiizumi et al., 1991b). However, geophysical data suggest that the use of integrated production rates will lead to errors in exposure age calculations and new radiocarbon ages suggest that the 11 ky calibration sites were probably exposed >13 ka (Clark et al, 1995).

Despite increasing use of  $^{26}\text{Al}$  and  $^{10}\text{Be}$  for high precision studies of climate change and glaciation in the Late Pleistocene e.g. (Evenson et al., 1993; Nishiizumi et al., 1993; Gosse et al., 1995), there exists no direct calibration of  $^{26}\text{Al}$  and  $^{10}\text{Be}$  production rates over the 20 ky time frame. This study empirically determines the production rates

of  $^{10}\text{Be}$  and  $^{26}\text{Al}$  from morainal boulders and outcrops having a calibrated  $^{14}\text{C}$  age of approximately 21.5 ky based on the dating of associated organic material. The boulders and outcrops have been sampled from the terminal moraine of the Laurentide ice sheet in northwestern New Jersey (Figure 3.1) where the Laurentide's Hudson-Champlain Lobe reached its terminus. This site was chosen based on the relatively well-constrained exposure age of the terminal moraine as well as the composition of the glacial erratics and outcrops, predominantly quartzite and gneiss. The data presented in this paper provide the first cosmogenic  $^{10}\text{Be}$  and  $^{26}\text{Al}$  production rate estimates over the 21,500 sidereal year time frame. In addition, our data provide a direct comparison between isotope abundance in boulder and outcrop sample sites with similar exposure ages, as well as a direct comparison between isotope abundances in different rock types, quartzite and gneiss. This study is the first to report cosmogenic isotope data from the Laurentide terminal moraine and addresses the accuracy of production rate estimates, a fundamental uncertainty in the application of cosmogenic isotopes to geologic studies.

## PREVIOUS RESEARCH

Existing cosmogenic exposure age and erosion rate calculations are based on the assumption that isotope production rates are temporally constant or are well represented by average values. However, numerous studies have shown that the strength of Earth's magnetic field and thus the production rate of cosmogenic nuclides have fluctuated over the past 140 ky (Bard et al., 1990; Kurz et al., 1990; Mazaud et al., 1991; Meynadier et al., 1992; Tric et al., 1992), particularly at low latitudes. Because accelerator mass spectrometer measurements can now be made with relatively high precision (several percent,  $1\sigma$ ), uncertainty in the rate of isotope production can easily become the dominant error term in any model used to interpret isotope abundances as exposure ages or erosion rates.



## Production rates of $^{10}\text{Be}$ and $^{26}\text{Al}$

Production rates for  $^{10}\text{Be}$  and  $^{26}\text{Al}$  have been calibrated empirically by measuring isotope abundances in samples collected from dated surfaces. Production rates of cosmogenic  $^{10}\text{Be}$  and  $^{26}\text{Al}$  were calculated over the 11 cal ky time period by Nishiizumi et al. (1989), the most recent ~2 My period in a study in Antarctica (Nishiizumi et al., 1991a) as well as an independent 50 ky calibration (Nishiizumi et al., 1991b). The production rates at sea level and  $> 50^\circ$  latitude for  $^{10}\text{Be}$  and  $^{26}\text{Al}$  were determined to be  $6.03 \pm 0.3$  atoms  $\text{g}^{-1} \text{y}^{-1}$  and  $36.8 \pm 2.7$  atoms  $\text{g}^{-1} \text{y}^{-1}$ , respectively, assuming that the 11 cal ky exposure age of the calibration surface is correct and that muon contribution to isotope production is well understood. The uncertainty term in Nishiizumi et al.'s (1989) production rates reflects only the scatter associated with measurement of different samples, not the uncertainty of the calibrated age.

The 11 cal ky calibration was performed on glacially polished granitic outcrops of Tioga age in the Sierra Nevada, California (Nishiizumi et al., 1989). The glacially polished surfaces sampled by Nishiizumi were assumed to date from recession of Tioga glaciers, assumed to be approximately 11 ka, and the glacial polish provided evidence that surface erosion had been negligible since initial exposure. The greatest uncertainty associated with this calibration is the uncertainty associated with the exposure age of the polished surfaces. Nishiizumi's age estimates, which have recently been called into question (Clark et al., 1995) and upon which the accuracy of the production rates rests, are based wholly on two bog-bottom radiocarbon dates. Nishiizumi et al. (1989) suggested that changes in the intensity of the earth's dipole field could affect their calculated production rates, (a potential decrease of 15%), they also assigned an uncertainty to the absolute exposure age of the samples, ( $\pm 10\%$ ). If these uncertainties were random, the dismissal of these two imprecisions could potentially result in as much as a 18% uncertainty in absolute production rates; however, most studies which have

utilized Nishiizumi et al.'s (1989) production rates have not propagated these uncertainties choosing to calculate errors in model exposure ages and erosion rates using only the imprecision of AMS measurements.

Production rates have apparently been verified by two studies over different time periods, one on Antarctic rocks with exposure ages of  $>2$  My (Nishiizumi et al., 1991a), and the other on rocks with exposure ages of about 50 thermoluminescence ky (Nishiizumi et al., 1991b). The latter, an independent study utilizing in-situ  $^{10}\text{Be}$  and  $^{26}\text{Al}$ , constrained exposure ages of dolomitic ejecta blocks at Meteor Crater, Arizona (Nishiizumi et al., 1991b), thereby dating the cratering event. The maximum  $^{10}\text{Be}/^{26}\text{Al}$  exposure age,  $49,200 \pm 1700$  years, was similar to that obtained by thermoluminescence,  $49,000 \pm 3000$  years, which was assumed to be correct, and was also similar to the mean of several cosmogenic  $^{36}\text{Cl}$  dates,  $49,200 \pm 700$  years. If the thermoluminescence age is correct, the  $^{10}\text{Be}$  and  $^{26}\text{Al}$  production rates averaged over the past 50 TL cal ky appears to be similar to the production rate averaged over the past 11 cal ky.

Although it appears reassuring that these independent production rate calibrations are in agreement, recent radiocarbon evidence, as well as calculations of dipole-field induced flux variations suggest that the 11 cal ky calibration is in error (Clark et al., 1995). A series of minimum limiting radiocarbon dates from basal lake sediments representing the end of Tioga glaciation in the Sierra Nevada suggests that the minimum exposure age for Nishiizumi et al's 11 cal ky calibration is no less than 13.1 cal ky BP and that the calibration sites of Nishiizumi et al. may have been exposed as early as 19 cal ky BP. The new Sierra Nevada radiocarbon evidence suggest that currently accepted 11 cal ky production rates are approximately 15-20% too high; this conclusion is confirmed by the Laurentide 21.5 ky calibration presented in this paper.



## Magnetic field fluctuation and variation in isotope production rates

There have been two studies which directly and distinctly correlate changing isotope production rates with the changing intensity of Earth's magnetic field. The first determined cosmogenic  $^3\text{He}$  production rates in young Hawaiian lava flows (Kurz et al., 1990), and the second documented changes in the production of atmospheric  $^{14}\text{C}$  over the last 30 ky (Bard et al., 1990).

Kurz et al. (1990) used Hawaiian lava flows of various ages to calculate production rates of cosmogenic  $^3\text{He}$ . Despite the absence of soil cover and negligible erosion rates, as suggested by flow morphology, they found considerable variation in apparent integrated  $^3\text{He}$  production rates with respect to time. For example, from present to 2000 years BP Kurz et al. determined a  $^3\text{He}$  production rate of  $125 \pm 30$  atoms  $\text{g}^{-1} \text{y}^{-1}$ . The production rate was  $55 \pm 15$  atoms  $\text{g}^{-1} \text{y}^{-1}$  from 2,000 to 7,000 years BP, and for 7,000 to >10,000 years BP the  $^3\text{He}$  production rate was found to be  $127 \pm 19$  atoms  $\text{g}^{-1} \text{y}^{-1}$ . The apparent production rate minima from 2,000 to 7,000 y BP corresponds to a maximum in the earth's dipole field strength, indicated by the archaeomagnetic measurements (McElhinny and Senanayake, 1982). The variations in  $^3\text{He}$  in-situ production rates should be much less at higher latitudes due to the dampened effect of the dipole field at increasing latitudes.

Measurements by Bard et al. (1990) established a link between variations in cosmogenically produced atmospheric  $^{14}\text{C}$  and temporal intensity variations in Earth's magnetic field. They compared U-Th ages and corresponding  $^{14}\text{C}$  ages of corals with over the last 30,000 years and found that  $^{14}\text{C}$  ages before 9000 years ago were systematically younger than corresponding U-Th ages, indicating increased atmospheric concentration of  $^{14}\text{C}$  and presumably increased production rates of atmospheric  $^{14}\text{C}$ . The U-Th ages, which are not influenced by the cosmic ray flux, were assumed to be accurate as they were in accord with a dendrochronological calibration of  $^{14}\text{C}$  production over the

first 10,000 years of the record. Ultimately, the authors concluded that the discrepancy between U/Th ages and  $^{14}\text{C}$  ages are the result of a time-variant magnetic field.

## **FIELD SITE**

Samples were taken primarily from two distinct geographic regions near the terminal moraine in north-central New Jersey (Figure 3.1, 3.2). Most of our samples were taken from either the Picatinny Military Arsenal, about 3 km north of Dover, New Jersey, or the from the Allamuchy State Forest, approximately 10 km north of Hacketstown, New Jersey. Two samples were taken from a large erratic near Weldon Road at approximately  $41^{\circ}\text{N}$  latitude, further north than the two main sample sites. The following physiographic and geologic descriptions will apply to the two primary geographic regions from which samples were taken.

### **Physiography**

The field area chosen for this study was the terminal moraine zone of the Laurentide ice sheet in the New Jersey Highlands Physiographic Province between  $74^{\circ}30'$  and  $74^{\circ}45'$  west longitude and  $40^{\circ}50'$  and  $41^{\circ}00'$  north geographic latitude (Figure 3.2) ranging in elevation from 250-375 meters above sea level. The average rainfall in northern New Jersey is approximately  $108\text{ cm yr}^{-1}$ , and is apparently evenly distributed throughout the year (Widmer, 1964). The terminal moraine of the Laurentide ice sheet runs latitudinally across the state of New Jersey at approximately  $40\text{-}41^{\circ}\text{N}$  geographic latitude. Historical land use in New Jersey has largely been dictated by climate and soil conditions and it is unlikely that either the Allamuchy State Forest or the hard, quartz-rich conglomeratic ridge within the Picatinny military arsenal have ever been used for agricultural purposes (Widmer, 1964). The bedrock is very shallow, the slopes are steep,

and the soil is extremely bouldery in the Allamuchy State Forest. The bedrock ridge in the Picatinny arsenal is comprised primarily of exposed quartzite which does not facilitate soil development. Soil is present only in thin and sporadic patches. The Weldon Road sample site, on the border of Sussex and Morris Counties may have been farmed historically. Although the soil is extremely bouldery, there is a remnant boulder wall that was probably built when the land was being used for agricultural purposes. Currently, the land in the Allamuchy State Forest is used for recreational purposes such as hiking and camping. The prominent conglomerate ridge in the Picatinny arsenal is currently used for weapons testing, environmental studies, and other military research. The land surrounding the Weldon Road site is privately owned and is currently not being used. Using tree size and abundance as an indicator, it is estimated that this land has not been used for agricultural or commercial purposes for at least 50-100 years.

## **Geology**

The bedrock geology in the Highlands Physiographic Province is dominated by two distinct rock types, Precambrian metamorphic rocks and Paleozoic sedimentary rocks (Figure 3.3). In the Allamuchy State Forest, both the bedrock and the erratics are gneissic in composition. The Losee Gneiss is characterized by its light color and quartz-feldspar composition. Within the Picatinny Arsenal, middle Paleozoic rocks form distinct, northeast trending ridges. The ridge forming Shawangunk conglomerate, or the stratigraphically equivalent Green Pond conglomerate (Smith, 1970), is characterized by rounded to angular white quartz pebbles and cobbles in an orange to purple quartz sand matrix.

## Glacial history

We have selected the terminal moraine zone of the Laurentide ice sheet in northwestern New Jersey (Figure 3.1) as a calibration site for *in-situ* produced cosmogenic isotope production rates because it meets four specific criteria: 1) Samples have well-constrained exposure ages (Table 3.1); 2) the effect of erosion and till cover appear to be negligible. 3) rocks have a significant amount of physically separable quartz, and 4) the geomorphic setting is well understood. Below, we document the published ice-sheet recession ages of several authors, all of which are in  $^{14}\text{C}$  years unless specified as calibrated  $^{14}\text{C}$  ages.

## Ice advance

Approximately 85 ka, the Laurentide ice sheet had begun to advance from the north, reaching its terminal position in New Jersey by 20  $^{14}\text{C}$  ky BP (Stanford, 1993). Based on mapping of surficial features, such as striations and drumlins and well log and auger hole data, Stanford (1993) mapped the bedrock topography and the subsurface stratigraphy of northeast New Jersey and concluded that the ice moved south across the highlands from the Wallkill-Kittatinny lowlands abutting a southwesterly flowing lobe from the Newark basin at a sutured border. The orientations of several glacial striations were measured and averaged on the Green Pond conglomerate in the Picatinny Arsenal which indicated a principle ice flow direction of approximately  $192^\circ$ . The striation orientations ranged from  $178$ - $196^\circ$ . Stanford (1993) also determined that nearly 40% of the area of the New Jersey Highlands contains glacially sculpted bedrock with a thin, patchy, discontinuous cover by surficial sediments (Figure 3.4), making this an ideal site for exposure age sampling. Stanford concludes, based on a series of radiocarbon dates



which are discussed below, that the ice sheet reached the terminal position by at least 20  $^{14}\text{C}$  ka BP and had receded from the terminal moraine prior to 18.5  $^{14}\text{C}$  ka BP.

### **Age Control for Laurentide recession**

Approximately 21-23 cal  $^{14}\text{C}$  ka, the Laurentide ice sheet began to retreat from the New Jersey Highlands depositing, among various lithologies, quartzite and gneissic glacial erratics as well as leaving polished, striated, and glacially molded bedrock. The age of the terminal moraine and glacial retreat has been determined by several independent investigators, on the basis of bog and lake sediment pollen assemblages, bog-bottom radiocarbon ages, as well as morphological sequence mapping and varve chronologies.

Cotter (1984), on the basis of pollen data and several radiocarbon dates, determined that deglaciation of the Ontario Lobe of the Laurentide ice sheet in western New Jersey had begun prior to 18.5  $^{14}\text{C}$  ka. Cotter's sample location, Francis Lake, is on the easternmost margin of the Ontario Lobe, adjacent to the Hudson-Champlain Lobe and is located at a latitude similar to the latitude of the sample sites chosen for our calibration (Figure 3.5). Due to the similarity of latitudes and the fact that Cotter's site is farther north than the majority of our sample locations, Cotter's calibrated  $^{14}\text{C}$  ages are assumed to be the minimum limiting exposure age for our production rate calibration. Cotter's age estimates were based on radiocarbon dates (Table 3.1) of basal lacustrine sediments which were correlated with tundra pollen assemblages in sediments from the same sedimentary horizon. The presence of the tundra pollen assemblages in the dated basal sediments led Cotter to the conclusion that the dated sediments were deposited shortly after deglaciation, and that deglaciation occurred prior to 18.5  $^{14}\text{C}$  ky (Cotter, 1984; p.1), which corresponds to approximately 21.5 calibrated  $^{14}\text{C}$  ky (Stuiver et al., 1991). As

organic bog-bottom dates, Cotter's  $^{14}\text{C}$  estimates provide an absolute minimum for the exposure of our samples.

In a similar study, Harmon (1968) collected an 18 m sediment core from Budd Lake just south of the terminal moraine in north-central New Jersey. Harmon obtained two radiocarbon dates, at 27 and 37 feet (8.23 m and 11.28 m), as well as pollen data from this 60 foot (18.29 m) core. The  $^{14}\text{C}$  age which corresponds with the 37 foot horizon,  $22,890 \pm 720$   $^{14}\text{C}$  years, but this date was rejected by Harmon as being too old based on extrapolation from pollen data to glacial chronology.

Evenson et al. (1983) used radiocarbon dates, stratigraphic relationships, and palynological evidence from the basal tundra pollen zone to argue that ice began to retreat from the terminal moraine in New Jersey prior to 18  $^{14}\text{C}$  ky BP. Matsch (1987) also concluded from regional overview that the growth of the Laurentide ice sheet ceased by 20 ka and that parts of the southern margin were retreating by 18 ka. Sirkin (1977) and Connally and Sirkin (1972), estimating deposition rates for sediments below radiocarbon dated organic horizons, suggested that recession from northern New Jersey began about 18  $^{14}\text{C}$  ky BP. In regional summaries, Fullerton (1986) and Stone and Borns (1986) assessed the regional array of limiting  $^{14}\text{C}$  ages of preglacial materials in drift (Sirkin and Stickenrath, 1982) and postglacial sediments and supported the estimate of deglaciation of western New Jersey prior to 18.5  $^{14}\text{C}$  ky BP. Oldale and Stone, (1987) further emphasized that the ice sheet in eastern New Jersey reached its terminal position 21-20  $^{14}\text{C}$  ky BP based on  $^{14}\text{C}$  dates on wood, bone, horn, peat, shells and whole sediment samples.

The quoted  $^{14}\text{C}$  dates are in radiocarbon years, uncorrected for the change in  $^{14}\text{C}$  production rates. Corrected ages would be several thousand years older (Table 3.1). In summary, evidence suggests that the actual exposure age of the moraine boulders and outcrops we sampled is approximately 21.5 calibrated  $^{14}\text{C}$  ky or siderial years.

## METHODS

### Field methods

Sample locations on the terminal moraine of the Laurentide ice sheet in north central New Jersey were identified, and samples collected during summer, 1994. Samples were collected from glacially striated bedrock as well as large erratics (>1.5 m). Two different lithologies were sampled, quartzite and gneiss (Figure 3.3). Each sample site was extensively documented using detailed geomorphic descriptions, photographs, and map locations. Sample sites were located, and elevations were estimated using 1:24,000 U.S.G.S. topographic maps and confirmed with GPS. Observations included elevation, latitude, sample thickness, slope of sampled surface, degree of horizon shielding, distance from all edges, and the condition of the sampled surface (striated or weathered). The location and nature of the sample sites are summarized in Table 3.2.

Sample sites were chosen based on several criteria which could significantly affect the abundances of  $^{10}\text{Be}$  and  $^{26}\text{Al}$ . Three of the most important criteria were: 1) the likelihood of little or no till cover since deglaciation 2) the stability of sampled erratics since deglaciation, and 3) little or no erosion of the rock surface since deglaciation. To ensure that an erratic had not been either moved or covered with till since deglaciation, only the largest boulders sitting near or atop ridges were selected (Figure 3.6). When choosing a bedrock sample site, surfaces were chosen which were either dipping, or were located on a prominent ridge top or cliff edge where till was present only in thin patches. The similarity of isotopic abundances between the boulder and outcrop samples suggests that the effects of till cover have been negligible. Of the two lithologies sampled, gneiss and quartzite, the quartzite was more resistant to weathering as indicated by the ubiquitous and well preserved glacial striations (Figure 3.7). The quartzite samples were extremely hard and dense, and few surfaces seemed to be affected significantly by

weathering. The gneiss appeared more susceptible to chemical and mechanical weathering. The physical and chemical degradation was indicated by the rough surface textures, lack of preserved striations, and differential weathering of quartz veins (< 4 cm of relief was observed) on the surface of the gneissic boulders and outcrops (Figure 3.8). However, the similarity of isotopic abundances between the striated quartzite and weathered gneiss sample indicates that erosion has been negligible over the past 21.5 ky.

Samples were taken using chisels and sledge hammers; however, slabs of rock were often easily removed by exploiting vulnerabilities in the rock, such as bedding planes, foliation planes, or pre-existing fractures. Sixteen samples were collected and in most cases, several kilograms of rock were taken to ensure sufficient sample for replicate preparations, as well as allowing for chemical experimentation during sample preparation.

### **Lab methods**

Samples were prepared at the University of Vermont. Samples were crushed inside a canvas bag and were reduced in size using a jaw crusher and a plate grinder. After each sample, all grinding and crushing equipment was vacuumed and washed with a wet towel in order to minimize sample contamination. Once the grinding was completed, the sample was sieved and the 250-710  $\mu\text{m}$  fraction retained. The fraction smaller than 250  $\mu\text{m}$  was disposed of, and the fraction larger than 710  $\mu\text{m}$  was re-introduced to the plate grinder and re-sieved.

The chemical sample preparation consists of three steps; quartz isolation and purification, quartz dissolution, and lastly, cation-exchange separation of  $^{10}\text{Be}$  and  $^{26}\text{Al}$ . The primary goal of the first chemical treatment is to separate and/or dissolve all secondary and accessory minerals. Samples containing less than 30% quartz were enriched in quartz using heavy liquid mineral separations (acetylene tetrabromide and



acetone). A small, powerful magnet was used to remove most magnetite and the iron filings introduced during grinding.

After mineral separations were completed, the sample, now >60% quartz, underwent a heated ultrasound treatment to dissolve selectively the remaining accessory minerals, as well as to etch the surface of the quartz and remove the adhered meteoric  $^{10}\text{Be}$ . Thirty to fifty grams of sample were placed in 4 liters of 1%HF-1%HNO<sub>3</sub> which was heated to approximately 70°C and sonicated for approximately 8 hours (Kohl and Nishiizumi, 1992). The ultrasound treatment was repeated with fresh acid at least two more times with leach durations of 14 and 24 hours, respectively. Following the third ultrasound treatment, the sample was rinsed with DI water and oven dried; and, in most cases, the result was a nearly pure quartz phase containing less than 200 ppm Al and Fe. Samples requiring further purification were subject to a series of heated 6N HCl leaches, until the leachant no longer dissolved significant Fe, as indicated by the straw yellow color of the leachate.

Quartz was dissolved using 4 times the sample weight of 48% HF, to which approximately 250 mg of Be carrier was added. Al carrier was not needed due to the high concentration of native aluminum in the samples (average ~157  $\mu\text{g/g}$ ,  $n = 24$ ). The HF solution was evaporated to dryness; the resulting cake was redissolved four times in 0.5 ml HClO<sub>4</sub> (to convert flouride to chloride) and evaporated to dryness each time. Be and Al were then separated from each other using cation exchange columns and varying strengths of HCl. BeOH and Al(OH)<sub>3</sub> were precipitated with NH<sub>4</sub>OH, dried down, converted to oxide form, mixed with Ag, and tamped into a target for analysis at the Lawrence Livermore National Laboratory's (LLNL) Center for Accelerator Mass Spectrometry (CAMS). Sample weights, ICP assays, and CAMS target numbers are summarized in Table 3.3.

## RESULTS

Average isotopic concentrations from 16 samples were used to calculate the production rates for  $^{10}\text{Be}$  and  $^{26}\text{Al}$  with an assumed exposure age of 21.5 cal  $^{14}\text{C}$  ky. Abundances for varying sample surfaces, 10 outcrop and 6 boulder samples, and rock types, 9 quartzite and 7 gneiss samples, have been compared to test the hypothesis that these populations are statistically inseparable.

### Isotope abundances and production rate interpretations

Isotopic ratios ( $^{10}\text{Be}/^9\text{Be}$ ,  $^{26}\text{Al}/^{27}\text{Al}$ ) were corrected for the background ratios measured in the process blanks. For Be, the blank correction ( $22.4 \pm 1.4 \times 10^{-15}$ ) was the mean of 13 process blanks plus or minus the standard error of the mean for these blanks. For Al, the blank correction ( $7.6 \pm 1.8 \times 10^{-15}$ ) was the mean of 11 process blanks plus or minus the standard error of the mean. It has been suggested that the standard deviation is the appropriate statistic when considering the uncertainty of the blank correction (J. Southon, personal communication). The standard error of the mean may be an optimistic estimate for the blank uncertainty; however, the choice of this statistic has no effect on the calculated values of mean isotopic abundances.

Ratios were then converted to abundances (atoms  $\text{g}^{-1}$  quartz) by converting the mass of the stable isotope ( $^9\text{Be}$ ,  $^{27}\text{Al}$ ), as determined by ICP or carrier addition, to atoms of the stable isotope and multiplying by the isotopic ratio. The total number of atoms of cosmogenic isotope were then divided by the sample weight to yield an atomic abundance (Tables 3.4 and 3.5). Samples SAF-B-10 and SAF-B-11 were taken from the same boulder, therefore the isotopic abundances for these two samples were averaged when calculating the isotopic production rates. The  $^{10}\text{Be}$  abundances were separated by less than 2% and the  $^{26}\text{Al}$  abundances were separated by approximately 8% for these two

samples.  $^{10}\text{Be}/^9\text{Be}$  ratios which required a boron correction of greater than 15% and sample targets which generated a beam current < 20% of the standard for that particular run were omitted from the data set because such targets give isotopic ratios of uncertain reliability (J. Southon, Pers. comm.).

Isotopic abundances were then corrected for sample geometry, thickness, and latitude and altitude, according to the data presented by Lal (1991). Dipping surfaces were adjusted according to the angular dependence of the cosmic ray flux, expressed as the function  $\text{Sin}^2/3\theta$  where  $\theta$  is the dip of the sampled surface. The dip correction does not incorporate foreshortening. For spallation reactions, in-situ production rates decrease exponentially with depth, therefore, isotopic abundances were adjusted for average sample thickness according to the integral:

$$P_x = \int_0^x P_o e^{-(x\rho/\Lambda)} \quad (1)$$

where  $P_x$  is the integrated production rate (atoms  $\text{g}^{-1} \text{yr}^{-1}$ ) over  $x$  depth (cm),  $P_o$  is the production rate at the surface,  $x$  is the average sample thickness (cm),  $\rho$  is the density of rock ( $2.7 \text{ g cm}^{-3}$ ), and  $\Lambda$  is the characteristic attenuation length for cosmic ray neutrons ( $165 \text{ g cm}^{-2}$ ). A correction for sample latitude and altitude was applied according to the empirically derived cosmic ray flux and cosmogenic isotope production estimates of Lal (1991) for the Earth's surface, considering only production by neutron spallation.

Production rates (atoms  $\text{g}^{-1} \text{yr}^{-1}$ ) were calculated using the equation

$$P = \frac{N\lambda}{(1 - e^{-(\lambda t)})} \quad (2)$$

where  $P$  is the production rate in atoms  $\text{g}^{-1} \text{ year}^{-1}$ ,  $N$  is the average isotopic abundance in atoms  $\text{g}^{-1}$ ,  $t$  is the assumed exposure age of the sample 21.5 ky, and  $\lambda$  is the decay constant ( $^{10}\text{Be}$ ;  $4.6 \cdot 10^{-7} \text{ yr}^{-1}$ ,  $^{26}\text{Al}$ ;  $9.9 \cdot 10^{-7} \text{ yr}^{-1}$ ).

The calculated production rates (Table 3.6) reflect production by neutron spallation as well as negative muon capture, however, the relative contribution for muon induced isotope production is probably negligible (1-3%; Brown et al., 1995).

### Statistical analyses for separability of populations

Statistical analyses were done to determine if the bedrock and erratic, as well as the gneiss and quartzite sample abundances could be considered as a single population for both  $^{10}\text{Be}$  and  $^{26}\text{Al}$ . The two-sample  $t$  test was used to test the significance of the difference between the means of two small ( $n_1 < 30$ ,  $n_2 < 30$ ) sample populations. The test statistic was calculated using the equation

$$t = \frac{\mu_1 - \mu_2}{\sqrt{\frac{(n_1 - 1)\sigma_1^2 + (n_2 - 1)\sigma_2^2}{n_1 + n_2 - 2}} * \sqrt{\left(\frac{1}{n_1} + \frac{1}{n_2}\right)}} \quad (3)$$

where  $\mu_1$  and  $\mu_2$  are the means of the two sample sets,  $\sigma_1$  and  $\sigma_2$  are the standard deviations of the two sample sets, and  $n_1$  and  $n_2$  are the number of samples in each population. The chosen level of significance was 0.05, and the degrees of freedom,  $n_1 + n_2 - 2$ , is 13 for  $^{26}\text{Al}$  and 11 for  $^{10}\text{Be}$ . Therefore  $-1.771 < t_{0.05} < 1.771$  for  $^{26}\text{Al}$ , and  $-1.796 < t_{0.05} < 1.796$  (Johnson and Wichern, 1982) for  $^{10}\text{Be}$  are the range of values upon which we rejected or accepted our hypotheses.

The null and alternative hypotheses tested for both  $^{26}\text{Al}$  and  $^{10}\text{Be}$  are  $H_0: A_B = A_O$ ,  $H_A: A_B \neq A_O$  and  $H_0: A_Q = A_G$ ,  $H_A: A_Q \neq A_G$  where  $A_B$  and  $A_O$  refer to boulder and outcrop isotope abundances, respectively, and  $A_Q$  and  $A_G$  refer to isotope



abundances in quartzite and gneiss, respectively. The test statistics calculated,  $^{10}\text{Be}$ :  $t=-1.01$ ,  $0.15$  and  $^{26}\text{Al}$ :  $t=-1.11$ ,  $-0.49$ , are all constrained within their respective rejection parameters, therefore, the null hypotheses could not be rejected. The acceptance of the null hypotheses would suggest that the differences in isotope abundances between boulder and outcrop samples and quartzite and gneiss samples may be reasonably attributed to chance.

The validity of two-sample  $t$  test rests on the assumption that the samples are independent, random and from populations which can be approximated by a normal distribution as well as similar population variances. The distribution of the test statistic is not affected by moderate variations in the assumption that the probability distribution is normal; however, the variances of the respective populations must be nearly equal for this test to be valid (Mendenhall, 1969). Based on the necessity of equal variances, calculations were done to test the hypothesis that population to population variation was equal. When samples are taken from normal distributions with equal variances, the ratio of the variances from each population,  $v_1/v_2$ , has an F distribution (Mendenhall, 1969). To test the null hypothesis,  $H_0: v_1=v_2$ , a test statistic was generated using the equation

$$F = \frac{v_1}{v_2} \quad (4)$$

where  $v_1$  is the variance of population 1 and  $v_2$  is the variance of population 2. The rejection parameters are determined using the degrees of freedom for both sample populations ( $n-1$ ), a 0.05 level of significance, and a table of  $F_{0.05}$  values (Merrington and Thompson, 1943).

The rejection parameters for the null hypothesis  $H_0: v_B=v_O$ , where  $v_B$  is the variance in the boulder isotope abundances and  $v_O$  is the variance in the outcrop isotope abundances, are  $F=6.09$  and  $6.00$  for  $^{10}\text{Be}$  and  $^{26}\text{Al}$  respectively. The F statistic calculated for each of these populations was  $1.40$  and  $1.07$  for  $^{10}\text{Be}$  and  $^{26}\text{Al}$

respectively. This would indicate that the null hypothesis could not be rejected and that the assumption of equal boulder and outcrop variances for the two-sample  $t$  test is a valid assumption.

The rejection parameters for the null hypothesis  $H_0: v_Q=v_G$ , where  $v_Q$  is the variance in the quartzite isotope abundances and  $v_G$  is the variance in the gneiss isotope abundances, are  $F=4.95$  and  $4.82$  for  $^{10}\text{Be}$  and  $^{26}\text{Al}$  respectively. The  $F$  statistic calculated for each of these populations was  $1.60$  and  $1.82$  for  $^{10}\text{Be}$  and  $^{26}\text{Al}$  respectively. Although the variance for the quartzite abundances seems to be much greater than the variance for the gneiss abundances, the calculated  $F$  statistics indicate that the population variances can still be assumed to be equal.

## DISCUSSION

Our calculated mean production rates ( $5.17\pm 0.15$ ,  $^{10}\text{Be}$ ;  $30.40\pm 1.01$ ,  $^{26}\text{Al}$ ; uncertainty represents the standard error of the mean) integrated over the last 21.5 cal ky are approximately 15-20% less than previously published production rates integrated over approximately 11.0 cal ky (Nishiizumi et al., 1989), 50 TL ky (Nishiizumi et al., 1991b), and 2.0 My (Nishiizumi et al., 1991a; Brown et al., 1991a), all of which appear to be approximately equal. There are several possible explanations for this discrepancy: 1) our sampled surfaces have eroded, moved, or been covered with till since deposition 2) sampled surfaces have had a history of snow cover 3) fluctuations in the intensity of the magnetic field 4) our independent age control for exposure age is inaccurate (too high) and 5) the exposure duration for Nishiizumi et al.'s (1989) sampled surfaces has been underestimated. We believe, based on the following arguments, that the bulk of the discrepancy most likely results from underestimation of exposure age for Nishiizumi et al.'s (1989) sampled surfaces as suggested by new  $^{14}\text{C}$  data from the Sierra Nevada

(Clark et al., 1995) indicating that the exposure age for Sierra Nevadan samples was likely underestimated by 15-20%.

## **Erosion**

If the sampled surfaces have eroded, been covered with till or snow, or in the case of boulders, moved since recession of the Laurentide ice sheet, the calculated production rates would underestimate actual production rates over the past 21,500 years. Any combination of these three variables would result in production rate values which would be less than the actual production rates over the assumed exposure age.

The presence of glacial striations on the quartzite bedrock surfaces we sampled suggests that it is unlikely that erosion has affected these sampled surfaces. There was evidence suggesting that gneissic surfaces had experienced some mass loss due to erosion (Figure 3.8); however, the similarity between isotope abundances in quartzite and gneiss samples (see statistical analyses above) indicate that the effects of weathering are negligible with respect to measured isotope abundances.

## **Post-depositional movement**

We believe it is unlikely that the sampled boulders have moved since deposition by the ice sheet. All but one of the boulders was located in a topographically high, flat-lying area, indicating the boulders have not rolled to their current position. Also, all sampled boulders were a minimum of 1 meter in diameter, making movement due to wind or water unlikely (Figure 3.6). The apparent agreement between boulder and outcrop sample abundances (see statistical analyses above) also suggests that the boulders have not undergone post-Laurentide movement. In the event of post-depositional



movement, we would expect the boulder isotope abundances to be less than the outcrop abundances.

### **Snow cover**

Cosmic ray shielding due to snow accumulation could lower apparent production rates. The potential effects of cosmic ray attenuation by snow cover were calculated using a variation on Equation 1. The density of snow, which ranges from  $0.05 \text{ g cm}^{-3}$  (newly fallen) to  $0.4 \text{ g cm}^{-3}$  (springtime pack), is assumed to have an average density of  $0.2 \text{ g cm}^{-3}$  (Dunne and Leopold, 1978). Mean monthly snow fall values (Figure 3.9, data from U.S. Climatology No. 20 CD ROM) were calculated using a 50 year record at the Sussex 1 SE station ( $41^{\circ}12' \text{ N}$ ,  $74^{\circ}36' \text{ W}$ , el. 120 m) and were assumed to not be cumulative. The mean snowfall values for this station are assumed to be similar to mean snowfall values for our sample sites, and are also assumed to be constant over the last 21.5 ky. If the preceding assumptions are valid, our samples would require less than a 1% correction to compensate for cosmic ray shielding due to snow cover. If snow cover were to account totally for the discrepancy between Laurentide and Sierra Nevadan production rates (~18%), there would have to have been a 150 cm (~5 ft) snowpack (assuming  $\rho=0.2 \text{ g cm}^{-3}$ ) covering our sample sites constantly over the last 21.5 ky. The results of these calculations suggest that it is unlikely that snow cover had any noticeable effect on the Laurentide-based production rates.

### **Till cover**

Finally, there is no evidence for extensive erosion of till cover from our sample sites. Till was present only in scattered thin patches on the quartzite outcrops and there is no mappable colluvium suggesting the presence of till eroded over the past 21.5 cal ky.



One would also expect to see remnant boulders on outcrops had there once been a significant till deposit which had subsequently been removed, which we do not. All boulders sampled were between 1 and 3 meters high making the possibility of extensive till or soil cover remote. The statistical agreement between boulder and outcrop sample abundances (see statistical analyses above) also suggests that till or soil cover on top of the boulders is not a factor influencing the Laurentide-based production rates.

The potential effects of till cover (assumed  $\rho=2.0 \text{ g cm}^{-3}$ ) on our production rates have been quantified using Equation 1. If we assume that, until recently, 1 meter of till covered the bedrock sample sites, leaving the tops of boulders (1-3 m high) exposed, the production rates for the bedrock sample sites would be approximately 70% less than those for continuously exposed boulder sample sites. If we assume that there was 25 cm till cover on the bedrock over the first 10,750 years after recession of the Laurentide and no till cover for the latter 10,750 years, we would expect the bedrock production rates to be approximately 15% less than boulder production rates. This calculation also assumes constant cosmic ray flux over the last 21.5 cal ky. These calculations suggest that any amount of till cover would result in low bedrock production rates with respect to boulder production rates. The possibility of till cover in excess of 1 meter is unlikely, however, we would still expect to see a discrepancy in the production rates of boulders and bedrock due to the observation that the boulders would be at least 1 meter closer to the surface of the till than the bedrock.

### **Variations due to paleomagnetic field**

Fluctuations in the intensity of Earth's magnetic field affect production rates of cosmogenic isotopes (Bard et al., 1990; Kurz et al., 1990). However, the existing paleomagnetic data (Mazaud et al., 1991; McElhinny and Senanayake, 1982; Meynadier et al., 1992) suggest production rates integrated over 21.5 cal ky should be greater than

those integrated over 11.0 cal ky because the intensity of Earth's magnetic field was stronger over the last 10 ky than it was from 10 ky to 20 ky BP.

Theoretical calculations have been made which model potential errors due to temporal magnetic field fluctuations (Clark et al., 1995) utilizing Nishiizumi's apparent paleolatitude formulation (1989, Eq. 5) and Lal's (1991) altitude/latitude scaling factors. The results of these calculations suggest that the effects of the magnetic field on instantaneous production rates will be most pronounced at high altitudes and low latitudes. Also, the Laurentide samples would be much less susceptible to the effects of a dynamic magnetic field due to the high latitude and low altitude of the sample sites. The effects of a temporally fluctuating magnetic field on the integrated production rates is significantly dampened, particularly with greater exposure ages.

The latitudinal effect on cosmic ray flux seems to be commonly accepted (Lal, 1991); however, there does not seem to be a consensus regarding the use of geomagnetic or geographic latitude when scaling production rates. The production rates of Nishiizumi et al. (1989) are based on the geomagnetic latitudes of the sample sites whereas the production rates of Nishiizumi et al. (1991b) are scaled according to the geographic latitude of the sample sites. Based on evidence which suggests that Earth's magnetic dipole approximates the geographic poles through time (Merrill and McElhinny, 1983), geographic latitude appears to be the appropriate variable when considering latitude scaling factors for cosmogenic production rates.

### **Exposure age constraints**

Our independent exposure age control relies on a series of  $^{14}\text{C}$  dates from bogs and lakes surrounding the terminal moraine (Table 3.1, Figure 3.7). We have adopted the youngest date ( $18,390 \pm 200$   $^{14}\text{C}$  years; Cotter, 1986) as the minimum limiting exposure age for our samples because was taken from a glacial lake several miles north of the

terminal moraine at a latitude which is higher than all but one of our sample sites. This conservative exposure age estimate ensures that the integrated production rates will be not be underestimated. There is evidence which suggests that the recession of the Laurentide ice sheet may have occurred 3,000-4,000 years prior to 21.5 cal  $^{14}\text{C}$  years (Stone, 1995, and Table 1); If correct, such evidence would indicate that our production rates are overestimated by as much as 15-20%.

Based on a series of limiting  $^{14}\text{C}$  dates for the Tiogan glaciation in the Sierra Nevada mountains (Clark et al., 1995), we believe that the assumed exposure ages for Nishiizumi et al.'s (1989) sample sites have been under-estimated by a minimum of 2,100 years. The limiting  $^{14}\text{C}$  ages taken from the basal layers of post-glacial lakes suggest that Tiogan deglaciation in the Sierra Nevada was complete by 13.1 cal ky  $^{14}\text{C}$  years BP. If we assume that the exposure age for Nishiizumi et al.'s sample sites is 13.1 cal ky  $^{14}\text{C}$  years, Sierran-based production rates are 5.11 atoms  $\text{g}^{-1} \text{yr}^{-1}$  and 30.64 atoms  $\text{g}^{-1} \text{yr}^{-1}$  for  $^{10}\text{Be}$  and  $^{26}\text{Al}$  respectively. These revised production rates are very similar to those calculated from the terminal moraine of the Laurentide ice sheet.

### $^{26}\text{Al}/^{10}\text{Be}$ ratios

The average  $^{26}\text{Al}/^{10}\text{Be}$  production rate ratio for our samples was calculated to be  $5.8 \pm 0.2$  (1sem,  $n=12$ ; Table 3.6). This ratio is consistent with the production rate ratio reported by Nishiizumi et al. (1989),  $6.0 \pm 0.5$ , for glacially polished surfaces in the Sierra Nevada. Sample SPA-O-6 has the lowest ratio at 4.7 and appears to be depleted in  $^{26}\text{Al}$  as indicated by comparison with the average concentration of  $^{26}\text{Al}$  (Table 3.6). This low ratio may indicate contamination from meteoric  $^{10}\text{Be}$ , making it appear as though it were depleted in  $^{26}\text{Al}$ . This seems unlikely, however, as the  $^{10}\text{Be}$  abundance for this sample is less than the mean abundance. The low ratio may also indicate a complex burial history. Contamination from meteoric  $^{10}\text{Be}$  is unlikely due to the extensive HF ultrasound

treatments, which dissolve and etch the surface of the quartz, where the meteoric  $^{10}\text{Be}$  would be adhered. If the uncertainties surrounding both the  $^{26}\text{Al}/^{10}\text{Be}$  ratio and the isotope abundances are considered (Figure 3.10), this sample may not be considered anomalous.

There are two samples which seem to be enriched in  $^{26}\text{Al}$ , SAF-O-13 and SPA-O-5, with respect to  $^{10}\text{Be}$  (Table 3.6). These elevated ratios could be due to radiogenic production of  $^{26}\text{Al}$  (Sharma and Middleton, 1989), biased production of  $^{26}\text{Al}$  by negative muon capture at depth (Lal, 1987; Middleton and Klein, 1987), or biased production of  $^{26}\text{Al}$  at depth due to changing energy spectrum of fast neutrons with depth in rock (Brown et al., 1991a). Sharma and Middleton (1989) showed that  $^{26}\text{Al}$  can be produced radiogenically as a result of Uranium and Thorium decay via the reaction  $^{23}\text{Na}(\alpha, n)^{26}\text{Al}$  (6000 at  $\text{g}^{-1}$ , average sandstone) whereas the radiogenic  $^{10}\text{Be}$  component is considered to be minor (24 at  $\text{g}^{-1}$ , average sandstone). Samples were not analyzed for uranium or thorium, therefore, this component has not been quantified. Muons, which penetrate rock much further than high-energy neutrons ( $\sim 1500 \text{ g cm}^{-2}$  in rock, Middleton and Klein, 1987), seem to have an empirically derived  $^{26}\text{Al}/^{10}\text{Be}$  production rate ratio of approximately 6 (Brown et al., 1992) despite theoretical calculations to the contrary (Lal and Arnold, 1985). Also, the contribution from muon-induced cosmogenic isotopes is negligible (1-3%) with respect to spallation induced cosmogenic isotopes (Brown et al., 1995). This would suggest that the muogenically produced  $^{26}\text{Al}$  would not be responsible for elevated  $^{26}\text{Al}/^{10}\text{Be}$  ratios.

### Implications

Data from the Laurentide, as well as the new age control evidence from the Sierra Nevada, suggest currently accepted late Pleistocene  $^{26}\text{Al}$  and  $^{10}\text{Be}$  in-situ production rates are probably 10-20% too high. The Laurentide data provide evidence which



suggests that boulder and outcrop sample abundances can be considered as a single population of samples and the use of both sample types can help reduce uncertainties with respect to sample history. The agreement between gneiss and quartzite sample abundances suggests that sample lithology and erosivity at these young exposure ages does not affect isotope abundance.

Our findings demonstrate that uncertainties associated with the accuracy of cosmogenic production rates and calculated exposure ages (15-20%) greatly exceeds the analytical precision (1-3 %). If cosmogenic isotopes are to be used for reliably dating geomorphic features associated with brief geologic events such as the Younger Dryas, the accuracy must be significantly improved. This is probably best accomplished with numerous production rate calibrations at various altitudes and latitudes, particularly for younger exposure ages.

## CONCLUSIONS

The production rate estimates for  $^{10}\text{Be}$  and  $^{26}\text{Al}$  introduced in this paper are the first from the terminal moraine of the Laurentide ice sheet and are the first estimates over the 21.5 cal ky time frame. Our data demonstrate that it is possible to make cosmogenic isotopic measurements in Fe, Ti rich quartzites of relatively young exposure age. The isotope abundances were seemingly unaffected by erosion as shown by in the agreement between abundances measured in striated and unstriated samples. Also, the sample abundances were seemingly uninfluenced by till or soil cover based on the agreement between abundances in very large erratics and bedrock samples. Finally, we can conclude that the sampled boulders have not moved since Laurentide deposition based on the agreement between bedrock and erratic sample abundances. The average production rate  $^{26}\text{Al}/^{10}\text{Be}$  ratio was determined to be 5.8, which is consistent with previously published values.

Our production rate estimates in quartz,  $5.17 \pm 0.15$  atoms  $g^{-1} yr^{-1}$  for  $^{10}Be$  and  $30.40 \pm 1.01$  atoms  $g^{-1} yr^{-1}$  for  $^{26}Al$ , are approximately 15-20% less than those published by Nishiizumi et al. (1989) for surfaces with an assumed exposure age of 11.0 ky cal  $^{14}C$  years. Laurentide and Sierra Nevadan production rates are indistinguishable if the new limiting Sierra Nevada  $^{14}C$  evidence constraining Tiogan exposure age is considered when calculating Nishiizumi et al.'s (1989) production rates.

## ACKNOWLEDGEMENTS

Isotopic measurements were made at the Center for Accelerator Mass Spectrometry, Lawrence Livermore National Laboratory with the help of John Southon, Marc Caffee, Bob Finkel, and Joe Koenig. Research was funded in part by the Geological Society of America-Field Research Grant #5394-94 to Larsen and NSF EAR 9396261 to Bierman. We acknowledge Jill Turner for assistance with sample preparation, Ruth Carswell for assistance drafting figures, and Christine Massey for field assistance. Personnel at the Picatinny Military Arsenal in Dover, New Jersey gave us access and allowed us to take samples from their installation.

## FIGURE CAPTIONS

Figure 3.1 Map of the state of New Jersey. Hatched line shows approximate location of the maximum extent of the Late Wisconsinan ice sheet. Field area is outlined by boxed zone. Samples were taken from Warren, Sussex, and Morris counties.

Figure 3.2 Locations of sample sites near the terminal moraine of the Laurentide ice sheet in the Highlands physiographic province in north-central New Jersey. Black swath represents the Laurentide terminal moraine.

Figure 3.3 Generalized map showing the bedrock geology of the field area in north central New Jersey. Map is simplified from Department of Environmental Protection-Division of Water Resources-Geological Survey Geologic Map of New Jersey (1985). Samples were taken from these two types of bedrock and erratics.

Figure 3.4 Distribution of glacial sediments in field area in the New Jersey Highlands physiographic province in north-central New Jersey. Map is simplified from Stanford (1993).

Figure 3.5 Map showing locations of independent  $^{14}\text{C}$  age controls for recession of the Laurentide ice sheet. References, details, and calibrated  $^{14}\text{C}$  ages can be seen in Table 1. Northernmost calibrated  $^{14}\text{C}$  ages of Cotter (1986) were assumed to be the minimum limiting exposure age for our samples.

Figure 3.6 Sampled gneissic erratic. Erratics dimensions are approximately 2.5 m high, 5m long, and 2m wide. The size of the boulder, as well as the location of the boulder

(perched on the top of a ridge) suggest that the boulder has not rolled since it was deposited by the Laurentide ice sheet. The size and location of the erratics also suggest that the boulder has not been covered with till following the recession of the ice sheet.

Figure 3.7 Preserved glacial striations. Photograph of glacially striated Shawangunk Conglomerate in the Picatinny Military Arsenal. Striations indicate that erosion of the bedrock surface has been negligible over the exposure age.

Figure 3.8 Gneissic surface displaying differential weathering of quartz vein and gneiss matrix. Statistical evidence suggests that the isotopic abundances from gneissic samples were the same as isotope abundances from quartzite samples, indicating the effects of weathering on the isotopic abundances of sampled gneissic surfaces are negligible.

Figure 3.9 Mean monthly snowfall values for Sussex, New Jersey. Values represent 50 year averages at Sussex 1 SE station (41°12' N, 74°36' W, el. 120 m). Data from U.S. Climatology No. 20 CD ROM.

Figure 3.10  $^{26}\text{Al}$  graphed versus  $^{10}\text{Be}$ . Production rate ratio has been shown to be equal to 6.0 (Nishiizumi et al., 1989). Thick line has a slope of 6.0 which is the expected ratio, and thin lines represent the standard deviation of the  $^{26}\text{Al}/^{10}\text{Be}$  ratio for our samples. All samples fall within the expected range.



TABLE 3.1. INDEPENDENT AGE CONTROL ON LAURENTIDE RECESSION

Location	Lat (°N)	Long (°W)	Lab ID	Reference	Dated Material	Basal date 14C yr BP	Basal Date cal. yr BP±
Budd Lake	40°52'	74°45'	I-2845	Harmon, 1968	organic sediment	22,890±720	26,470 *
Jenny Jump Mtn	42°54'23"	74°55'08"	GX-4279	Cadwell' Pers Com	bog-bottom	19,340±695	22,920 *
Francis Lake	40°58'30"	74°50'30"	SI-5273	Cotter, 1986	basal seds	18,570±250	22,150 *
Francis Lake	40°58'30"	74°50'30"	SI-4921	Cotter, 1986	basal seds	18,390±200	21,970±281
Lake Passaic	40°52'	74°45'	OC-1304	Stone, 1989	concretion	20,180±500	23,760 *
Long Island	40°	74°	SI-1590	Sirkin, 1980	organic silt	21750±750	25,330 *

\* No model exists to calibrate these 14C uncertainties.

+ Calibrated according to 'calib' program (Stuiver and Reimer, 1993)

TABLE 3.2 SAMPLE SITE LOCATIONS AND CHARACTERISTICS

Sample	Site	Lithology	Sampled surface	Elevation (m)	Location	
					Latitude (°N)	Longitude (°W)
SPA-O-1	Picatinny Arsenal	Quartzite	Bedrock	342	40°57'	74°32'
SPA-O-2	Picatinny Arsenal	Quartzite	Bedrock	342	40°57'	74°32'
SPA-O-3	Picatinny Arsenal	Quartzite	Bedrock	342	40°57'	74°32'
SPA-O-4	Picatinny Arsenal	Quartzite	Bedrock	342	40°57'	74°32'
SPA-O-5	Picatinny Arsenal	Quartzite	Bedrock	336	40°58'	74°31'
SPA-O-6	Picatinny Arsenal	Quartzite	Bedrock	336	40°58'	74°31'
SWR-B-7	Weldon Road	Gneiss	Erratic	375	41°00'	74°36'
SWR-B-8	Weldon Road	Gneiss	Erratic	375	41°00'	74°36'
SMH-B-9	Lake Denmark	Quartzite	Erratic	253	40°57'	74°31'
SAF-B-10	Allamuchy Forest	Gneiss	Erratic	323	40°55'	74°45'
SAF-B-11	Allamuchy Forest	Gneiss	Erratic	323	40°55'	74°45'
SAF-B-12	Allamuchy Forest	Gneiss	Erratic	323	40°55'	74°45'
SAF-O-13	Allamuchy Forest	Gneiss	Erratic	299	40°55'	74°45'
SAF-O-14	Allamuchy Forest	Gneiss	Bedrock	278	40°55'	74°45'
SPA-O-15	Picatinny Arsenal	Quartzite	Bedrock	336	40°57'	74°33'
SPA-O-16	Picatinny Arsenal	Quartzite	Bedrock	336	40°57'	74°33'

TABLE 3.3 LABORATORY SAMPLE DATA

Sample	Al target #	Be target #	Sample size (g)	Total Al ( $\mu$ g)	9-Be added ( $\mu$ g)
SPA-O-1	AL1498	BE4610	28.918	6521	311
SPA-O-2X	AL1443	BE4348	29.785	7065	270
SPA-O-3	AL1499	BE4615	24.130	5011	311
SPA-O-4X	AL1639	BE4726	27.997	6869	252
SPA-O-5	N.D.	BE3970	11.885	1637	409
SPA-O-5X	AL1348	BE4227	28.980	N.D.	254
SPA-O-5XX	AL1642	BE4727	29.030	4734	254
SPA-O-6	AL1151	BE3973	20.604	2636	410
SPA-O-6X	AL1445	BE4337	30.189	N.D.	258
SPA-O-6XX	AL1641	BE4728	29.134	7993	259
SWR-B-7	AL1497	BE4614	21.786	2598	306
SWR-B-8	AL1222	BE3986	20.043	1033	243
SWR-B-8X	AL1446	BE4343	29.860	1759	252
SMH-B-9	AL1221	BE3994	15.655	2012	235
SMH-B-9X	AL1441	BE4339	32.694	4670	254
SMH-B-9XX	AL1638	BE4730	29.712	3979	252
SAF-B-10	AL1217	BE3992	18.050	1534	233
SAF-B-10X	AL1496	BE4612	29.877	3650	309
SAF-B-11	AL1450	BE4334	22.360	1900	249
SAF-B-12	AL1350	BE4216	28.232	3664	391
SAF-O-13	AL1219	BE3955	17.057	1483	238
SAF-O-13X	AL1449	BE4341	25.210	2357	250
SAF-O-13XX	AL1640	N.D.	28.062	13481	252
SAF-O-14	AL1349	BE4217	27.680	2650	243
SPA-O-15	AL1500	BE4613	28.038	6230	309
SPA-O-16X	AL1643	BE4729	34.785	8139	256

N.D. No data for these samples

X indicates replicate measurement

XX indicates triplicate measurement

TABLE 3.4  $^{10}\text{Be}$  AMS DATA AND ABUNDANCES

Sample	$^9\text{Be}/^{10}\text{Be}$ ratio measured ( $\times 10^{15}$ )	Blank corrected ratio ( $\times 10^{15}$ )	$^{10}\text{Be}$ abundance ( $\times 10^5$ atoms $\text{g}^{-1}$ ) (sea level, high latitude)
SPA-O-1	$245.2 \pm 12.0$	$222.8 \pm 15.2$	$1.25 \pm 0.09$
SPA-O-2X	$236.1 \pm 9.0$	$213.7 \pm 13.0$	$1.04 \pm 0.06$
SPA-O-3	$208.4 \pm 15.0$	$186.0 \pm 17.7$	$1.25 \pm 0.12$
SPA-O-4X	$282.1 \pm 18.0$	$259.7 \pm 20.3$	$1.25 \pm 0.10$
SPA-O-5X	$211.7 \pm 8.4$	$189.3 \pm 12.6$	$0.91 \pm 0.06$
SPA-O-5XX	$249.9 \pm 13.0$	$227.5 \pm 16.0$	$1.09 \pm 0.08$
SPA-O-6	$114.0 \pm 5.8$	$91.6 \pm 11.0$	$0.99 \pm 0.12$
SPA-O-6X	$255.3 \pm 8.5$	$232.9 \pm 12.7$	$1.08 \pm 0.06$
SPA-O-6XX	$252.4 \pm 22.0$	$230.0 \pm 23.9$	$1.11 \pm 0.12$
SWR-B-8	$183.0 \pm 7.1$	$160.6 \pm 11.8$	$1.02 \pm 0.07$
SWR-B-8X	$259.4 \pm 9.4$	$237.0 \pm 13.3$	$1.04 \pm 0.06$
SMH-B-9	$127.2 \pm 6.8$	$104.8 \pm 11.6$	$0.90 \pm 0.10$
SMH-B-9X	$239.5 \pm 9.9$	$217.1 \pm 13.7$	$0.97 \pm 0.06$
SAF-B-10	$159.5 \pm 9.0$	$137.1 \pm 13.0$	$0.97 \pm 0.09$
SAF-B-10X	$245.2 \pm 12.0$	$222.8 \pm 15.2$	$1.29 \pm 0.09$
SAF-B-11	$209.9 \pm 8.9$	$187.5 \pm 12.9$	$1.15 \pm 0.08$
SAF-B-12	$168.1 \pm 7.5$	$145.7 \pm 12.0$	$1.10 \pm 0.09$
SAF-O-13	$137.1 \pm 4.9$	$114.7 \pm 10.6$	$0.93 \pm 0.09$
SAF-O-13X	$204.3 \pm 7.1$	$181.9 \pm 11.8$	$1.04 \pm 0.07$
SAF-O-14	$268.8 \pm 21.0$	$246.4 \pm 23.0$	$1.22 \pm 0.11$



TABLE 3.5 <sup>26</sup>Al AMS DATA AND ABUNDANCES

Sample	<sup>26</sup> Al/ <sup>27</sup> Al ratio measured (x10 <sup>15</sup> )		Blank corrected ratio (x10 <sup>15</sup> )	<sup>26</sup> Al abundance (x10 <sup>5</sup> atoms g <sup>-1</sup> ) (sea level, high latitude)
SPA-O-1	184.9 ± 13.0	177.3 ± 14.3	6.99 ± 0.56	
SPA-O-2X	139.9 ± 11.0	132.3 ± 12.5	5.65 ± 0.53	
SPA-O-3	204.6 ± 16.0	197.0 ± 17.1	7.15 ± 0.62	
SPA-O-4X	156.7 ± 13.0	149.1 ± 14.3	6.52 ± 0.63	
SPA-O-5XX	256.0 ± 18.0	248.6 ± 19.0	7.40 ± 0.56	
SPA-O-6XX	108.0 ± 13.0	100.4 ± 14.3	4.99 ± 0.71	
SWR-B-8	680.0 ± 24.0	672.4 ± 24.7	6.04 ± 0.22	
SWR-B-8X	553.0 ± 35.0	545.4 ± 35.5	5.60 ± 0.36	
SMH-B-9	239.3 ± 9.0	231.7 ± 10.8	5.71 ± 0.27	
SMH-B-9X	166.0 ± 11.0	158.4 ± 12.5	4.34 ± 0.34	
SMH-B-9XX	212.3 ± 12.0	204.7 ± 13.4	5.26 ± 0.34	
SAF-B-10	475.1 ± 21.0	467.5 ± 21.8	7.30 ± 0.34	
SAF-B-10X	302.6 ± 25.0	295.0 ± 25.7	6.75 ± 0.59	
SAF-B-11	393.4 ± 23.0	385.8 ± 23.8	6.03 ± 0.37	
SAF-B-12	291.5 ± 18.0	283.9 ± 19.0	6.71 ± 0.45	
SAF-O-13	398.3 ± 16.0	390.7 ± 17.1	6.57 ± 0.29	
SAF-O-13X	493.7 ± 34.0	486.1 ± 34.5	8.79 ± 0.62	
SAF-O-13XX	67.4 ± 9.7	59.7 ± 11.4	5.55 ± 1.06	
SAF-O-14	393.4 ± 12.0	385.8 ± 13.4	6.96 ± 0.24	
SPA-O-15	194.7 ± 15.0	187.1 ± 16.1	7.47 ± 0.64	
SPA-O-16X	154.3 ± 11.0	146.7 ± 12.5	6.11 ± 0.52	

TABLE 3.6 AVERAGE ABUNDANCES AND PRODUCTION RATES

Sample	Average $^{10}\text{Be}$ abundances* (sea level, >60°) atoms $\text{g}^{-1}\times 10^5$	$^{10}\text{Be}$ production rate† (sea level, >60°) atoms $\text{g}^{-1}\text{y}^{-1}$	Average $^{26}\text{Al}$ abundances* (sea level, >60°) atoms $\text{g}^{-1}\times 10^5$	$^{26}\text{Al}$ production rate† (sea level, >60°) atoms $\text{g}^{-1}\text{y}^{-1}$	$^{26}\text{Al}/^{10}\text{Be}$ ratio
SPA-O-1	1.25 ± 0.09	5.86 ± 0.40	6.99 ± 0.56	32.84 ± 2.65	5.6 ± 0.6
SPA-O-2	1.04 ± 0.06	4.88 ± 0.30	5.65 ± 0.53	26.54 ± 2.51	5.4 ± 0.6
SPA-O-3	1.25 ± 0.12	5.86 ± 0.56	7.15 ± 0.62	33.61 ± 2.91	5.7 ± 0.7
SPA-O-4	1.25 ± 0.10	5.83 ± 0.46	6.52 ± 0.63	30.65 ± 2.94	5.2 ± 0.6
SPA-O-5	1.00 ± 0.07	4.66 ± 0.32	7.40 ± 0.56	34.77 ± 2.65	7.4 ± 0.8
SPA-O-6	1.06 ± 0.10	4.96 ± 0.46	4.99 ± 0.71	23.48 ± 3.35	4.7 ± 0.8
SWR-B-8	1.03 ± 0.07	4.81 ± 0.31	5.82 ± 0.29	27.34 ± 1.38	5.7 ± 0.5
SMH-B-9	0.94 ± 0.08	4.38 ± 0.38	5.11 ± 0.32	24.00 ± 1.49	5.5 ± 0.6
SAF-B-10a	1.14 ± 0.09	5.32 ± 0.41	6.69 ± 0.43	31.45 ± 2.04	5.9 ± 0.6
SAF-B-12	1.10 ± 0.09	5.14 ± 0.42	6.71 ± 0.45	31.55 ± 2.11	6.1 ± 0.6
SAF-O-13	0.99 ± 0.08	4.61 ± 0.36	6.97 ± 0.66	32.78 ± 3.09	7.1 ± 0.9
SAF-O-14	1.22 ± 0.11	5.70 ± 0.53	6.96 ± 0.24	32.72 ± 1.14	5.7 ± 0.6
SPA-O-15	N.D.	N.D.	7.47 ± 0.64	35.10 ± 3.03	N.D.
SPA-O-16	N.D.	N.D.	6.11 ± 0.52	28.74 ± 2.45	N.D.
Average§	1.11 ± 0.03	5.17 ± 0.15	6.47 ± 0.22	30.40 ± 1.01	5.8 ± 0.22

\*Abundances for each sample reflect the average of all replicates.

†Production rates based on 21,500 years exposure.

§Uncertainties on averages are standard errors of the mean.

Figure 3.1

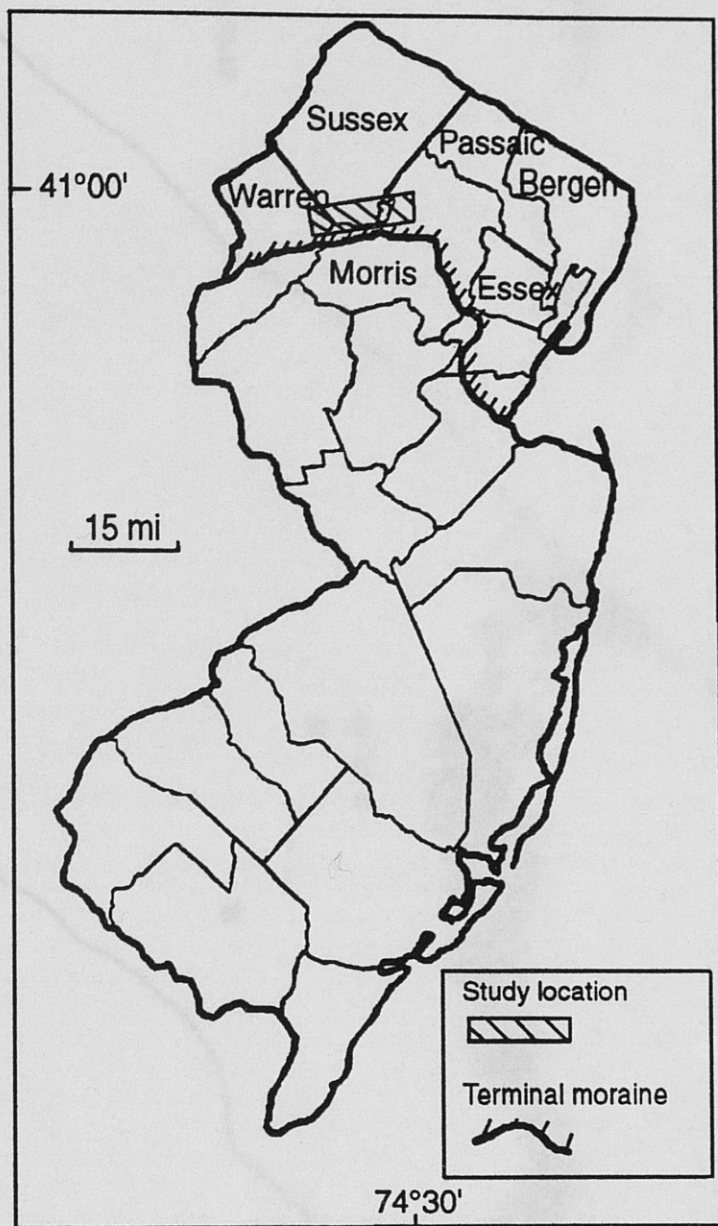


Figure 3.2

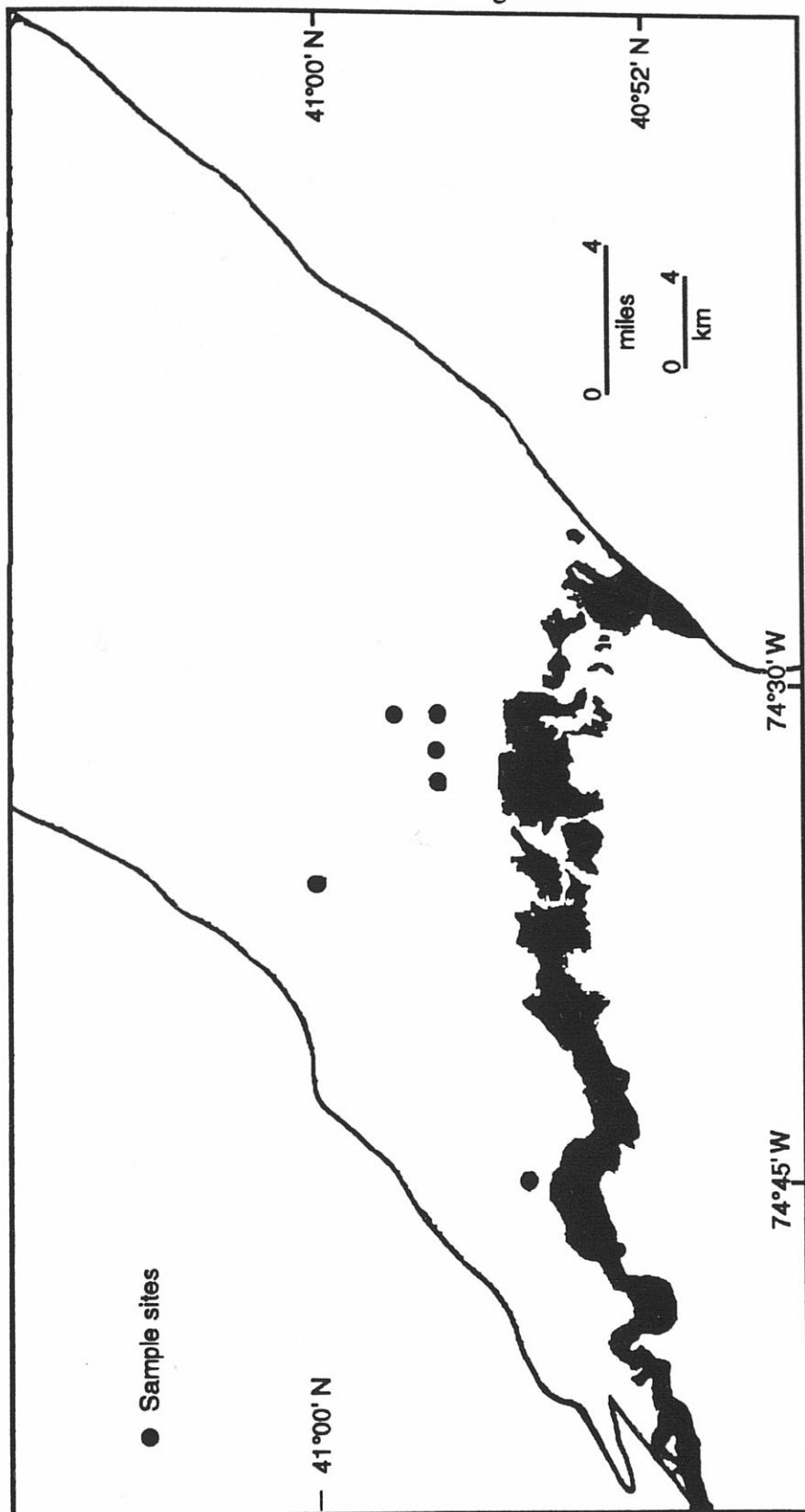




Figure 3.3

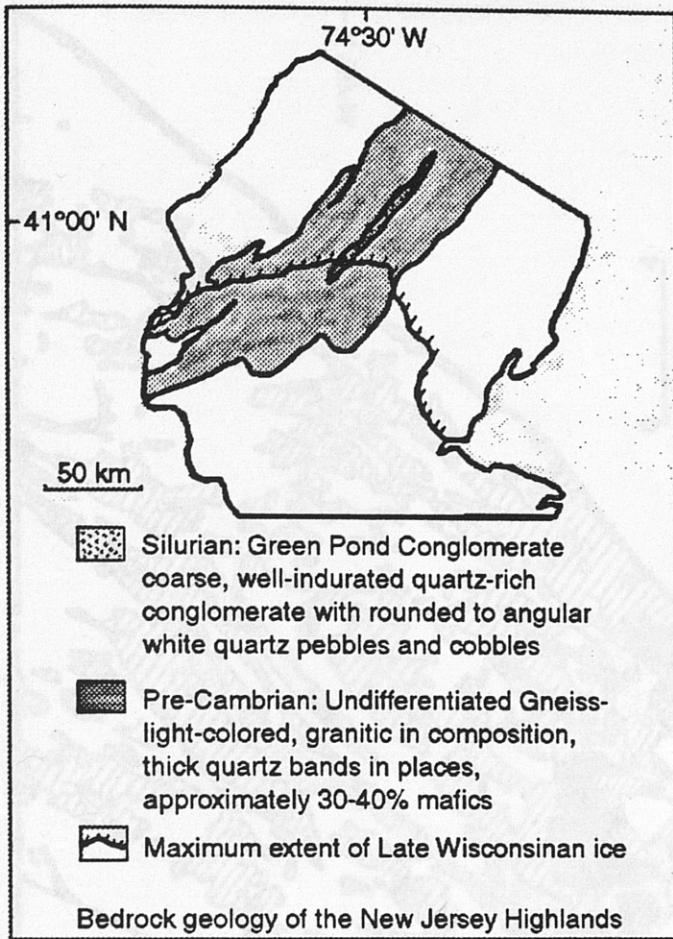


Figure 3.4

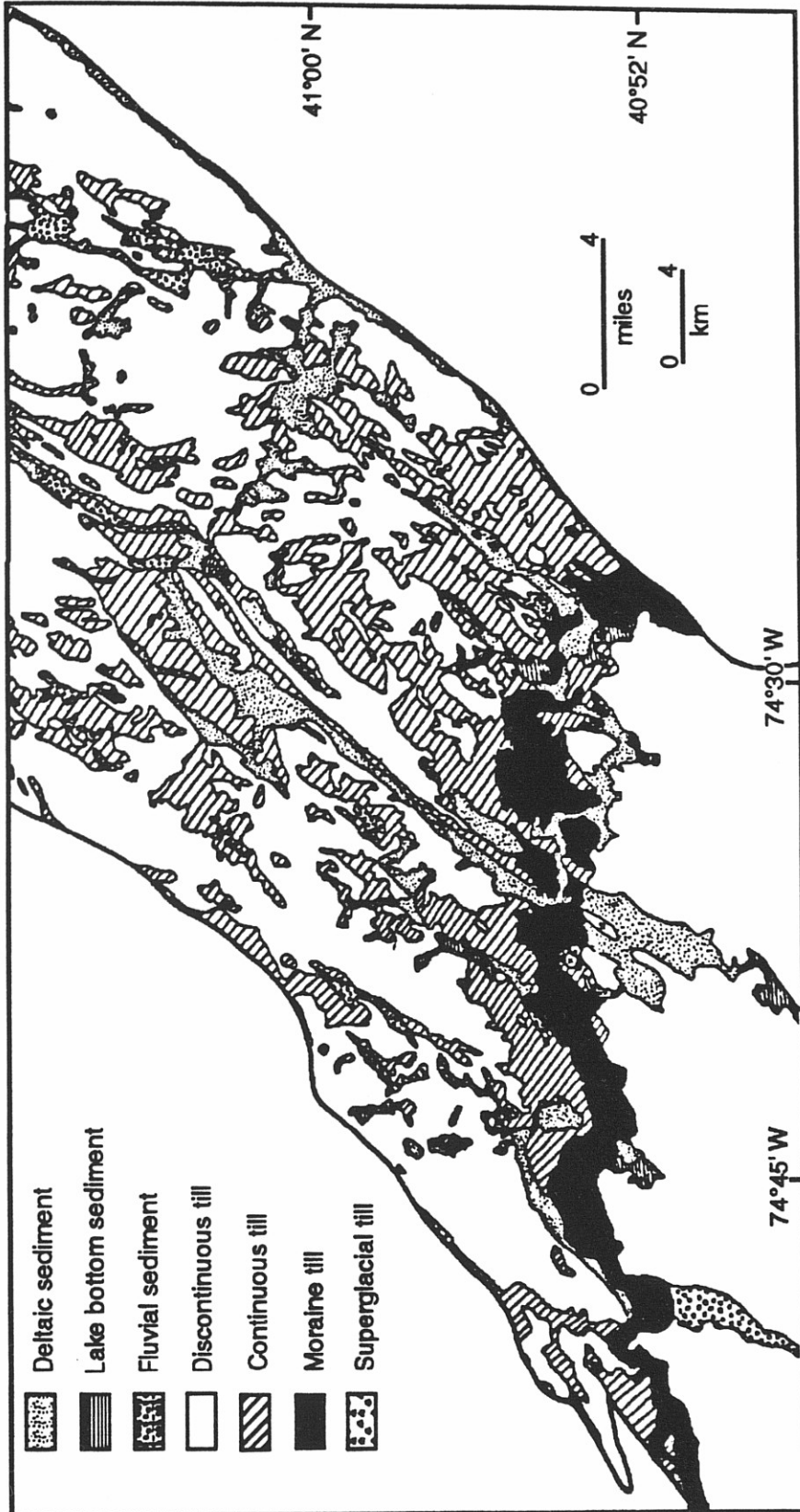


Figure 3.5

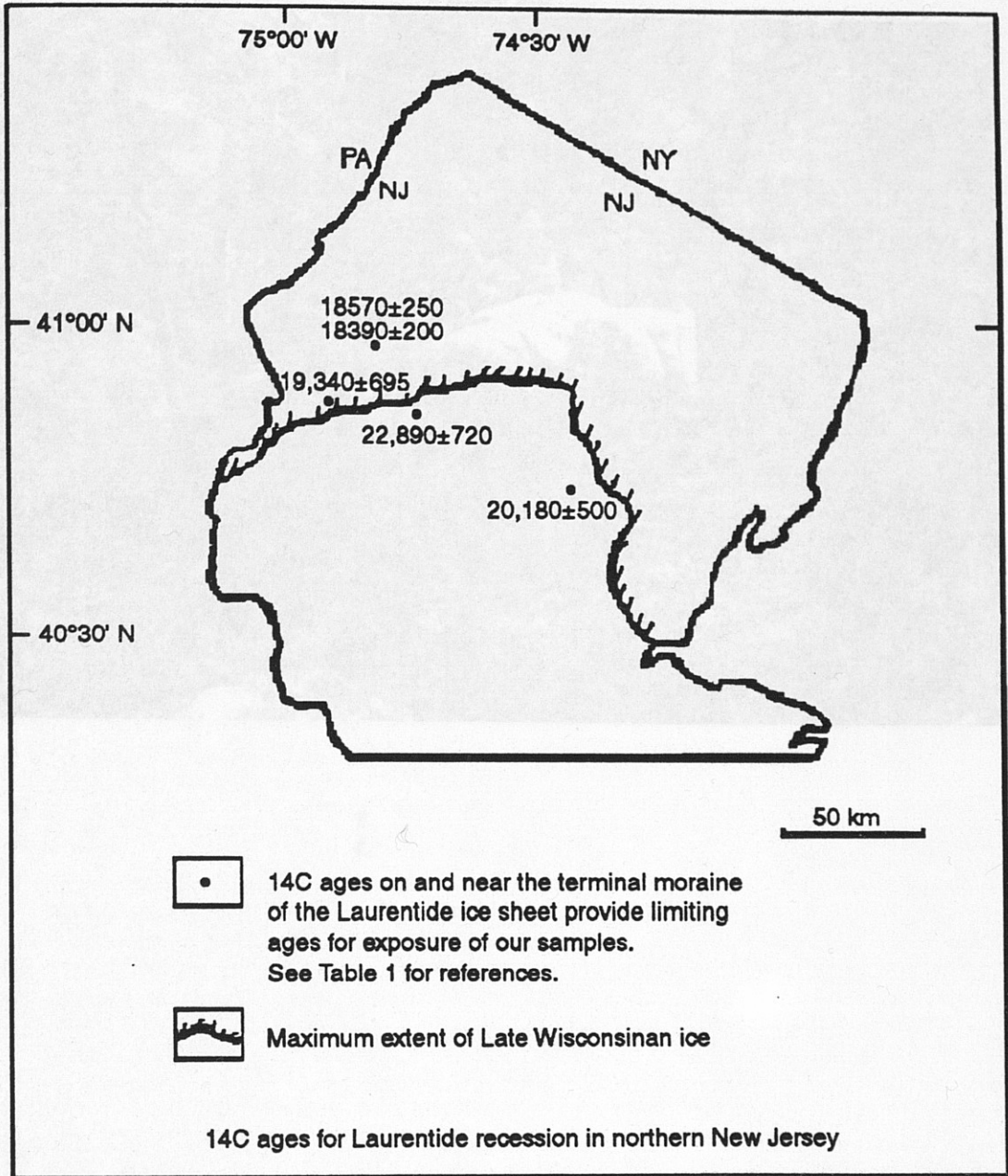




Figure 3.6

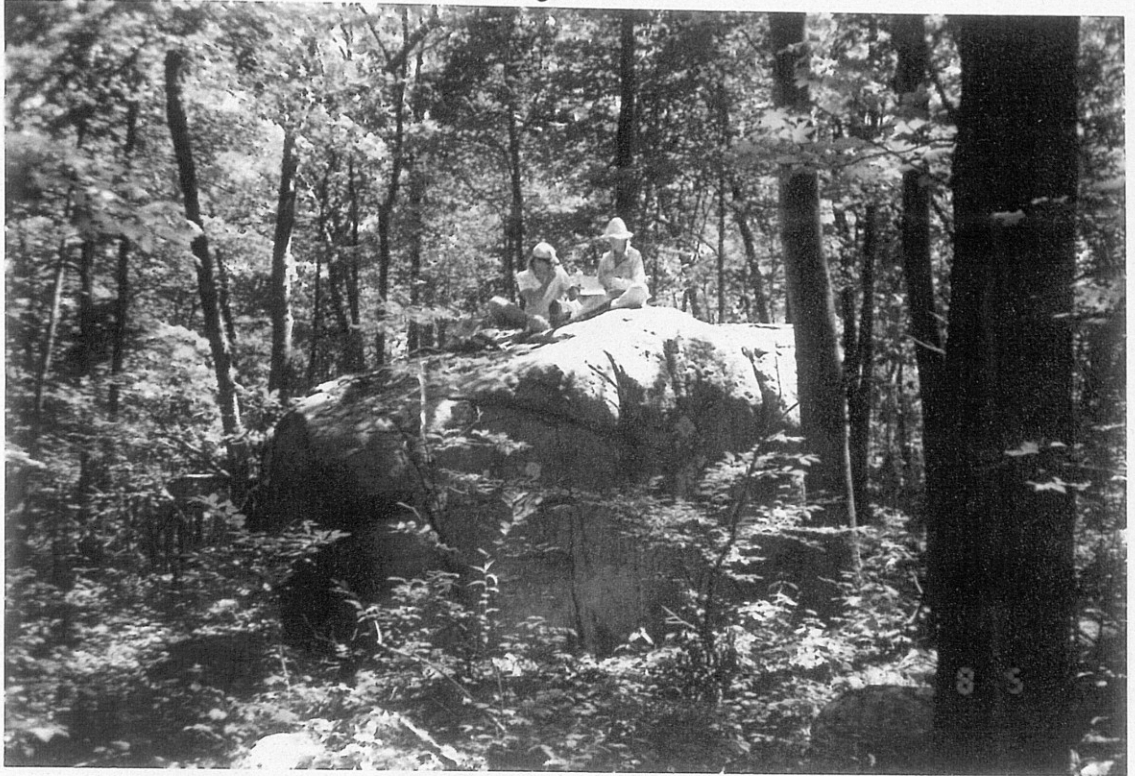




Figure 3.7



Figure 3.8





Figure 3.9

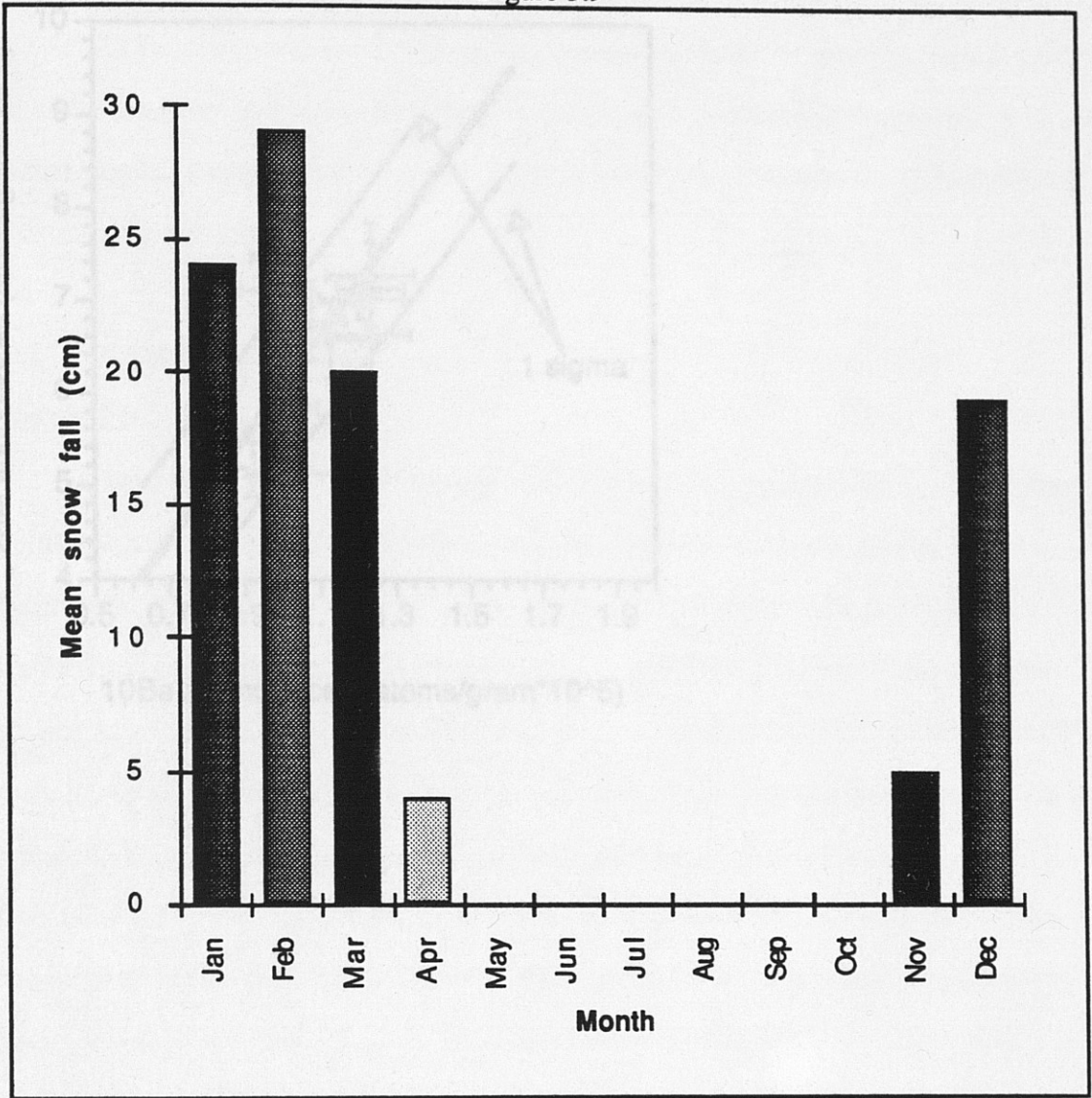
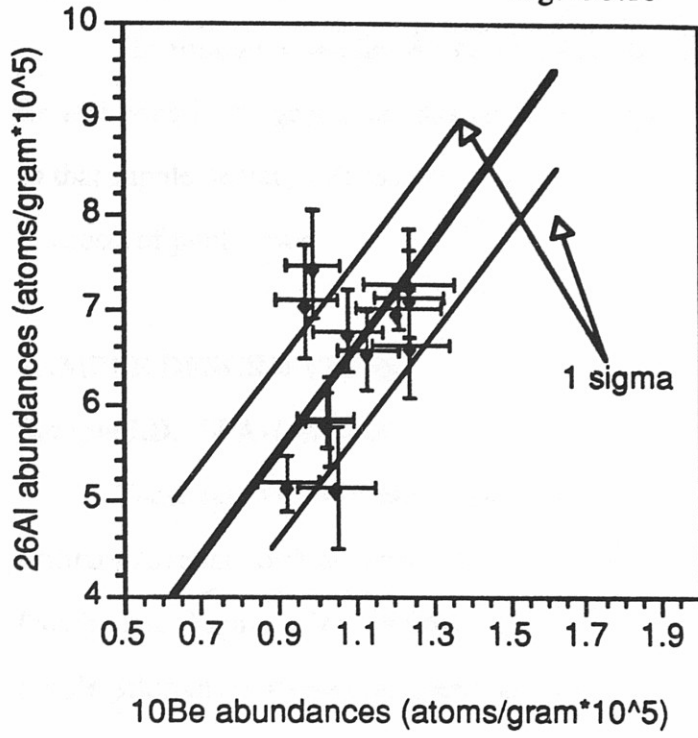


Figure 3.10





## **DATA REPOSITORY**

The following sample site descriptions are to be submitted with the journal article for archiving in the geological Society of America's data repository. The repository exists so that supplementary information may be available to interested parties while defraying the costs of publication.

## **SAMPLE DESCRIPTIONS**

### **Sample I.D.: SPA-O-1,2,3,4**

These samples was taken from an extensive bedrock ridge within the Picatinny Military Arsenal north of Dover New Jersey. They can be located on the Dover Quadrangle (Figure 3.26). The bedrock lithology, the Green Pond conglomerate, is a purple Silurian conglomerate comprised mostly of quartz sand with white quartz clasts ranging in size from 1mm to several cm's in diameter. The quartz clasts were planed off, probably by moving ice, and they had less than 5mm relief. The bedrock displays nearly horizontal sheeting, the sheets ranging in thickness from cm's to 10's of cm's, with abundant slickenlines. The sheeting, which is nearly parallel with the topography, may be due to glacial unloading. There were also a few scattered white quartzite erratics which were generally less than a meter in diameter. The bedrock surface sampled showed striations which were consistent at S10°W. These surfaces were not glacially polished, however it is not likely that the bedrock surface has eroded more than a cm, based on the presence of the glacial stria.

Vegetation is very sparse on the ridge and there is almost no soil development. The vegetation is primarily scrub oak, blueberry bushes, and other scrubby plants. lichens are also present on about 5-15% of the bedrock surface. It is unlikely that this outcrop has been heavily forested since deglaciation. It is also unlikely that snow accumulation will be a significant factor affecting the isotope abundance due to the fact that there is little vegetation and it is a ridge top with high wind and sun exposure.

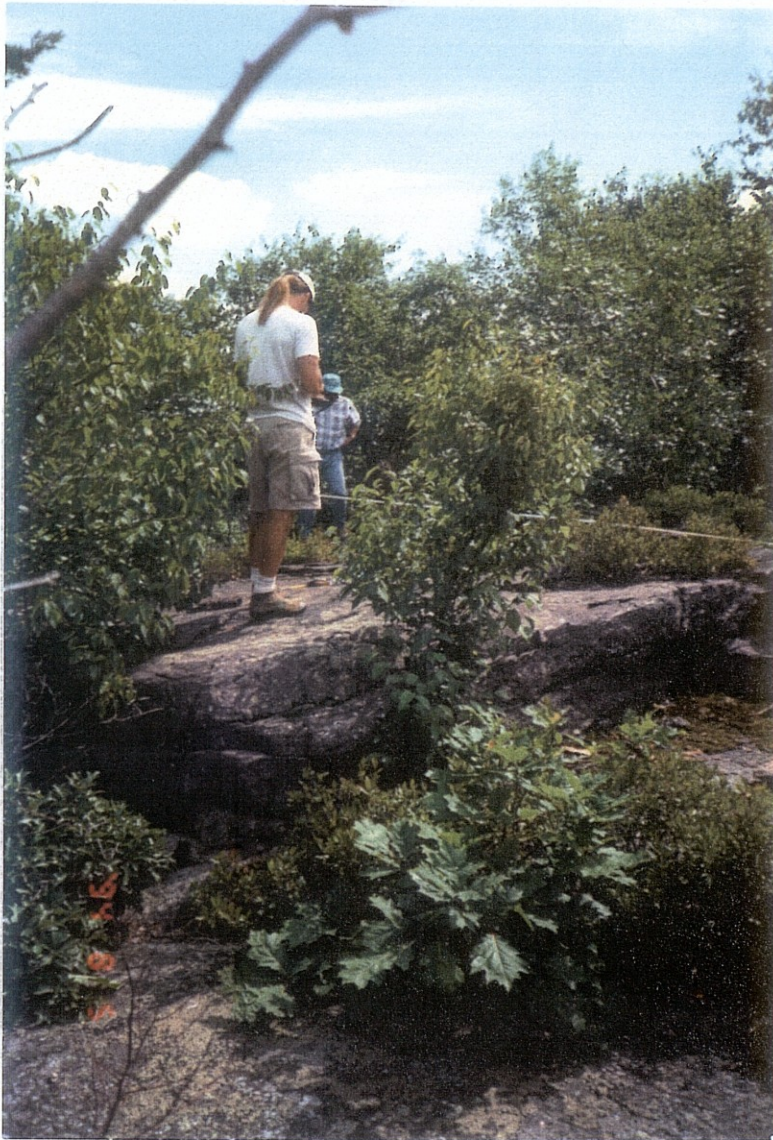


Figure 3.11. Bedrock ridge from which samples 1-4 were taken.



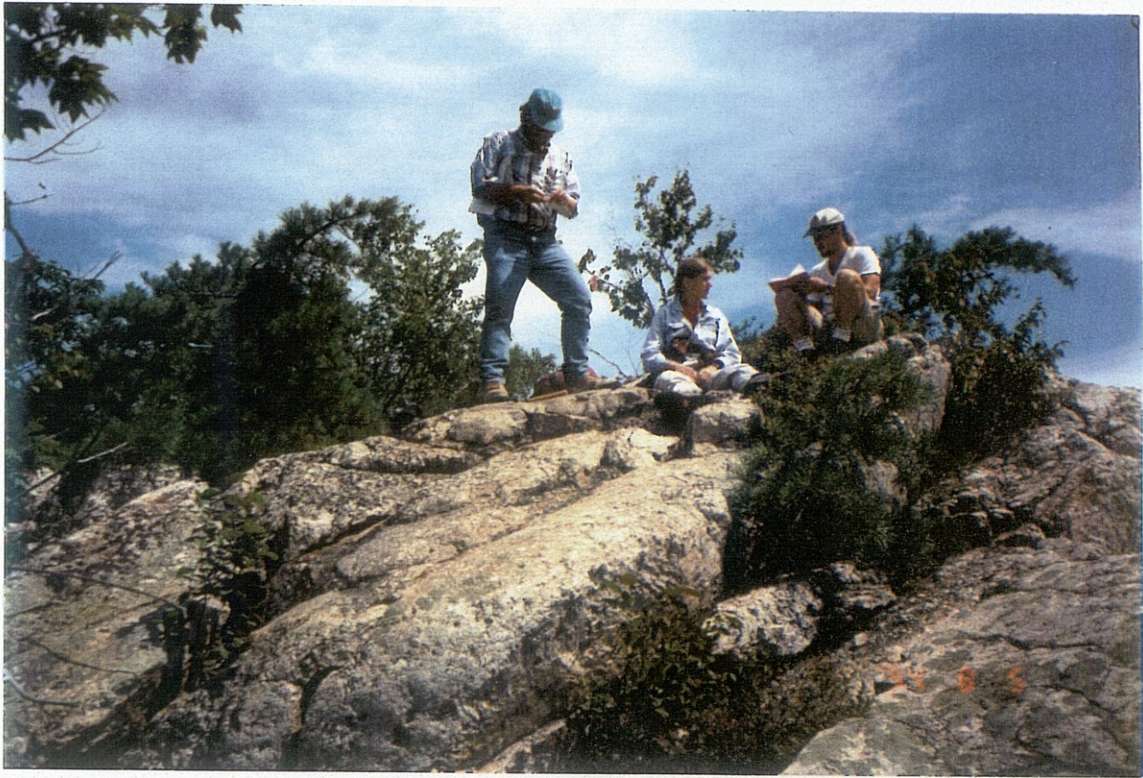


Figure 3.13. Bedrock ridge from which sample 5 was taken. Sample was taken from area between standing persons feet.



Figure 3.14. Bedrock surface from which sample 6 was taken.



### **Sample I.D.: SWR-B-7,8**

These two samples were taken from a gneiss erratic perched atop a relatively flat ridge in the Franklin Quadrangle (Figure 3.27). The boulder, which was flat-topped with vertical sides, most likely joint planes, was surrounded by other 1 meter diameter erratics. There were no other erratics comparable in size, however. The erratic was located in an old pasture with 50-75 year oaks. The forest floor was covered with a soil horizon and erratics spaced approximately 1-3 meters apart. The erratic was covered with lichens. There is no evidence of fire damage, however, the boulder has lost some mass due to chemical weathering. The evidence for this can be seen where quartz veins stand proud (<3 cm) of the rest of the boulder (Figure 3.8), due to the variable weathering rates of quartz and the relatively mafic matrix. It is unlikely that this erratic has either been moved or covered with till based on its sheer size ( up-facing surface >2 m above the forest floor, 5mX3m). The uncertainty regarding this sample will be associated with surface denudation due to weathering. There were two samples taken from this boulder, SWR-B-8 from a quartz vein (> 80% quartz), and SWR-B-7 from the granitic gneiss matrix (15%-25% quartz). This will be a test for spatial variability within a boulder, variability between lithologies, and may also help to establish the erosion rates for the two lithologies.



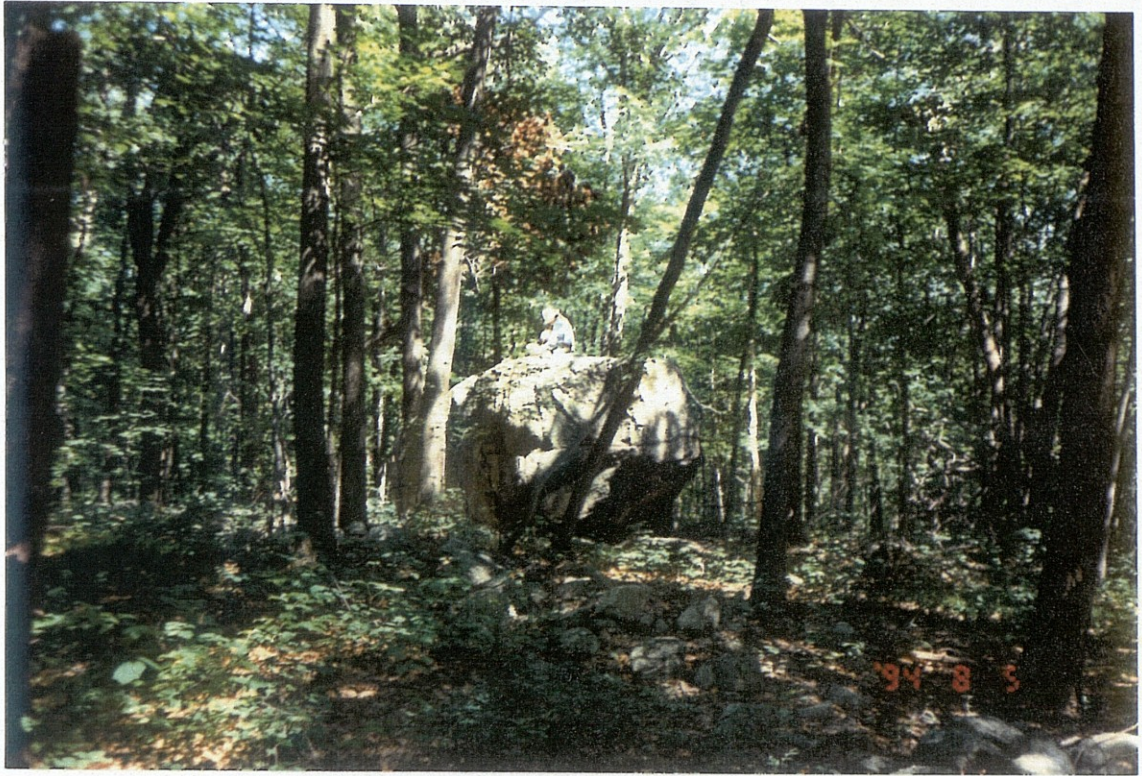


Figure 3.15. Glacial erratic from which samples 7 and 8 were taken.



Figure 3.16. Surface of glacial erratic.

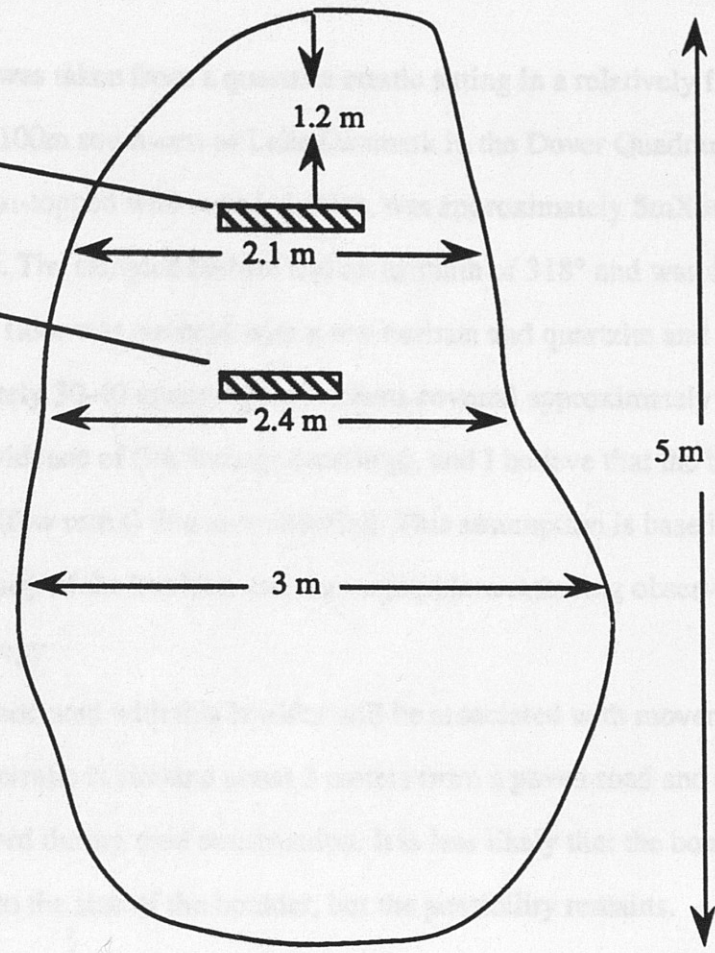


**MAP VIEW**

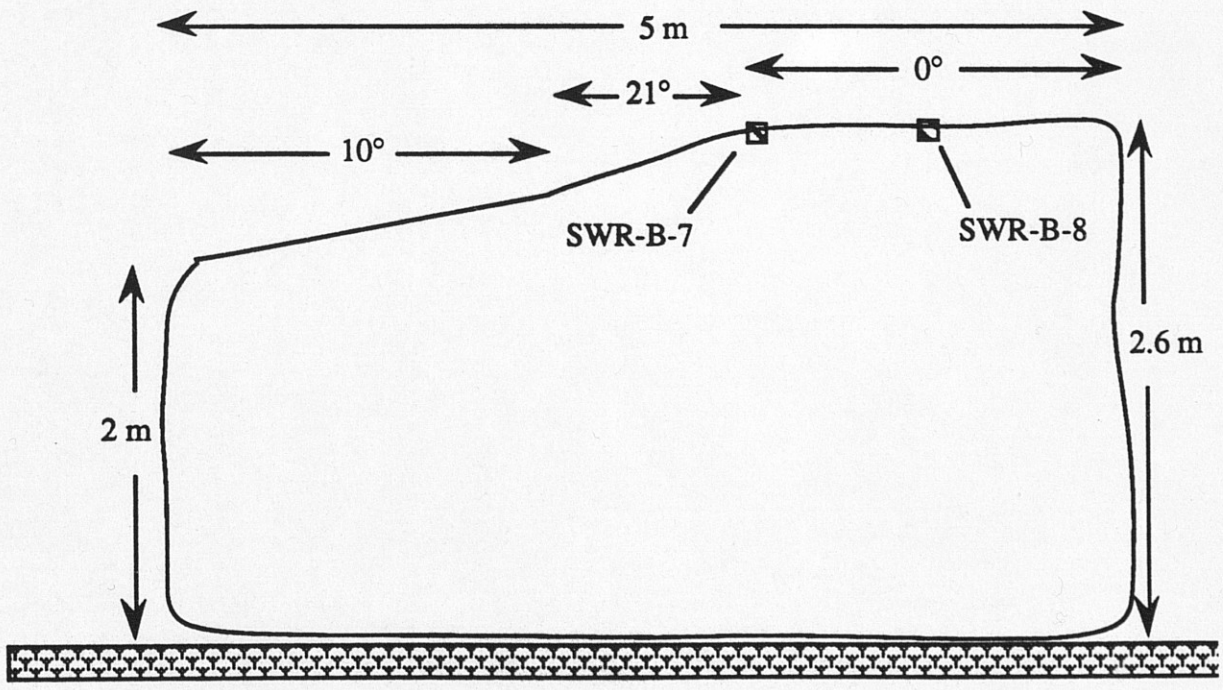
SWR-B-8

SWR-B-7

S64°W



**CROSS SECTION**



### **Sample I.D.: SMH-B-9**

Sample SMH-B-9 was taken from a quartzite erratic sitting in a relatively flat lying area, approximately 100m southwest of Lake Denmark in the Dover Quadrangle. The boulder, which was flat-topped with rounded sides, was approximately 5mX3m and was over a meter in height. The sampled surface had an azimuth of 318° and was dipping 15° to the East. The forest floor was covered with a soil horizon and quartzite and gneiss erratics spaced approximately 30-40 meters apart. Lichens covered approximately 5% of the boulder. There is no evidence of fire damage (spalling), and I believe that the boulder has lost little surface area (few mm's) due to weathering. This assumption is based on the extreme hardness and density of the boulder, and the negligible weathering observed in bedrock of the same lithology.

The uncertainty associated with this boulder will be associated with movement and till or soil cover. The erratic is situated about 3 meters from a paved road and could have potentially been moved during road construction. It is less likely that the boulder has been shielded by till, due to the size of the boulder, but the possibility remains.





Figure 3.18. Quartzite erratic. Sample SMH-B-9 was taken from the top of this erratic.



### **Sample I.D.: SAF-B-10,11,12**

Samples 10 through 12 were taken from adjacent gneissic boulders within the Allamuchy State Forest on the terminal moraine of the Laurentide ice sheet. These samples can be located on the Tranquility Quadrangle (Figure 3.28). The boulders were located near the top of a ridge and were situated among a group of six, similarly sized boulders. The lithology for SAF-O-10 through SAF-O-12 was a white-gray colored granitic gneiss. The gneiss was approximately 30% mafics and 70% felsics with about 20% quartz. The surfaces of the boulders were moderately weathered and displayed a pebbly texture, however, they were extremely hard to chisel. It is not likely that the bedrock surface has eroded more than a few cm's, based on the minimal amount of relief (5-15 cm) on the sampled surfaces, as well as the absence of spalls. Samples 10 and 11 were both taken from the surface of the same boulder. The surface for sample 10 was a knob striking at 90° and had an average dip of 20°S. Sample 11 was taken from a horizontal, planar surface on a lower spot on the same boulder. This part of the boulder could have possibly been exposed due to spalling. These two samples will allow a direct comparison for spatial variability within the same boulder, as well as a check for variability within differing sample geometries. Sample SAF-B-12 was taken from the surface of an adjacent boulder. The surface was dipping at 20°S. Sample 12, along with samples 10 and 11 will provide the means for testing the spatial variability within a boulder field.

The vegetation is best described as forest flora. The vegetation consists primarily of oaks, maples, blueberry bushes, and other scrubby plants and grasses. The boulders are resting on a well-developed soil horizon, however, it is unlikely that the boulders have been covered by either till or soil since deglaciation, based on the size of the boulders (1-2m high). It is also highly improbable that the boulders have moved since deglaciation, based on their size as well as the fact that they are sitting at the top of a ridge.





Figure 3.19. Gneissic erratic from which samples 10 and 11 were taken.



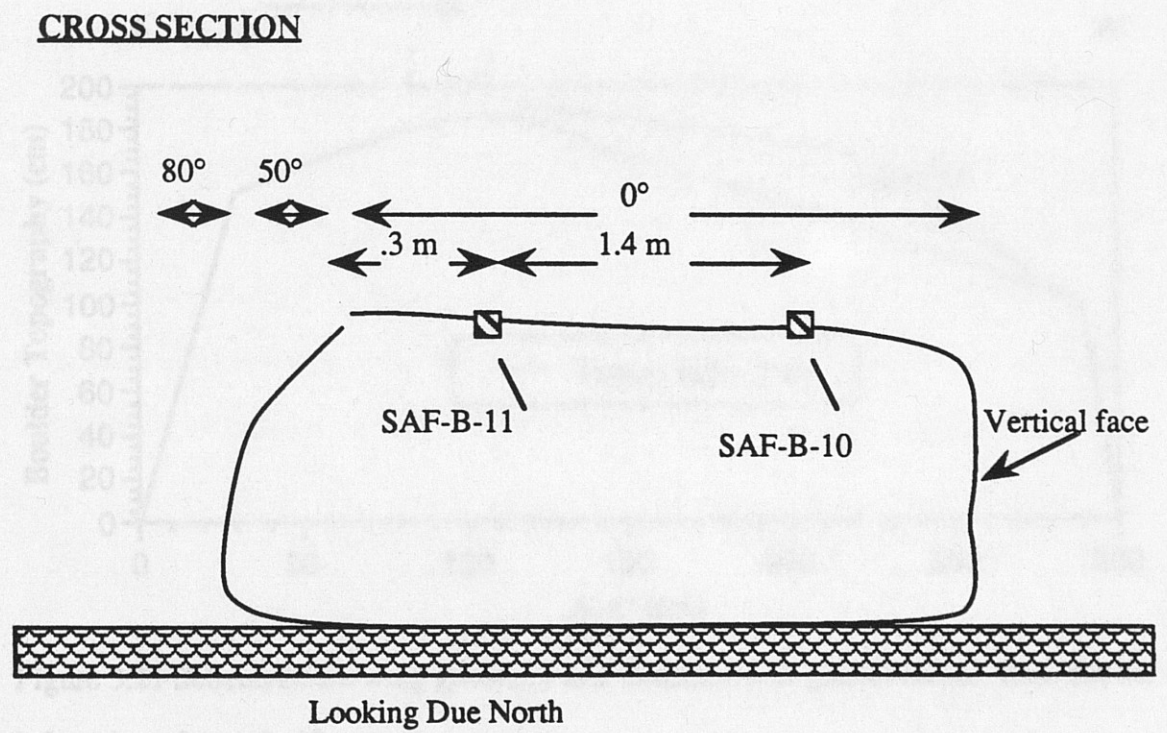
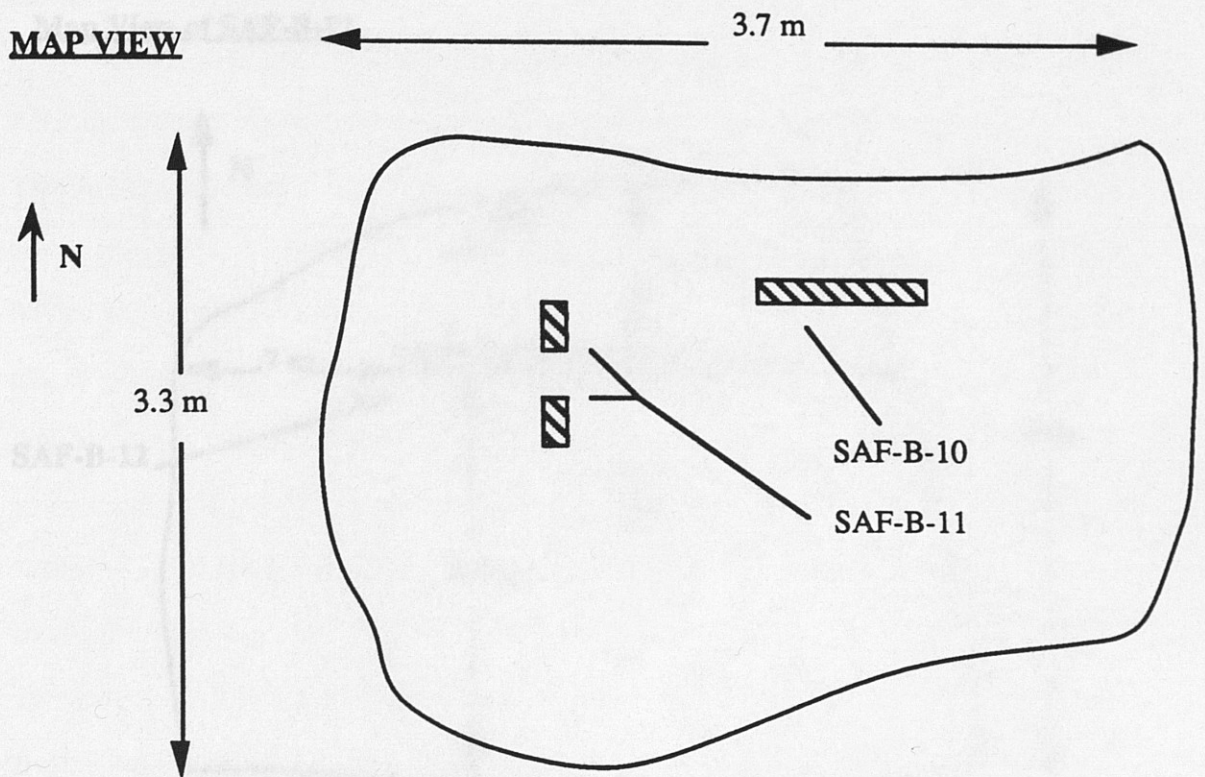


Figure 3.20 Schematic showing dimensions of erratic and location of samples 10 and 11

**Map View of SAF-B-12**

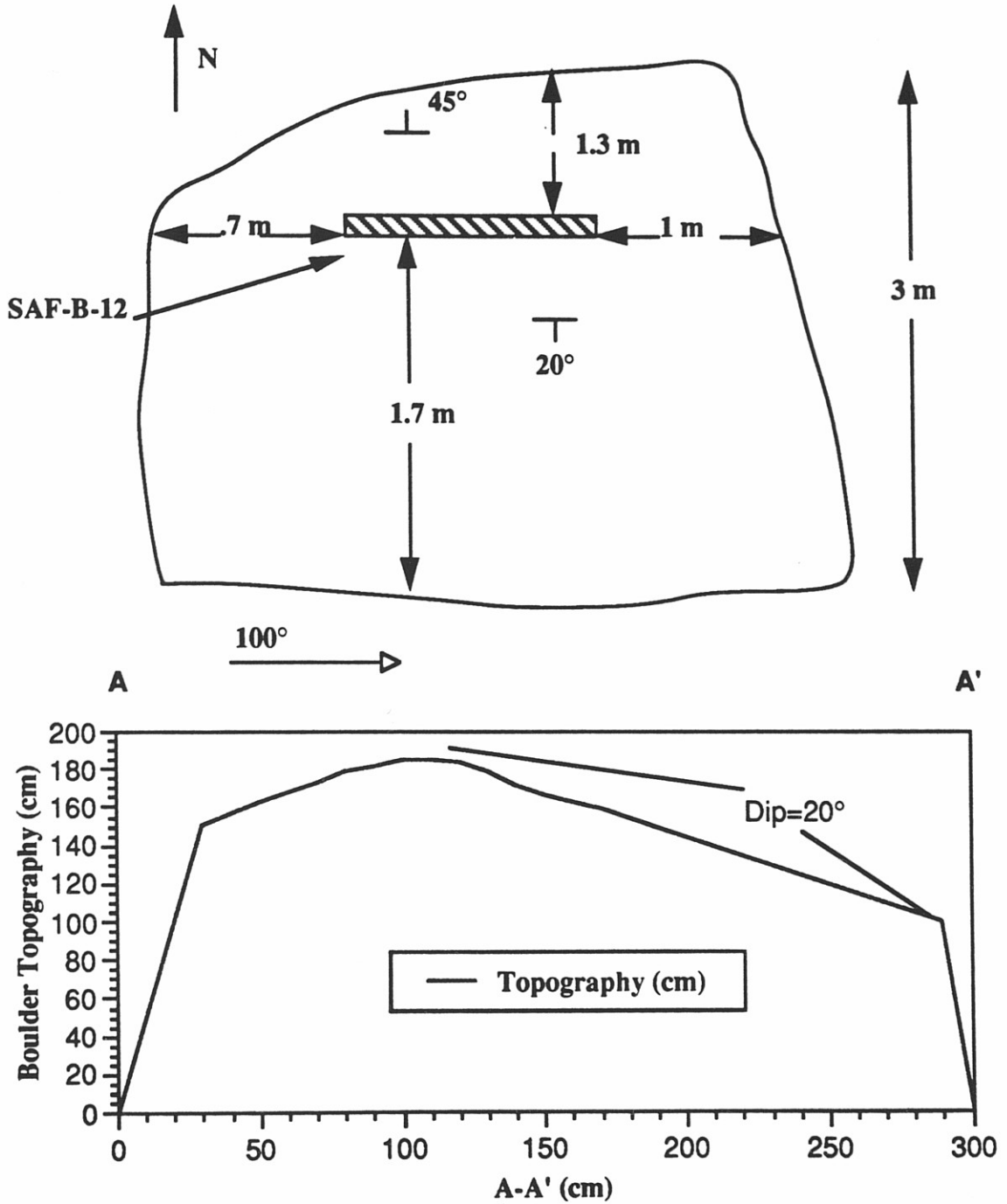


Figure 3.21 Schematic showing geometry and dimensions of glacial erratic. Also shown is location of sample 12



### Sample LD.: SPA-O-13,14

Samples 13 and 14 were taken from adjacent gneissic bedrock outcrops within the Allamuchy State Forest on the terminal moraine of the Laurentide ice sheet, in the Tranquility Quadrangle. The bedrock lithology for SPA-O-13 AND SPA-O-14 was a white-gray colored granitic gneiss. The gneiss was approximately 30% mafics and 70% felsics with about 20% quartz. The surfaces of the outcrops were moderately weathered and displayed a pebbly texture. It is not likely that the bedrock surface has eroded more than a few cm's, based on the preservation of the glacial contouring and the minimal amount of relief (<5 cm) on the sampled surfaces, as well as the absence of spalls. Sample 13 was taken from a planar surface on the side of what appeared to be a meltwater channel. The surface was striking at 176° and had an average dip of 31°. The adjacent channel was filled with boulders averaging 1m diameter. Sample 14 was taken from a horizontal, planar surface near the edge of a cliff. These two samples will allow a direct comparison for spatial variability, as well as a check for variability within differing sample geometries.

The vegetation is best described as mixed hardwood/softwood forest flora. The vegetation consists primarily of oaks, maples, blueberry bushes, and other scrubby plants and grasses. There is a soil horizon in most of the non-cliff, low slope areas and this could be a source of shielding for sample 14. It is unlikely, however, that sample 13 has ever had a soil cover due to the 30° slope. Surficial deposits are believed to be less than 2-3 m thick. Lichens are also present on about 5-10% of the bedrock surface.

Figure 3.23 Glacial moraine crest from which sample 14 was taken.





Figure 3.22. Glacially molded outcrop from which sample 13 was taken.



Figure 3.23 Glacially molded outcrop from which sample 14 was taken.



### **Sample I.D.: SPA-O-15,16**

Samples 15 and 16 were taken from an extensive bedrock ridge within the Picatinny Military Arsenal overlooking Picatinny Lake in the Dover Quadrangle. The strike of the bedrock is  $242^{\circ}$  and the beds are dipping almost vertically. The bedrock lithology for SPA-O-15 AND SPA-O-16 was a purple colored (Fe?) Silurian quartzite matrix with white quartz clasts ranging in size from 1mm to several cm's in diameter. The quartz clasts were shaved off, most likely from the overriding ice sheet, and they had less than 5mm relief. The bedrock surfaces sampled showed striations which were averaged at  $S02^{\circ}E$ . It is not likely that the bedrock surface has eroded more than a few mm's, based on the presence of glacial striations as well as evidence of glacial polish. Sample 15 was taken from a striated horizontal surface on the outcrop. The sample was extracted from the edge of a weathered, silty, less-resistant strata. Sample 16 was taken approximately 2 meters from SPA-O-15 from very hard quartzite on a surface dipping approximately  $30^{\circ}$  on the same outcrop. These two samples will allow a direct comparison between variable grain sizes, silt and sand, as well as a check for varying sample geometries in close proximity to one another.

Vegetation is very sparse on the ridge. The vegetation is primarily scrub oak, blueberry bushes, and other scrubby plants. There is shallow soil in most of the depressions. Lichens are also present on about 5-15% of the bedrock surface. It is unlikely that this outcrop has been forested since deglaciation, as the quartzite bedrock does not seem to support substantial vegetation, nor does it facilitate the formation of soil. It is also unlikely that snow accumulation will be a significant factor due to the fact that there is little vegetation and it is a ridge top on the edge of a steep gorge, with high wind and sun exposure.



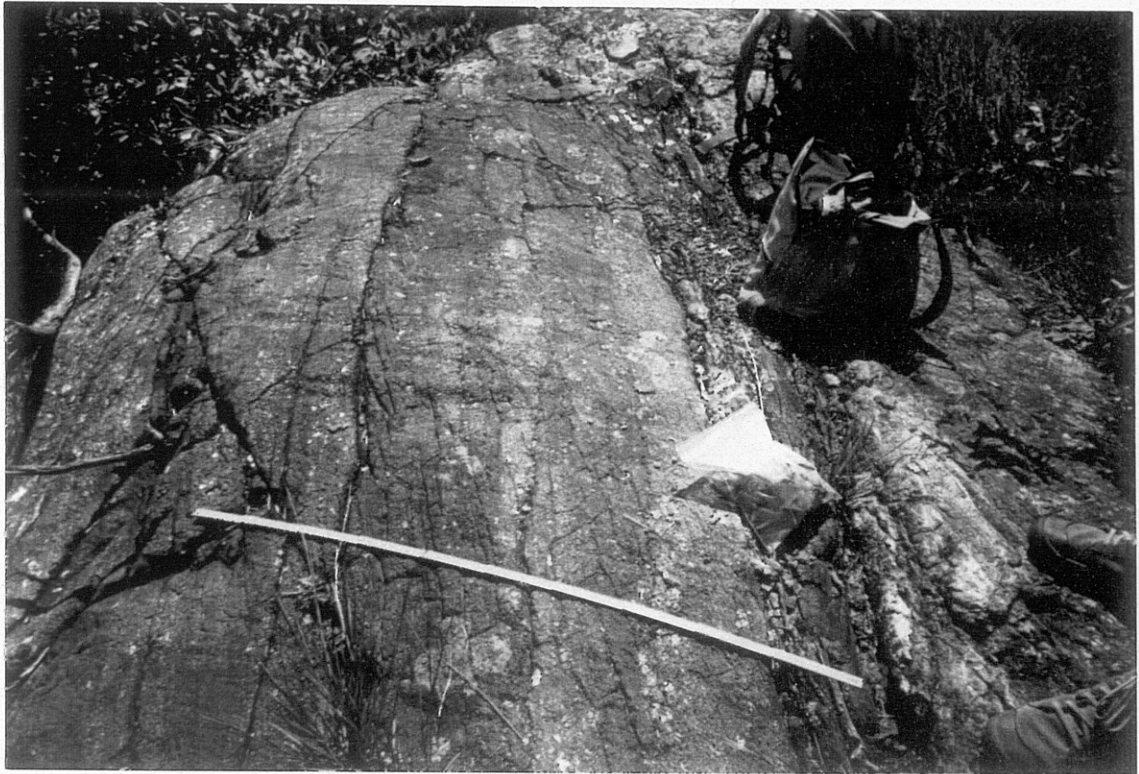


Figure 3.24. Striated outcrop. Samples 15 and 16 were taken from this surface.

**MAP VIEW**

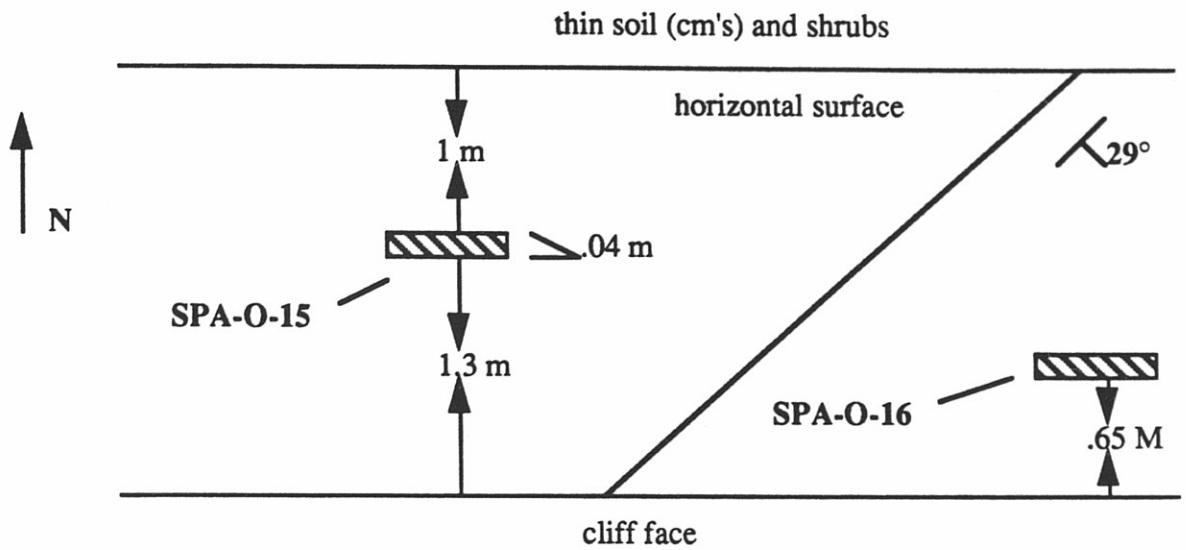


Figure 3.25 Schematic showing outcrop geometry and location of samples 15 and 16

Figure 3.26. Topographic map showing location of samples 1,2,3,4,5,6,9,15 and 16.

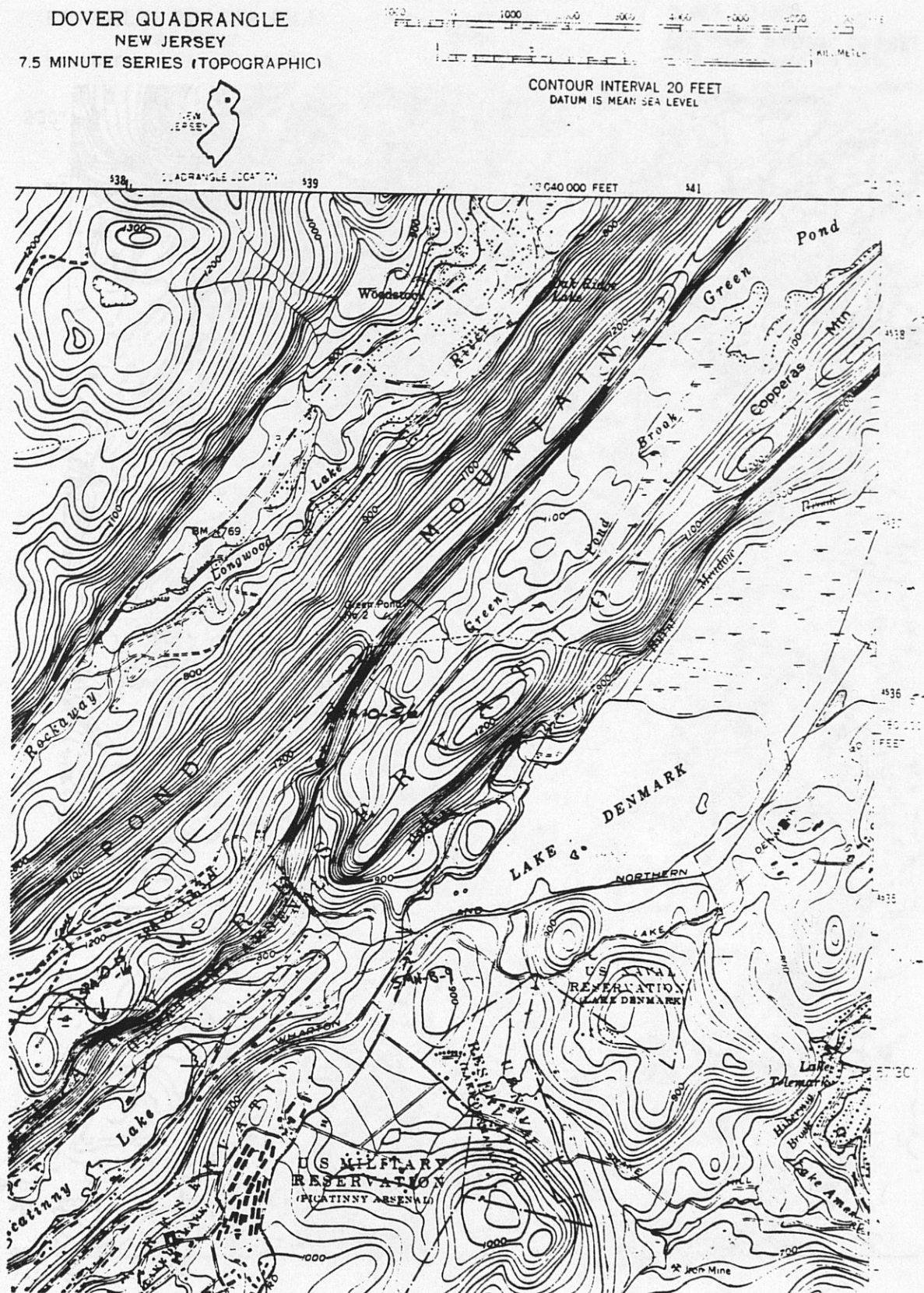




Figure 3.27. Topographic map showing location of samples 7 and 8.

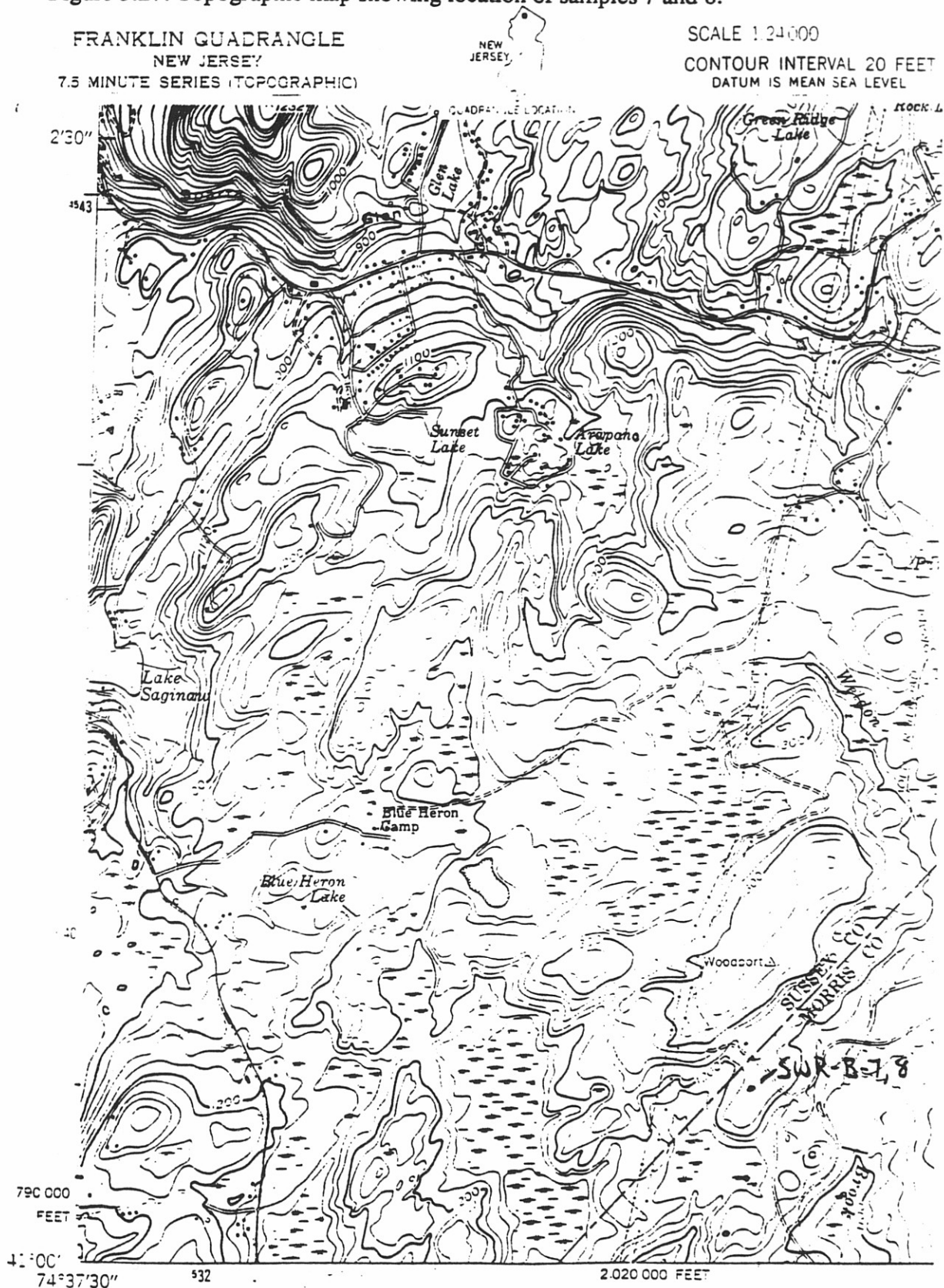
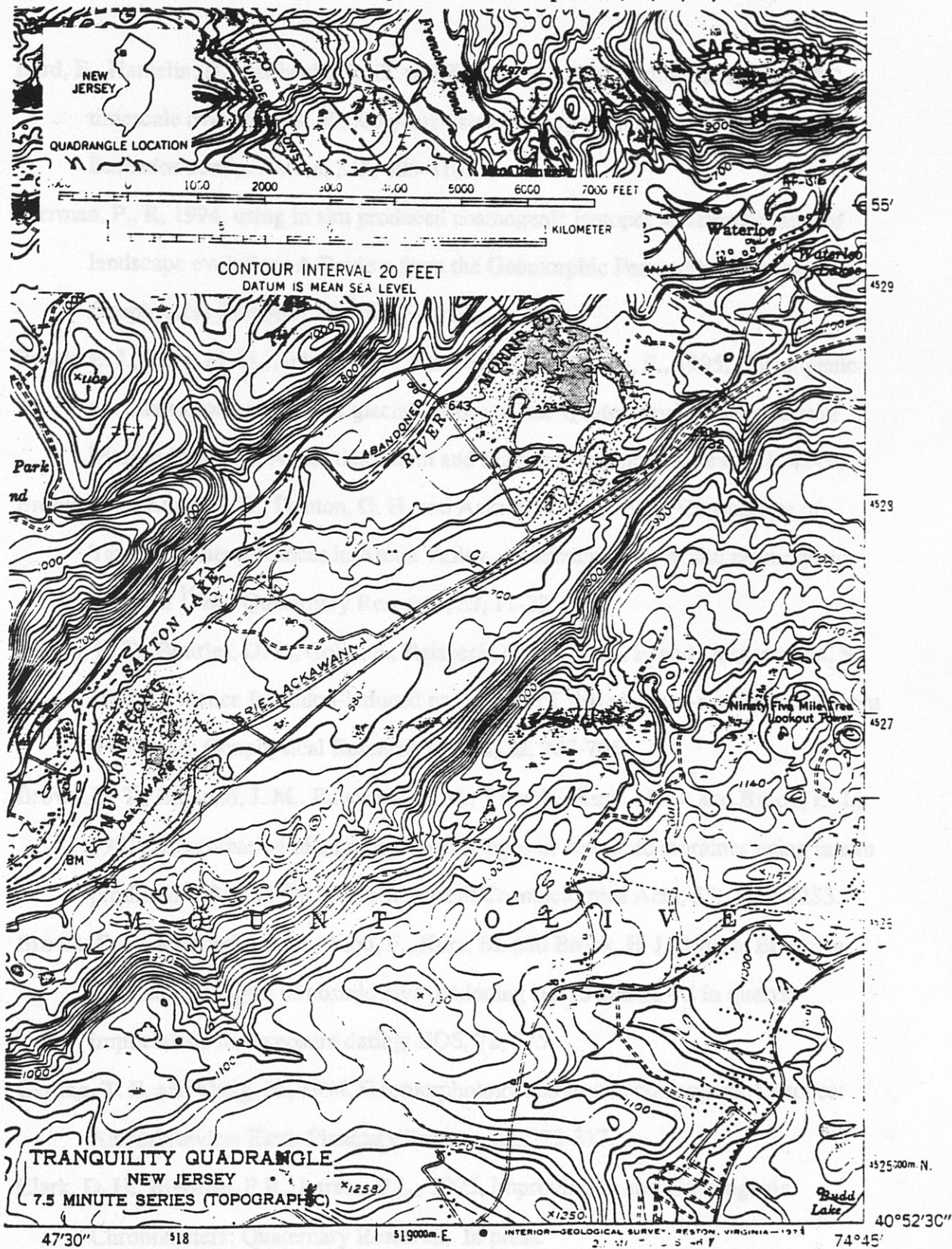


Figure 3.28. Topographic map showing location of samples 10, 11, 12, 13, and 14.



## REFERENCES CITED

- Bard, E., Hamelin, B., Fairbanks, R. G. and Zindler, A., 1990, Calibration of the  $^{14}\text{C}$  timescale over the past 30,000 years using mass spectrometric U-Th ages from Barbados corals: *Nature*, 345, 405-410.
- Bierman, P., R., 1994, using in situ produced cosmogenic isotopes to estimate rates of landscape evolution: A Review from the Geomorphic Perspective: *Journal of Geophysical Research*, 99, 13885-13896.
- Brook, E. J., Kurz, M. D., Ackert, R. P., Raisbeck, G. and Yiou, F., 1995, Cosmogenic nuclide exposure ages and glacial history of late Quaternary Ross Sea drift in McMurdo Sound, Antarctica: *Earth and Planetary Science Letters*, 131, 41-56.
- Brook, E. J., Kurz, M. D., Denton, G. H. and Ackert, R. P. J., 1993, Chronology of Taylor Glacier advances in Arena Valley, Antarctica using in situ cosmogenic  $^3\text{He}$  and  $^{10}\text{Be}$ : *Quaternary Research*, 39, 11-23.
- Brown, E. T., Bourles, D. L., Colin, F., Raisbeck, G. M., Yiou, F. and Desgarceaux, S., 1995, Evidence for muon-induced production of  $^{10}\text{Be}$  in near-surface rocks from the Congo: *Geophysical Research Letters*, 22, 703-706.
- Brown, E. T., Edmond, J. M., Raisbeck, G. M., Yiou, F., Kurz, M. D. and Brook, E. J., 1991a, Examination of surface exposure ages of Antarctic moraines using in situ produced  $^{10}\text{Be}$  and  $^{26}\text{Al}$ : *Geochimica et Cosmochimica Acta*, 55, 2269-2283.
- Brown, E. T., Raisbeck, G. M., Yiou, F., Kurz, M. and Brook, E. J., 1991b, Effective attenuation lengths of cosmic rays producing Be-10 and 26-Al in quartz: implications for exposure dating: *EOS*, 72, 575.
- Cerling, T. E. and Craig, H., 1994, Geomorphology and in-situ cosmogenic isotopes: *Annual Review Earth Planetary Science*, 22, 273-317.
- Clark, D. H., Bierman, P.R., Larsen, P.L., 1995, Improving *In situ* Cosmogenic Chronometers: *Quaternary Research*, In press.



- Connally, G.G. and Sirkin, L.A., 1973, Wisconsinan history of the Hudson-Champlain  
Lobe: The Wisconsinan Stage; Geological Society of America Memoir, 136, 47-  
69.
- Cotter, J. F., 1984, The minimum age of the Woodfordian deglaciation of northeastern  
Pennsylvania and northwestern New Jersey: Lehigh University, Ph.D.
- Dunne, T., Leopold, L.B., 1978, Water in Environmental Planning: W.H. Freeman and  
Company, New York.
- Elmore, D. and Phillips, F., 1987, Accelerator mass spectrometry for measurement of  
long-lived radioisotopes: Science, 236, 543-550.
- Evenson, E.B., Cotter, J.F., Ridge, J.C., Sevon, W.D., Sirkin, L., Stuckenrath, R., 1983,  
The mode and chronology of deglaciation of the Great Valley, northwestern New  
Jersey: Geological Society of America Abstracts with Programs, 15, 133.
- Evenson, E.B. and Gosse, J., 1993, Application of in situ produced cosmogenic nuclide  
exposure ages to reconstruct glacial histories at the Pinedale type locality,  
Wyoming: Geological Society of America Abstracts with Programs, 25, A308.
- Fabryka-Martin, J. T., 1988, Production of radionuclides in the earth and their  
hydrogeologic significance, with emphasis on Chlorine-36 and Iodine-129:  
University of Arizona, Ph.D.
- Finkle, R. C. and Suter, M., 1993, AMS In the Earth Sciences: Technique and  
Applications: Advances in Analytical Geochemistry, 1, 1-114.
- Friedlander, M. W., 1989, Cosmic Rays: Harvard, Cambridge, 160.
- Fullerton, D.S., 1986, Stratigraphy and correlation of glacial deposits from Indiana to  
New York and New Jersey: Quaternary Science Reviews, 5, 23-37.
- Gosse, J. C., Klein, J., Evenson, E. B., Lawn, B. and Middleton, R., 1995, Beryllium-10  
dating of the Duration and Retreat of the Last Pinedale Glacial Sequence: Science,  
268, 1329-1333.

- Harmon, K. P., 1968, Late Pleistocene forest succession in northern New Jersey: Rutgers University, Ph.D. dissertation
- Johnson, R. A. and Wichern, D. W., 1982, Applied Multivariate Statistical Analysis: Prentice-Hall, Inc., .
- Klein, J., Giegengack, R., Middleton, R., Sharma, P., Underwood, J. R. and Weeks, R. A., 1986, Revealing histories of exposure using in situ produced  $^{26}\text{Al}$  and  $^{10}\text{Be}$  in Libyan desert glass: Radiocarbon, 28, 547-555.
- Kohl, C. P. and Nishiizumi, K., 1992, Chemical isolation of quartz for measurement of *in-situ* -produced cosmogenic nuclides: Geochimica et Cosmochimica Acta, 56, 3583-3587.
- Kurz, M. D., 1986, *In situ* production of terrestrial cosmogenic helium and some applications to geochronology: Geochimica et Cosmochimica Acta, 50, 2855-2862.
- Kurz, M. D., Colodner, D., Trull, T. W., Moore, R. and O'Brien, K., 1990, Cosmic ray exposure dating with in situ produced cosmogenic  $^3\text{He}$ : results from young Hawaiian lava flows: Earth and Planetary Science Letters, 97, 177-189.
- Lal, D., 1987, Cosmogenic isotopes produced in situ in terrestrial solids: Nuclear Instruments and Methods in Physics Research, B29, 238-245.
- Lal, D., 1991, Cosmic ray labeling of erosion surfaces: *In situ* production rates and erosion models: Earth and Planetary Science Letters, 104, 424-439.
- Lal, D. and Arnold, J. R., 1985, Tracing quartz through the environment: Proceedings of the Indian Academy of Science (Earth and Planetary Science), 94, 1-5.
- Larsen, P. L., Bierman, P. R. and Caffee, M., 1995, Cosmogenic  $^{26}\text{Al}$  chronology of the Late Wisconsinan glacial maximum in North-Central New Jersey: GSA Abstracts with Programs, 27, 63.

- Mazaud, A., Laj, C., Bard, E., Arnold, M. and Tric, E., 1991, Geomagnetic field control of  $^{14}\text{C}$  production over the last 80 ky: implications for the radiocarbon time scale: *Geophysical Research Letters*, 18, 1885-1888.
- Matsch, C.L., 1987, retreat of the southern margin of the Laurentide ice sheet: *International Union for Quaternary Research*, XII, 221.
- McElhinny, M. W. and Senanayake, W. E., 1982, Variations in the geomagnetic dipole 1: the past 50,000 years: *Journal of Geomagnetism and Geoelectricity*, 34, 39-51.
- Mendenhall, W., 1969, *Introduction to Probability and Statistics*, Wadsworth Publishing Company, Inc., Belmont, California, 393.
- Merrill, R.T., McElhinny, M.W., 1983, *The Earth's Magnetic Field: Its History, Origin and Planetary Perspective*: William L. Donn (ed.) Academic Press, New York.
- Merrington, M. and Thompson, C. M., 1943, Tables of Percentage Points of the Inverted Beta (F) Distribution: *Biometrika*, 33, 73-88.
- Meynadier, L., Valet, J., Weeks, R., Shackleton, N. and Hagee, V., 1992, Relative geomagnetic intensity of the field during the last 140 ka: *Earth and Planetary Science Letters*, 114, 39-57.
- Middleton, R. and Klein, J., 1987,  $^{26}\text{Al}$ : measurement and applications: *Philosophical Transactions of the Royal Society of London*, A 323, 121-143.
- Monaghan, M. C., McKean, J., Dietrich, W. E. and Klein, J., 1992,  $^{10}\text{Be}$  Chronometry of bedrock-to-soil conversion rates: *Earth and Planetary Science Letters*, 111, 483-492.
- Nishiizumi, K., Kohl, C. P., Arnold, J. R., Dorn, R. I., Klein, J., Fink, D., Middleton, R. and Lal, D., 1993, Role of in situ cosmogenic nuclides  $^{10}\text{Be}$  and  $^{26}\text{Al}$  in the study of diverse geomorphic processes: *Earth Surface Processes and Landforms*, 18, 407-425.



- Nishiizumi, K., Kohl, C. P., Arnold, J. R., Klein, J., Fink, D. and Middleton, R., 1991a, Cosmic ray produced  $^{10}\text{Be}$  and  $^{26}\text{Al}$  in Antarctic rocks: exposure and erosion history: *Earth and Planetary Science Letters*, 104, 440-454.
- Nishiizumi, K., Kohl, C. P., Shoemaker, E. M., Arnold, J. R., Klein, J., Fink, D. and Middleton, R., 1991b, *In situ*  $^{10}\text{Be}$ - $^{26}\text{Al}$  exposure ages at Meteor Crater, Arizona: *Geochimica et Cosmochimica Acta*, 55, 2699-2703.
- Nishiizumi, K., Lal, D., Klein, J., Middleton, R. and Arnold, J. R., 1986, Production of  $^{10}\text{Be}$  and  $^{26}\text{Al}$  by cosmic rays in terrestrial quartz *in situ* and implications for erosion rates: *Nature*, 319, 134-136.
- Nishiizumi, K., Winterer, E. L., Kohl, C. P., Klein, J., Middleton, R., Lal, D. and Arnold, J. R., 1989, Cosmic ray production rates of  $^{10}\text{Be}$  and  $^{26}\text{Al}$  in quartz from glacially polished rocks: *Journal of Geophysical Research*, 94, 17907-17915.
- Oldale, R.N., Stone, B.D., 1987, The Late Wisconsinan glaciation in southern New England: International Union for Quaternary Research XII<sup>th</sup> International Congress, 234.
- Phillips, F. M., Zreda, M. G., Smith, S. S., Elmore, D., Kubik, P. W. and Sharma, P., 1990, Cosmogenic Chlorine-36 chronology for glacial deposits at Bloody Canyon, eastern Sierra Nevada: *Science*, 248, 1529-1532.
- Raisbeck, G. M., Yiou, F., Klein, J. and Middleton, R., 1983, Accelerator mass spectrometer measurement of cosmogenic  $^{26}\text{Al}$  in terrestrial and extraterrestrial matter: *Nature*, 301, 690-692.
- Sarda, P., Staudacher, T., Allegre, C. and Lecomte, A., 1993, Cosmogenic neon and helium at Reunion: measurement of erosion rate: *Earth and Planetary Science Letters*, 119, 405-417.
- Sharma, P. and Middleton, R., 1989, Radiogenic production of  $^{10}\text{Be}$  and  $^{26}\text{Al}$  in uranium and thorium ores: Implications for studying terrestrial samples containing low levels of  $^{10}\text{Be}$  and  $^{26}\text{Al}$ : *Geochimica et Cosmochimica Acta*, 53, 709-716.

- Sirkin, L.A., 1977, Late Pleistocene vegetation and environments in the middle Atlantic region; in Newman, W.S. and Salwen, B., Amerinds and their paleoenvironments in northeastern North America: New York Academy of Science Annals, 288, 206-217.
- Smith, N. D., 1970, The Braided Stream Depositional Environment: Comparison of the Platte River with Some Silurian Clastic Rocks, North-Central Appalachians: Geological Society of America Bulletin, 81, 2993-3014.
- Stanford, S. D., 1993, Late Wisconsinan Glacial Geology of the New Jersey Highlands: Northeastern Geology, 15, 210-223.
- Stone, B.D., Borns, H.W., 1986, Pleistocene glacial and interglacial stratigraphy of New England, Long Island, and adjacent Georges Bank and Gulf of Maine: Quaternary Science Reviews, 5, 39-52.
- Stuiver, M., Braziunas, T. F., Becker, B. and Kromer, B., 1991, Climatic, Solar, Oceanic, and Geomagnetic Influences on Late-Glacial and Holocene Atmospheric  $^{14}\text{C}/^{12}\text{C}$  Change: Quaternary Research, 35, 1-24.
- Stuiver, M., and Reimer, P. J., 1993, Extended  $^{14}\text{C}$  database and revised CALIB radiocarbon calibration program, Radiocarbon, 35, 215-230.
- Tric, E., Valet, J. P., Tucholka, P., Paterne, m., Labeyrie, L., Guichard, F., Tauxe, L. and Fontugne, M., 1992, Paleointensity of the geomagnetic field during the last 80,000 years: Journal of Geophysical Research, 97, 9337-9351.
- Widmer, K., 1964, The Geology and Geography of New Jersey: The New Jersey Historical Series, D. Van Nostrand Company, Inc., Princeton, New Jersey, 19, 193.

## APPENDIX A. BATCH DATA

Appendix A contains original lab data as well as ICP assays which are necessary to reproduce the results of this thesis. Samples were run in batches of 8, one of which was a process blank. For each batch, there are four tables of data. The first table contains original lab data such as sample weight and carrier amounts. The second table contains the raw ICP data. Each sample was analyzed three times, along with our own 25ppm standard, on the ICP in the Plant & Soil Science Department at the University of Vermont. The third table contains the reduced ICP data. The three assays for each sample were averaged and the standard deviation calculated. The fourth table contains the reduced data which is used to calculate cosmogenic isotope abundances. This includes the concentrations of aluminum and beryllium in the quartz. The aluminum is assumed to be entirely  $^{27}\text{Al}$  and the beryllium is assumed to be entirely  $^9\text{Be}$ .

Sample Data  
Batch # 14  
Start date 11/6/94

COLUMAN SAMPLE QZ1.WT AL.CARRIER BE.CARRIER

USED	SPRINK	B	(1000 ppm)	(1500 ppm)
A	BLANK	20.014	0	0.239
G	SPRINK	20.123	0	0.239
C	SPRINK 2	20.713	0	0.268
E	SPRINK	20.043	0	0.248
B	SPRINK 4	15.655	0	0.235
D	SPRINK 5	18.05	0	0.237
F	SPRINK 10	17.017	0	0.238
H	SPRINK 13			



Sample Data

Batch # 14  
 start date 11/8/94

checked 3/29/95

COLUMN USED	SAMPLE	QTZ WT grams	AL CARRIER g (1000 ppm)	BE CARRIER g (1000 ppm)	ADD ACID grams	INTO ICP grams	TOTAL ICP grams	HF ADDED
A	BLANK		2.003	0.432	10.667	0.979	5.7023	10
G	smsap	20.014	0	0.239	9.665	0.994	6.699	80
C	mhbq 2	20.123	0	0.233	9.327	0.947	6.124	80
E	ybg2	20.713	0	0.266	11.648	0.916	5.808	83
B	swr b-8	20.043	0	0.243	9.689	0.88	6.127	80
D	smh b 9	15.655	0	0.235	10.526	0.902	6.19	63
F	saf b 10	18.05	0	0.233	10.55	0.954	6.083	73
H	saf o 13	17.057	0	0.238	10.21	0.971	5.433	68

**Sample Data**

**Batch #** 8  
**start date** October 5  
 1994

**checked 3/29/95**

SAMPLE	QTZ WT	AL CARRIER	BE CARRIER	ADD ACID	INTO ICP	TOTAL HF ADDED
	grams	g	g	grams	grams	ICP grams
BLANK	0	1.911	0.416	10.83	0.955	6.323
DB 92-6 (250-500)	12.25	0	0.411	11.841	0.998	6.406
DB 92-3 (250-500)	17.468	0	0.414	10.349	1.006	6.648
DB 92-1 (500-750)	20.157	0	0.411	9.433	0.723	6.755
SPA-0-5	11.885	0	0.409	11.032	0.951	6.66
SPA-0-6	20.604	0	0.41	10.435	0.952	6.544
DC-9	10.508	0	0.411	9.906	0.909	6.357
DC-29	17.994	0	0.434	11.389	0.975	6.877

**RAW ICP DATA (Based on 1N acid Blank and 50 ppm Acid Standard)**

Batch #	8								
	Be-1	Al-1	Be-2	Al-2	Be-3	Al-3	Be-3	Al-3	Al-3
BLANK		5.53	25.9	5.57	26.1	5.57	26.4	5.57	26.4
DB 92-6 (250-500)		5.4	8.87	5.45	8.92	5.36	8.82	5.36	8.82
DB 92-3 (250-500)		5.76	12.8	5.84	12.9	5.78	12.9	5.78	12.9
DB 92-1 (500-750)		4.55	10.2	4.45	10.1	4.46	10.1	4.46	10.1
25 ppm stan		28	26	28.2	26.2	28.3	26.4	28.3	26.4
SPA-0-5		5.08	20.8	5.06	20.9	5.08	20.8	5.08	20.8
SPA-0-6		5.02	33.2	5.05	33.4	5.21	34.2	5.21	34.2
DC-9		5.71	8.05	5.8	8.01	5.85	8.3	5.85	8.3
DC-29		5.18	36.6	5.22	36.8	5.33	37.7	5.33	37.7
25 ppm stan		28.2	26.3	28.3	26.4	29	26.7	29	26.7



BATCH	8	Al (avg)	+/- 1s	Be (avg)	+/- 1s
BLANK		26.13	0.25	5.56	0.02
DB 92-6 (250-500)		8.87	0.05	5.40	0.05
DB 92-3 (250-500)		12.87	0.06	5.79	0.04
DB 92-1 (500-750)		10.13	0.06	4.49	0.06
25 ppm stan		26.20	0.20	28.17	0.15
		(25.45) = real value		(28.12) = real value	
SPA-0-5		20.83	0.06	5.07	0.01
SPA-0-6		33.60	0.53	5.09	0.10
DC-9		8.12	0.16	5.79	0.07
DC-29		37.03	0.59	5.24	0.08
25 ppm stan		26.47	0.21	28.50	0.44
		(25.45) = real value		(28.12) = real value	

Batch # 8

Al in ICP Aliquot	Total Al in sample	Total Al in corrected for Be yield	Al added as carrier	Al from quartz	Al in quartz	Al Yield	Al Yield
(mc grams)	(mc grams) by ICP	(mc grams)	(mc grams)	(mc grams)	(ppm)	(ICP based) (%)	(Be- corrected) (%)
160.51	1820.24	1903.62	1911.00	-7.38		95.25	99.61
55.19	654.87	656.46	0.00	656.46	53.59		
83.09	854.76	894.63	0.00	894.63	51.22		
66.49	867.51	903.19	0.00	903.19	44.81		
133.42	1547.73	1636.84	0.00	1636.84	137.72		
211.43	2317.54	2635.96	0.00	2635.96	127.93		
49.64	540.92	562.07	0.00	562.07	53.49		
244.90	2860.63	2987.40	0.00	2987.40	166.02		

**RAW ICP DATA (Based on 1N acid Blank and 50 ppm Acid Standard)**

Batch #	14								
	Be-1	Al-1	Be-2	Al-2	Be-3	Al-3	Be-3	Al-3	Al-3
BLANK		7.19	33.70	7.23	34.00	7.16	33.70		
smsap		3.69	28.70	3.70	28.90	3.62	28.60		
mhbq 2		3.91	13.80	3.94	13.90	3.85	13.80		
ybg2		3.71	18.50	3.72	18.50	3.77	18.40		
25 ppm stan		28.00	26.50	28.00	26.90	28.20	26.80		
swr b-8		3.43	14.70	3.40	14.80	3.48	15.10		
smh b 9		3.29	28.70	3.23	27.90	3.22	28.30		
saf b 10		3.48	23.30	3.45	22.90	3.44	23.30		
saf o 13		4.08	25.80	4.14	26.20	4.12	26.30		
25 ppm stan		28.40	26.00	28.40	26.10	28.40	26.40		



BATCH	14	Al (avg)	+/- 1s	Be (avg)	+/- 1s
BLANK		33.8	0.2	7.19	0.04
smsap		28.7	0.2	3.67	0.04
mhbg 2		13.8	0.1	3.90	0.05
ybg2		18.5	0.1	3.73	0.03
25 ppm stan		26.73	0.208	28.07	0.12
		(25.45) = real value		(28.12) = real value	
swr b-8		14.9	0.2	3.44	0.04
smh b 9		28.3	0.4	3.25	0.04
saf b 10		23.2	0.2	3.46	0.02
saf o 13		26.1	0.3	4.11	0.03
25 ppm stan		26.17	0.208	28.40	0.000
		(25.45) = real value		(28.12) = real value	
				Al/Be	
				0.952	
				(0.905) = real value	
				Al/Be	
				0.921	
				(0.905) = real value	

Batch # 14

Al in ICP Aliquot (mc grams)	Total Al in sample by ICP (mc grams)	Total Al in corrected for as carrier Be yield (mc grams)	Al added as carrier (mc grams)	Al from quartz (mc grams)	Al in quartz (ppm)	Al Yield (ICP based) (%)	Al Yield (Be-corrected) (%)
BLANK	183.49	1999.22	1928.77	2003.00	-74.23	99.81	96.29
smsap	183.24	1781.75	1777.98	0.00	1777.98	88.84	
mhbq 2	80.65	794.31	785.29	0.00	785.29	39.02	
ybg2	102.11	1298.39	1250.21	0.00	1250.21	60.36	
swr b-8	88.59	975.43	1032.58	0.00	1032.58	51.52	
smh b 9	170.38	1988.26	2012.14	0.00	2012.14	128.53	
saf b 10	137.06	1515.74	1533.93	0.00	1533.93	84.98	
saf o 13	137.92	1450.19	1483.43	0.00	1483.43	86.97	
Be in ICP Aliquot (mc grams)	Total Be in sample (mc grams)	Be added as carrier (mc grams)	Be Yield (%)				
BLANK	41.10	447.78	432	103.65			
smsap	24.63	239.51	239	100.21			
mhbq 2	23.93	235.68	233	101.15			
ybg2	21.72	276.25	266	103.85			
swr b-8	20.85	229.55	243	94.47			
smh b 9	19.90	232.21	235	98.81			
saf b 10	20.82	230.24	233	98.81			
saf o 13	22.13	232.67	238	97.76			
average				99.84			
high				103.85			
low				94.47			

checked 3/29/95

start date 12/9/94

Batch # 20

COLUMN USED	SAMPLE	QTZ WT grams	AL CARRIER g (1000 ppm)	BE CARRIER g (1000 ppm)	ADD ACID grams	INTO ICP grams	TOTAL ICP grams	HF ADDED
A	BLANK		2.075	0.595	8.640	1.010	6.136	10.000
C	DC-35	31.543	0.000	0.258	6.320	1.008	6.336	125.000
E	YBG-3	25.004	0.000	0.255	6.890	1.010	6.617	100.000
G	LUI-20	22.558	0.000	0.260	7.700	1.009	6.418	90.000
B	SPA-O-5	28.980	0.000	0.254	6.580	0.972	6.471	115.000
D	SPA-O-6	30.189	0.000	0.258	9.530	1.041	6.208	120.000
F	SAF-B-12	28.232	0.497	0.391	8.180	0.971	6.452	120.000
H	SAF-O-14	27.680	0.512	0.243	7.500	1.040	6.368	115.000



**RAW ICP DATA (Based on 1N acid Blank and 50 ppm Acid Standard)**

Batch #	20	Be-1	Al-1	Be-2	Al-2	Be-3	Al-3	
BLANK			10.30	38.80	11.00	42.50	11.30	43.10
DC-35			5.13	133.00	5.57	144.00	5.56	145.00
YBG-3			4.35	38.90	4.70	41.00	4.77	41.40
LUI-20			4.05	53.60	4.38	58.10	4.41	57.80
25 ppm stan			27.90	26.80	30.30	29.20	30.80	28.90
SPA-O-5								
SPA-O-6								
SAF-B-12			5.95	58.90	5.99	59.50	5.94	59.30
SAF-O-14			3.98	60.30	3.96	59.60	3.82	59.70
25 ppm stan			28.00	26.60	27.70	26.60	26.80	26.00

BATCH	20	Al (avg)	+/- 1s	Be (avg)	+/- 1s
BLANK		41.5	2.3	10.87	0.51
DC-35		140.7	6.7	5.42	0.25
YBG-3		40.4	1.3	4.61	0.23
LUI-20		56.5	2.5	4.28	0.20
25 ppm stan		28.30	1.308	29.67	1.55
		(25.45) = real value		(28.12) = real value	
SPA-O-5	No Data	No Data	No Data	No Data	No Data
SPA-O-6	No Data	No Data	No Data	No Data	No Data
SAF-B-12		59.2	0.3	5.96	0.03
SAF-O-14		59.9	0.4	3.92	0.09
25 ppm stan		26.40	0.346	27.50	0.624
		(25.45) = real value		(28.12) = real value	

Al/Be  
0.954  
(0.905) = real value

Al/Be  
0.960  
(0.905) = real value

**Batch # 20**

	Al in ICP Aliquot (mc grams)	Total Al in sample by ICP (mc grams)	Total Al in corrected for Be yield (mc grams)	Al added as carrier (mc grams)	Al from quartz (mc grams)	Al in quartz (ppm)	Al Yield (ICP based) (%)	Al Yield (Be-corrected) (%)
BLANK	229	1957	2154	2075	79		94.33	103.81
DC-35	802	5025	6353	0	6353	201.40		
YBG-3	241	1641	2123	0	2123	84.93		
LUI-20	326	2489	3256	0	3256	144.36		
SPA-O-5	No Data	No Data	No Data	0	No Data	No Data		
SPA-O-6	No Data	No Data	No Data	0	No Data	No Data		
SAF-B-12	368	3104	3664	497	3167	112.16		
SAF-O-14	368	2650	3499	512	2987	107.90		
								average 80.69
								high 90.87
								low 75.75
BLANK	63	541	595	90.87				
DC-35	33	204	258	79.10				
YBG-3	29	197	255	77.30				
LUI-20	26	199	260	76.42				
SPA-O-5	No Data	No Data	No Data	No Data				
SPA-O-6	No Data	No Data	No Data	No Data				
SAF-B-12	39	331	391	84.72				
SAF-O-14	26	184	243	75.75				



start date 1/6/95 checked bierman 3/22/95

Batch # 23

SAMPLE	QTZ WT grams	AL CARRIER g (1000 ppm)	BE CARRIER g (1000 ppm)	ADD ACID grams	INTO ICP grams	TOTAL ICP grams
BLANK	0.000	2.966	0.252	10.610	1.006	6.649
lfp-16	16.134	0.987	0.250	10.950	0.968	6.820
lpf-6	23.790	0.996	0.252	10.520	1.018	6.623
spa-0-2 X	29.785	0.000	0.270	10.260	1.013	6.661
swrb-8 X	29.856	0.000	0.252	9.940	1.015	6.482
smh b-9 X	32.694	0.000	0.254	10.690	1.013	6.770
saf b 11	22.364	0.000	0.249	8.820	1.003	6.752
saf 0 13 X	25.210	0.000	0.250	9.640	1.015	6.823

**RAW ICP DATA (Based on 1N acid Blank and 50 ppm Acid Standard)**

Batch # 23	Batch # 23					
	Be-1	Al-1	Be-2	Al-2	Be-3	Al-3
BLANK	3.46	41.10	3.46	41.10	3.46	41.60
lfp-16	3.19	36.50	3.16	36.40	3.14	36.40
lpf-6	3.52	116.00	3.46	115.00	3.48	115.00
spa-0-2 X	3.74	104.00	3.75	103.00	3.74	103.00
25 ppm stan	28.00	26.80	28.10	26.60	27.90	26.80
swrb-8 X	3.80	28.10	3.79	28.20	3.78	28.10
smh b-9 X	3.35	65.50	3.34	65.70	3.37	65.50
saf b 11	4.12	33.30	4.05	32.90	4.08	33.20
saf 0 13 X	3.72	37.40	3.71	37.10	3.75	37.60
25 ppm stan	27.50	26.60	27.50	26.40	27.80	26.70

BATCH23

	Al (avg)	+/- 1s	Be (avg)	+/- 1s
BLANK	41.27	0.29	3.46	0.00
lfp-16	36.43	0.06	3.16	0.03
lpf-6	115.33	0.58	3.49	0.03
spa-0-2 X	103.33	0.58	3.74	0.01
25 ppm stan	26.73	0.12	28	0.1
	(25.45) = real value		(28.12) = real value	
swrb-8 X	28.13	0.06	3.79	0.01
smh b-9 X	65.57	0.12	3.35	0.02
saf b 11	33.13	0.21	4.08	0.04
saf 0 13 X	37.37	0.25	3.73	0.02
25 ppm stan	26.57	0.15	27.60	0.17
	(25.45) = real value		(28.12) = real value	
			Al/Be	
			0.95	
			(0.905) = real value	
			Al/Be	
			0.96	
			(0.905) = real value	



Batch # 23

Al in ICP Aliquot (mc grams)	Total Al in sample by ICP (mc grams)	Total Al in corrected for as carrier Be yield (mc grams)	Al added (mc grams)	Al from quartz (mc grams)	Al in quartz (ppm)	Al Yield (ICP based) (%)	Al Yield (Be-corrected) (%)
BLANK	261.21	2754.91	2849.06	2966	-116.94	92.88	96.06
lfp-16	236.55	2675.82	2729.43	987	1742.43	108.00	
lpf-6	727.18	7514.71	7901.73	996	6905.73	290.28	
spa-0-2 X	655.26	6636.70	7065.18	0	7065.18	237.21	
swrb-8 X	174.70	1710.81	1758.84	0	1758.84	58.91	
smh b-9 X	425.23	4487.36	4669.65	0	4669.65	142.83	
saf b 11	214.31	1884.59	1899.74	0	1899.74	84.95	
saf 0 13 X	244.24	2319.64	2356.94	0	2356.94	93.49	
Be in ICP Aliquot (mc grams)	Total Be in sample (mc grams)	Be added as carrier (mc grams)	Be added as carrier Yield (%)				
BLANK	23.10	243.67	252	96.70			
lfp-16	21.67	245.09	250	98.04			
lpf-6	23.19	239.66	252	95.10			
spa-0-2 X	25.04	253.63	270	93.94			
swrb-8 X	25.03	245.12	252	97.27			
smh b-9 X	23.13	244.08	254	96.10			
saf b 11	28.09	247.01	249	99.20			
saf 0 13 X	25.91	246.04	250	98.42			
				average	96.84		
				high	99.20		
				low	93.94		

start date 3/1/95 checked 3/29/95

Batch # 32

COLUMN USED	SAMPLE	QTZ WT grams	AL CARRIER g (1000 ppm)	BE CARRIER g (1000 ppm)	ADD ACID grams	INTO ICP grams	TOTAL ICP grams	HF ADDED
C	BLANK		0.966	11.300	11.030	0.969	6.615	10.000
A	SPA-O-3	24.130	0.000	12.200	12.200	1.021	6.153	100.000
B	SPA-O-1	28.918	0.000	13.610	13.610	1.013	6.006	115.000
G	SPA-O-4	29.862	0.000	11.980	11.980	1.008	6.414	120.000
D	SWR-B-7	21.786	0.943	14.340	14.340	1.041	7.377	85.000
E	SAF-B-10	29.877	0.915	10.430	10.430	0.967	6.762	120.000
H	SPA-O-15	28.038	0.000	11.220	11.220	1.005	6.680	120.000
F	SPA-O-16	29.972	0.000	11.100	11.100	1.028	6.092	120.000

**RAW ICP DATA (Based on 1N acid Blank and 50 ppm Acid Standard)**

Batch #	32								
	Be-1	Al-1	Be-2	Al-2	Be-3	Al-3	Be-3	Al-3	Al-3
BLANK	-	4.33	13.50	4.40	13.40	4.29	13.50	4.29	13.50
SPA-O-3	-	4.26	72.00	4.34	70.50	4.25	69.80	4.25	69.80
SPA-O-1	-	3.83	82.80	3.84	81.90	3.78	81.50	3.78	81.50
SPA-O-4	-	-	-	-	-	-	-	-	-
25 ppm stan	-	28.80	26.90	28.80	26.50	28.60	26.60	28.60	26.60
SWR-B-7	-	2.98	26.10	2.99	25.60	2.94	25.90	2.94	25.90
SAF-B-10	-	4.33	52.70	4.31	51.70	4.28	52.20	4.28	52.20
SPA-O-15	-	4.14	85.20	4.08	83.90	4.05	84.70	4.05	84.70
SPA-O-16	-	-	-	-	-	-	-	-	-
25 ppm stan	-	28.50	26.40	27.90	25.70	27.60	25.90	27.60	25.90



REDUCED ICP DATA

BATCH32

	Al (avg)	+/- 1s	Be (avg)	+/- 1s
BLANK	13.47	0.06	4.34	0.06
SPA-O-3	70.77	1.12	4.28	0.05
SPA-O-1	82.07	0.67	3.82	0.03
SPA-O-4	0	0	0	0
25 ppm stan	26.67	0.21	28.73	0.12
	(25.45) = real value		(28.12) = real value	
		Al/Be		
		0.93		
		(0.905) = real value		
SWR-B-7	25.87	0.25	2.97	0.03
SAF-B-10	52.20	0.50	4.31	0.03
SPA-O-15	84.60	0.66	4.09	0.05
SPA-O-16	0	0	0	0
25 ppm stan	26.00	0.36	28.00	0.46
	(25.45) = real value		(28.12) = real value	
		Al/Be		
		0.93		
		(0.905) = real value		

**Batch # 32**

	Al in ICP Aliquot (mc grams)	Total Al in sample by ICP (mc grams)	Total Al in corrected for Be yield (mc grams)	Al added as carrier (mc grams)	Al from quartz (mc grams)	Al in quartz (ppm)	Al Yield (ICP based) (%)	Al Yield (Be- corrected) (%)
BLANK	85	968	935	966	-31		100.18	96.79
SPA-O-3	416	4966	5011	0	5011	207.65		
SPA-O-1	470	6320	6521	0	6521	225.51		
SPA-O-4	0	0	#DIV/0!	0	#DIV/0!	#DIV/0!		
SWR-B-7	187	2573	2598	943	1655	75.95		
SAF-B-10	346	3727	3650	915	2735	91.56		
SPA-O-15	553	6176	6230	0	6230	222.19		
SPA-O-16	0	0	#DIV/0!	0	#DIV/0!	#DIV/0!		
	Be in ICP Aliquot (mc grams)	Total Be in sample (mc grams)	Be added as carrier (mc grams)	Be Yield (%)				
BLANK	28	320	309	103.50				
SPA-O-3	26	308	311	99.10				
SPA-O-1	22	301	311	96.91				
SPA-O-4	0	0	309					
SWR-B-7	22	303	306	99.05				
SAF-B-10	29	315	309	102.09				
SPA-O-15	27	306	309	99.13				
SPA-O-16	0	0	309					
							average	99.97
							high	103.50
							low	96.91

start date 4/10/95

Batch # 41

COLUMN USED	SAMPLE	QTZ WT grams	AL CARRIER g (1000 ppm)	BE CARRIER g (1000 ppm)	ADD ACID grams	INTO ICP grams	TOTAL ICP grams	HF ADDED
B	BLANK	-	2.721	0.251	9.620	0.934	6.282	10.000
A	spa-0-6XX	29.134	0.000	0.259	15.550	0.913	6.142	120.000
H	spa-0-5XX	29.030	0.000	0.254	19.270	0.750	6.394	120.000
C	saf-o-13xx	28.062	0.884	0.252	13.100	0.797	7.850	120.000
F	spa-o-16x	34.785	0.000	0.256	17.070	1.013	6.468	135.000
E	smh-b-9xx	29.712	0.000	0.252	14.210	1.001	7.289	120.000
D	spa-0-4x	27.997	0.000	0.252	8.410	1.007	7.057	115.000
G	smibg-3	26.395	0.889	0.251	12.760	0.818	6.899	105.000

RAW ICP DATA (Based on 1N acid Blank and 50 ppm Acid Standard)

	Batch # 41					
	Be-1	Al-1	Be-2	Al-2	Be-3	Al-3
BLANK	4.03	42.9	4.09	43.8	4.1	43.9
spa-0-6XX	2.3	75.6	2.41	79.6	2.35	78.6
spa-0-5XX	1.43	29.1	1.57	31.4	1.54	30.3
saf-o-13xx	1.76	100	1.83	106	1.81	104
25 ppm stan	27.1	26.1	28.3	27.9	28	27
spa-o-16x	2.26	77.1	2.33	77.6	2.21	75.9
smh-b-9xx	2.41	40.5	2.5	42.3	2.47	41.5
spa-0-4x	2.5	72.8	2.56	74	2.5	73
smibg-3	2.02	23.4	2.08	23.3	2.05	23.4
25 ppm stan	27.8	26.8	28	26.9	27.8	27



REDUCED ICP DATA

BATCH 41

	Al (avg)	+/- 1s	Be (avg)	+/- 1s
BLANK	43.53	0.55	4.07	0.04
spa-0-6XX	77.93	2.08	2.35	0.06
spa-0-5XX	30.27	1.15	1.51	0.07
saf-0-13xx	103.33	3.06	1.80	0.04
25 ppm stan	27	0.9	27.8	0.62
	(25.45) = real value		(28.12) = real value	
Al/Be			0.97	
			(0.905) = real value	
spa-o-16x	76.87	0.87	2.27	0.06
smh-b-9xx	41.43	0.90	2.46	0.05
spa-0-4x	73.27	0.64	2.52	0.03
smibg-3	23.37	0.06	2.05	0.03
Al/Be			0.97	
			(0.905) = real value	
25 ppm stan	26.9	0.1	27.87	0.12
	(25.45) = real value		(28.12) = real value	

Batch # 41

	Al in ICP Aliquot (mc grams)	Total Al in sample by ICP (mc grams)	Total Al in corrected for as carrier Be yield (mc grams)	Al added (mc grams)	Al from quartz (mc grams)	Al in quartz (ppm)	Al Yield (ICP based) (%)	Al Yield (Be-corrected) (%)
BLANK	257.78	2655.05	2499.77	2721.00	-221.23		97.58	91.87
spa-0-6XX	451.19	7684.52	7992.69	0.00	7992.69	274.34		
spa-0-5XX	182.42	4686.86	4733.88	0.00	4733.88	163.07		
saf-o-13xx	764.60	12567.45	13481.00	884.00	12597.00	448.90		
spa-o-16x	470.37	7926.25	8139.46	0.00	8139.46	233.99		
smh-b-9xx	285.73	4056.14	3979.43	0.00	3979.43	133.93		
spa-0-4x	489.17	4085.34	6869.29	0.00	6869.29	245.36		
smibg-3	152.52	2379.12	2682.39	889.00	1793.39	67.94		
	Be in ICP Aliquot (mc grams)	Total Be in sample (mc grams)	Be added as carrier (mc grams)	Be Yield (%)				
BLANK	25.88	266.59	251	106.21				
spa-0-6XX	14.62	249.01	259	96.14				
spa-0-5XX	9.79	251.48	254	99.01				
saf-o-13xx	14.29	234.92	252	93.22				
spa-o-16x	14.79	249.29	256	97.38				
smh-b-9xx	18.09	256.86	252	101.93				
spa-0-4x	17.95	149.87	252	59.47				
smibg-3	14.27	222.62	251	88.69				
				average	92.76			
				high	106.21			
				low	59.47			

## APPENDIX B. LEACH EXPERIMENT

An experiment was run in which one sample, SPA-O-2, was subjected to numerous variations of leach times, mesh sizes and acid concentrations. Sample SPA-O-2 was chosen for the experiment based on the large quantity of sample obtained, several kilograms, as well as its inherent aversion to the quartz purification procedure. The results of this experiment would indicate that a minimum of two ultrasounds is required for adequate clean up, and that for more than four ultrasound treatments, the benefits become negligible. The most effective treatment (clean-up, and cost) seems to be the two ultrasound treatment with an extended first leach time. Experiments were also done with a subsequent HCl leach in an attempt to dissolve the residual Fe and Al. Approximately 30 grams of HF etched quartz was added to 250 ml of 6N HCl and heated to approximately 90-100°C for 24 hours. It was determined almost immediately that the HCl was removing Fe as the leachate turned a rich yellow color after approximately one hour of leach time.

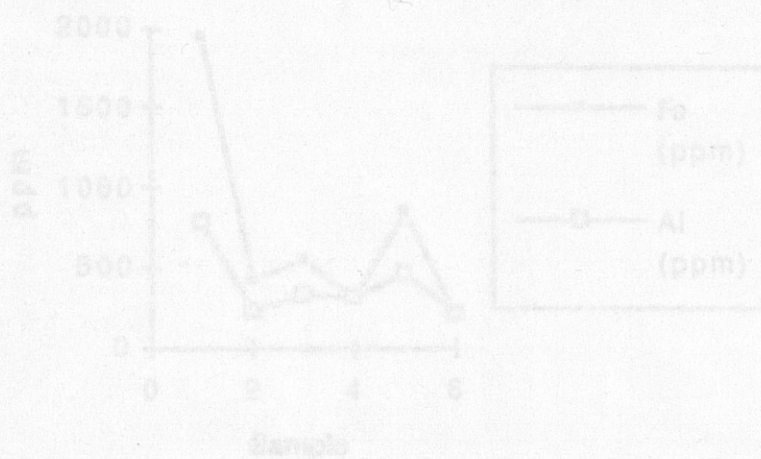




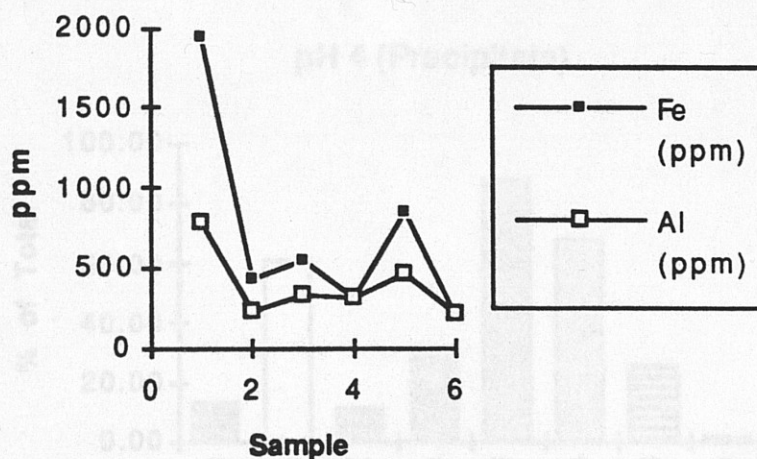
Table B.1. Leach experiment parameters and results

<b>Sample: SPA-O-2</b>		<b>Strengths:</b>		<b>HF (ml)</b>	<b>HNO3 (ml)</b>
30 g of sample in 4 liters d.i.-acid solution		F		80	50
		H		40	25

<b>I.D.</b>	<b>Leach Parameters</b>				<b>Fe (ppm)</b>	<b>Al (ppm)</b>
	<b>Hrs</b>	<b>Strengths</b>	<b>Mag Sep</b>	<b>microns</b>		
1 U.S.	20.5	F	N	250-710	1948.77	785.73
2 U.S.	27.5, 14	F,H	N	250-710	439.91	234.1
3 U.S.	20.5,14,6.25	F,H,H	N	250-710	554.33	338.84
4 U.S.	20.5,14,6.25,11	F,H,H,H	N	250-710	312.32	308.85
3 F	8,14,24	F,F,F	Y	250-500	845.49	464.77
3F+6N HCl	24	6 M		250-500	191.75	207.35

Figure B.1. Graphical representation of leach experiment results. Sample axis corresponds to I.D. column in Table B.1.





## APPENDIX C. PRECIPITATION EXPERIMENT

There were some samples which, despite numerous ultrasound treatments, remained relatively enriched in Fe, Ti, and native Al. Therefore, a post-dissolution treatment was developed with the goal of removing these elements without affecting the concentration of  $^{10}\text{Be}$  in the quartz. For this experiment, the dissolved quartz solution (HCl) was raised to incrementally higher pH's with 1N  $\text{NH}_4\text{OH}$  and the resulting precipitates and supernatant liquids were analyzed on the ICAP at Middlebury College. Uncertainties in this experiment arise from the use of pH paper. The colors on the pH paper were often not easily differentiated, therefore the pH values are assumed to be  $\pm 1$  pH. The results of this experiment are shown graphically in Figure C.1 (a-e). I would recommend repeating this experiment with an accurate and precise pH meter for more reliable results.

Figure C.1a

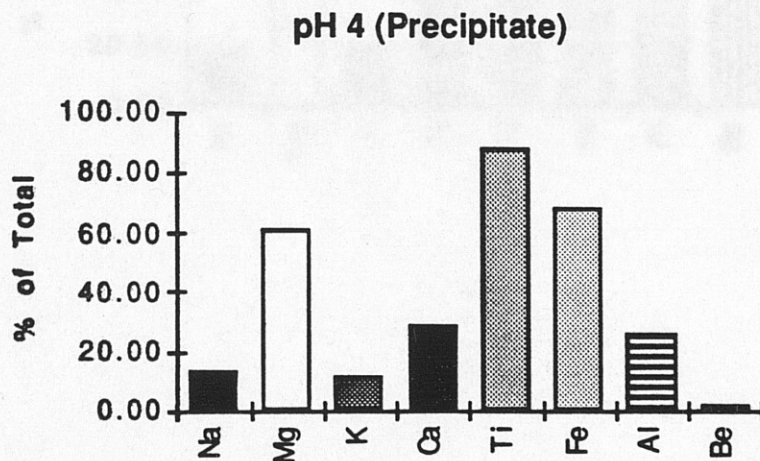


Figure C.1b

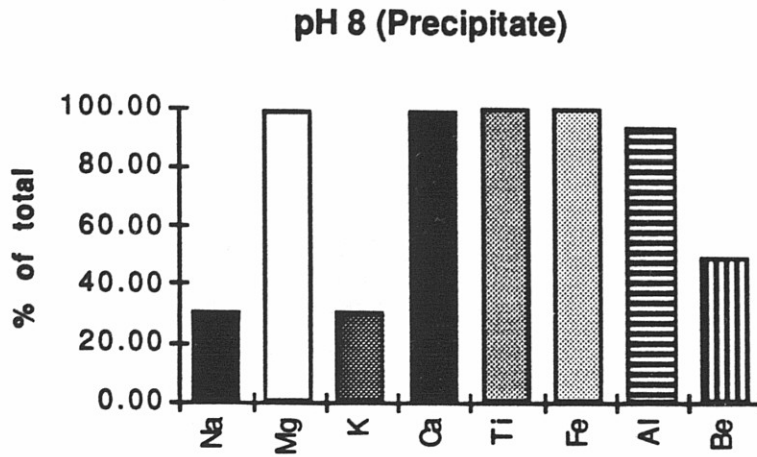


Figure C.1c

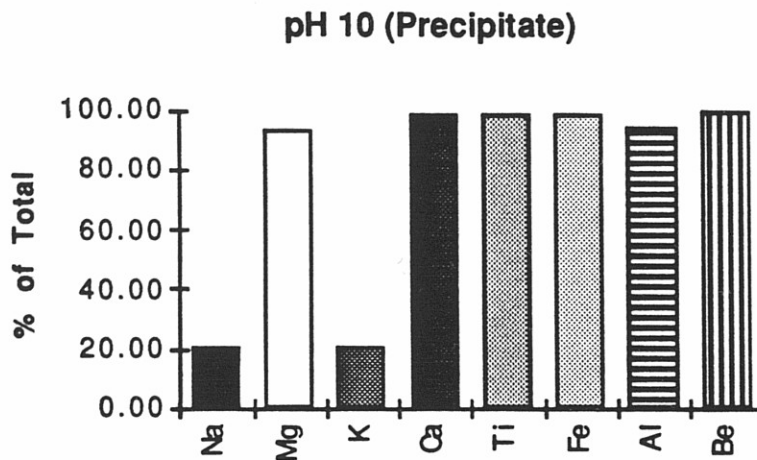


Figure C.1d

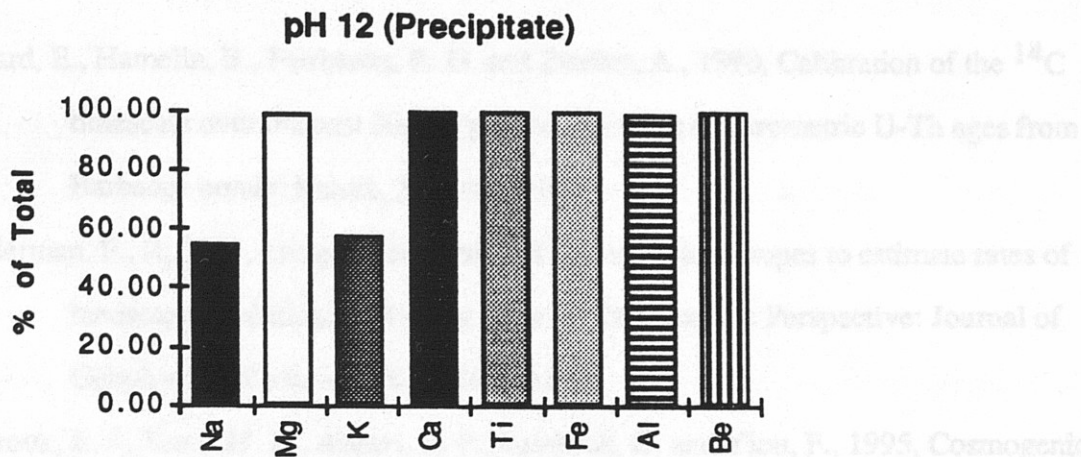
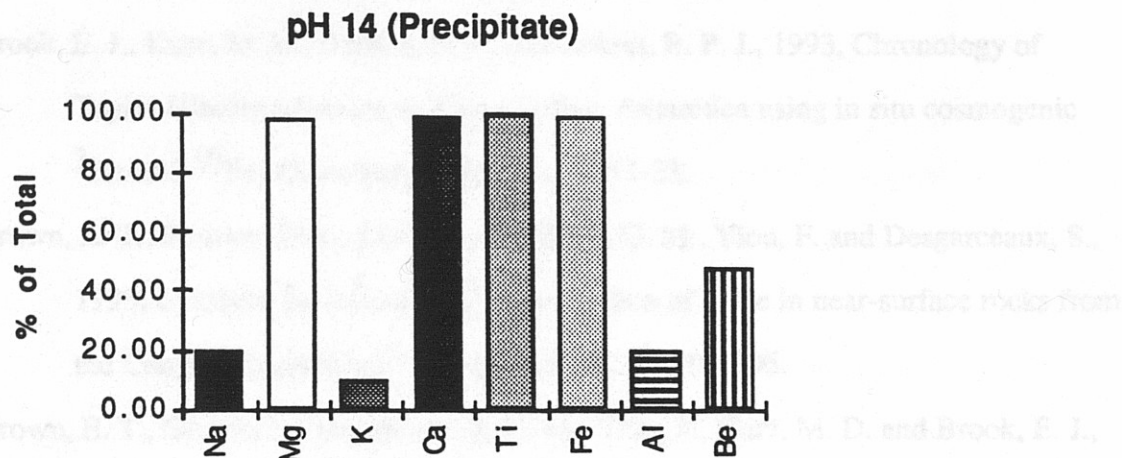


Figure C.1e



## COMPREHENSIVE BIBLIOGRAPHY

- Bard, E., Hamelin, B., Fairbanks, R. G. and Zindler, A., 1990, Calibration of the  $^{14}\text{C}$  timescale over the past 30,000 years using mass spectrometric U-Th ages from Barbados corals: *Nature*, 345, 405-410.
- Bierman, P., R., 1994, using in situ produced cosmogenic isotopes to estimate rates of landscape evolution: A Review from the Geomorphic Perspective: *Journal of Geophysical Research*, 99, 13885-13896.
- Brook, E. J., Kurz, M. D., Ackert, R. P., Raisbeck, G. and Yiou, F., 1995, Cosmogenic nuclide exposure ages and glacial history of late Quaternary Ross Sea drift in McMurdo Sound, Antarctica: *Earth and Planetary Science Letters*, 131, 41-56.
- Brook, E. J., Kurz, M. D., Denton, G. H. and Ackert, R. P. J., 1993, Chronology of Taylor Glacier advances in Arena Valley, Antarctica using in situ cosmogenic  $^3\text{He}$  and  $^{10}\text{Be}$ : *Quaternary Research*, 39, 11-23.
- Brown, E. T., Bourles, D. L., Colin, F., Raisbeck, G. M., Yiou, F. and Desgarceaux, S., 1995, Evidence for muon-induced production of  $^{10}\text{Be}$  in near-surface rocks from the Congo: *Geophysical Research Letters*, 22, 703-706.
- Brown, E. T., Edmond, J. M., Raisbeck, G. M., Yiou, F., Kurz, M. D. and Brook, E. J., 1991a, Examination of surface exposure ages of Antarctic moraines using in situ produced  $^{10}\text{Be}$  and  $^{26}\text{Al}$ : *Geochimica et Cosmochimica Acta*, 55, 2269-2283.
- Brown, E. T., Raisbeck, G. M., Yiou, F., Kurz, M. and Brook, E. J., 1991b, Effective attenuation lengths of cosmic rays producing Be-10 and 26-Al in quartz: implications for exposure dating: *EOS*, 72, 575.
- Cerling, T. E. and Craig, H., 1994, Geomorphology and in-situ cosmogenic isotopes: *Annual Review Earth Planetary Science*, 22, 273-317.
- Clark, D. H., Bierman, P.R., Larsen, P.L., 1995, Improving *In situ* Cosmogenic Chronometers: *Quaternary Research*, In press .



- Connally, G.G. and Sirkin, L.A., 1973, Wisconsinan history of the Hudson-Champlain Lobe: The Wisconsinan Stage; Geological Society of America Memoir, 136, 47-69.
- Cotter, J. F., 1984, The minimum age of the Woodfordian deglaciation of northeastern Pennsylvania and northwestern New Jersey: Lehigh University, Ph.D.
- Dunne, T., Leopold, L.B., 1978, Water in Environmental Planning: W.H. Freeman and Company, New York.
- Elmore, D. and Phillips, F., 1987, Accelerator mass spectrometry for measurement of long-lived radioisotopes: Science, 236, 543-550.
- Evenson, E.B., Cotter, J.F., Ridge, J.C., Sevon, W.D., Sirkin, L., Stuckenrath, R., 1983, The mode and chronology of deglaciation of the Great Valley, northwestern New Jersey: Geological Society of America Abstracts with Programs, 15, 133.
- Evenson, E.B. and Gosse, J., 1993, Application of in situ produced cosmogenic nuclide exposure ages to reconstruct glacial histories at the Pinedale type locality, Wyoming: Geological Society of America Abstracts with Programs, 25, A308.
- Fabryka-Martin, J. T., 1988, Production of radionuclides in the earth and their hydrogeologic significance, with emphasis on Chlorine-36 and Iodine-129: University of Arizona, Ph.D.
- Finkle, R. C. and Suter, M., 1993, AMS In the Earth Sciences: Technique and Applications: Advances in Analytical Geochemistry, 1, 1-114.
- Friedlander, M. W., 1989, Cosmic Rays: Harvard, Cambridge, 160.
- Fullerton, D.S., 1986, Stratigraphy and correlation of glacial deposits from Indiana to New York and New Jersey: Quaternary Science Reviews, 5, 23-37.
- Gosse, J. C., Klein, J., Evenson, E. B., Lawn, B. and Middleton, R., 1995, Beryllium-10 dating of the Duration and Retreat of the Last Pinedale Glacial Sequence: Science, 268, 1329-1333.

- Harmon, K. P., 1968, Late Pleistocene forest succession in northern New Jersey: Rutgers University, Ph.D. dissertation
- Johnson, R. A. and Wichern, D. W., 1982, Applied Multivariate Statistical Analysis: Prentice-Hall, Inc., .
- Klein, J., Giegengack, R., Middleton, R., Sharma, P., Underwood, J. R. and Weeks, R. A., 1986, Revealing histories of exposure using in situ produced  $^{26}\text{Al}$  and  $^{10}\text{Be}$  in Libyan desert glass: Radiocarbon, 28, 547-555.
- Kohl, C. P. and Nishiizumi, K., 1992, Chemical isolation of quartz for measurement of *in-situ* -produced cosmogenic nuclides: Geochimica et Cosmochimica Acta, 56, 3583-3587.
- Kurz, M. D., 1986, *In situ* production of terrestrial cosmogenic helium and some applications to geochronology: Geochimica et Cosmochimica Acta, 50, 2855-2862.
- Kurz, M. D., Colodner, D., Trull, T. W., Moore, R. and O'Brien, K., 1990, Cosmic ray exposure dating with in situ produced cosmogenic  $^3\text{He}$ : results from young Hawaiian lava flows: Earth and Planetary Science Letters, 97, 177-189.
- Lal, D., 1987, Cosmogenic isotopes produced in situ in terrestrial solids: Nuclear Instruments and Methods in Physics Research, B29, 238-245.
- Lal, D., 1991, Cosmic ray labeling of erosion surfaces: *In situ* production rates and erosion models: Earth and Planetary Science Letters, 104, 424-439.
- Lal, D. and Arnold, J. R., 1985, Tracing quartz through the environment: Proceedings of the Indian Academy of Science (Earth and Planetary Science), 94, 1-5.
- Larsen, P. L., Bierman, P. R. and Caffee, M., 1995, Cosmogenic  $^{26}\text{Al}$  chronology of the Late Wisconsinan glacial maximum in North-Central New Jersey: GSA Abstracts with Programs, 27, 63.

- Mazaud, A., Laj, C., Bard, E., Arnold, M. and Tric, E., 1991, Geomagnetic field control of  $^{14}\text{C}$  production over the last 80 ky: implications for the radiocarbon time scale: *Geophysical Research Letters*, 18, 1885-1888.
- Matsch, C.L., 1987, retreat of the southern margin of the Laurentide ice sheet: *International Union for Quaternary Research*, XII, 221.
- McElhinny, M. W. and Senanayake, W. E., 1982, Variations in the geomagnetic dipole 1: the past 50,000 years: *Journal of Geomagnetism and Geoelectricity*, 34, 39-51.
- Mendenhall, W., 1969, *Introduction to Probability and Statistics*, Wadsworth Publishing Company, Inc., Belmont, California, 393.
- Merrill, R.T., McElhinny, M.W., 1983, *The Earth's Magnetic Field: Its History, Origin and Planetary Perspective*: William L. Donn (ed.) Academic Press, New York.
- Merrington, M. and Thompson, C. M., 1943, Tables of Percentage Points of the Inverted Beta (F) Distribution: *Biometrika*, 33, 73-88.
- Meynadier, L., Valet, J., Weeks, R., Shackleton, N. and Hagee, V., 1992, Relative geomagnetic intensity of the field during the last 140 ka: *Earth and Planetary Science Letters*, 114, 39-57.
- Middleton, R. and Klein, J., 1987,  $^{26}\text{Al}$ : measurement and applications: *Philosophical Transactions of the Royal Society of London*, A 323, 121-143.
- Monaghan, M. C., McKean, J., Dietrich, W. E. and Klein, J., 1992,  $^{10}\text{Be}$  Chronometry of bedrock-to-soil conversion rates: *Earth and Planetary Science Letters*, 111, 483-492.
- Nishiizumi, K., Kohl, C. P., Arnold, J. R., Dorn, R. I., Klein, J., Fink, D., Middleton, R. and Lal, D., 1993, Role of in situ cosmogenic nuclides  $^{10}\text{Be}$  and  $^{26}\text{Al}$  in the study of diverse geomorphic processes: *Earth Surface Processes and Landforms*, 18, 407-425.

- Nishiizumi, K., Kohl, C. P., Arnold, J. R., Klein, J., Fink, D. and Middleton, R., 1991a, Cosmic ray produced  $^{10}\text{Be}$  and  $^{26}\text{Al}$  in Antarctic rocks: exposure and erosion history: *Earth and Planetary Science Letters*, 104, 440-454.
- Nishiizumi, K., Kohl, C. P., Shoemaker, E. M., Arnold, J. R., Klein, J., Fink, D. and Middleton, R., 1991b, *In situ*  $^{10}\text{Be}$ - $^{26}\text{Al}$  exposure ages at Meteor Crater, Arizona: *Geochimica et Cosmochimica Acta*, 55, 2699-2703.
- Nishiizumi, K., Lal, D., Klein, J., Middleton, R. and Arnold, J. R., 1986, Production of  $^{10}\text{Be}$  and  $^{26}\text{Al}$  by cosmic rays in terrestrial quartz *in situ* and implications for erosion rates: *Nature*, 319, 134-136.
- Nishiizumi, K., Winterer, E. L., Kohl, C. P., Klein, J., Middleton, R., Lal, D. and Arnold, J. R., 1989, Cosmic ray production rates of  $^{10}\text{Be}$  and  $^{26}\text{Al}$  in quartz from glacially polished rocks: *Journal of Geophysical Research*, 94, 17907-17915.
- Oldale, R.N., Stone, B.D., 1987, The Late Wisconsinan glaciation in southern New England: International Union for Quaternary Research XII<sup>th</sup> International Congress, 234.
- Phillips, F. M., Zreda, M. G., Smith, S. S., Elmore, D., Kubik, P. W. and Sharma, P., 1990, Cosmogenic Chlorine-36 chronology for glacial deposits at Bloody Canyon, eastern Sierra Nevada: *Science*, 248, 1529-1532.
- Raisbeck, G. M., Yiou, F., Klein, J. and Middleton, R., 1983, Accelerator mass spectrometer measurement of cosmogenic  $^{26}\text{Al}$  in terrestrial and extraterrestrial matter: *Nature*, 301, 690-692.
- Sarda, P., Staudacher, T., Allegre, C. and Lecomte, A., 1993, Cosmogenic neon and helium at Reunion: measurement of erosion rate: *Earth and Planetary Science Letters*, 119, 405-417.
- Sharma, P. and Middleton, R., 1989, Radiogenic production of  $^{10}\text{Be}$  and  $^{26}\text{Al}$  in uranium and thorium ores: Implications for studying terrestrial samples containing low levels of  $^{10}\text{Be}$  and  $^{26}\text{Al}$ : *Geochimica et Cosmochimica Acta*, 53, 709-716.



- Sirkin, L.A., 1977, Late Pleistocene vegetation and environments in the middle Atlantic region; in Newman, W.S. and Salwen, B., Amerinds and their paleoenvironments in northeastern North America: New York Academy of Science Annals, 288, 206-217.
- Smith, N. D., 1970, The Braided Stream Depositional Environment: Comparison of the Platte River with Some Silurian Clastic Rocks, North-Central Appalachians: Geological Society of America Bulletin, 81, 2993-3014.
- Stanford, S. D., 1993, Late Wisconsinan Glacial Geology of the New Jersey Highlands: Northeastern Geology, 15, 210-223.
- Stone, B.D., Borns, H.W., 1986, Pleistocene glacial and interglacial stratigraphy of New England, Long Island, and adjacent Georges Bank and Gulf of Maine: Quaternary Science Reviews, 5, 39-52.
- Stuiver, M., Braziunas, T. F., Becker, B. and Kromer, B., 1991, Climatic, Solar, Oceanic, and Geomagnetic Influences on Late-Glacial and Holocene Atmospheric  $^{14}\text{C}/^{12}\text{C}$  Change: Quaternary Research, 35, 1-24.
- Stuiver, M., and Reimer, P. J., 1993, Extended  $^{14}\text{C}$  database and revised CALIB radiocarbon calibration program, Radiocarbon, 35, 215-230.
- Tric, E., Valet, J. P., Tucholka, P., Paterne, m., Labeyrie, L., Guichard, F., Tauxe, L. and Fontugne, M., 1992, Paleointensity of the geomagnetic field during the last 80,000 years: Journal of Geophysical Research, 97, 9337-9351.
- Widmer, K., 1964, The Geology and Geography of New Jersey: The New Jersey Historical Series, D. Van Nostrand Company, Inc., Princeton, New Jersey, 19, 193.